THE ROLE OF FREE RADICAL STRESS IN THE ETIOLOGY OF PENDRED SYNDROME

IN A MOUSE MODEL.

by

RUCHIRA SINGH

B.Tech., Jawaharlal Nehru Technological University, Hyderabad, India, 2001

AN ABSTRACT OF A DISSERTATION

submitted in partial fulfillment of the requirements for the degree

DOCTOR OF PHILOSOPHY

Department of Anatomy & Physiology
College of Veterinary Medicine

KANSAS STATE UNIVERSITY
Manhattan, Kansas

2008

Abstract

Pendred syndrome is characterized by sensorineural deafness and post-pubertal goiter. It is caused by mutations in the anion exchanger, pendrin (*SLC26A4*). The purpose of this study was to understand the etiology of Pendred syndrome using a mouse model. Different methods of amplification from nanogram amounts of starting RNA were evaluated for gene array application. Gene arrays were performed and free radical stress markers were compared between the stria vascularis and the thyroid of the *Slc26a4*$^{+/-}$ and *Slc26a4*$^{-/-}$ mice. Hearing loss in *Slc26a4*$^{-/-}$ mice is linked to the loss of Kcnj10 protein expression and consequently the loss of endocochlear potential. To understand the mechanism of hearing loss in *Slc26a4*$^{-/-}$ mice, progressive loss of Kcnj10 protein expression in stria vascularis of *Slc26a4*$^{-/-}$ mice was assessed, the modulation of Kcnj10 protein expression by free radical stress in cultured stria vascularis and in an heterologous expression system was evaluated. To characterize the thyroid pathology, *Slc26a4* expression in the thyroid of *Slc26a4*$^{+/-}$ mice was measured in a developmental study and correlated with serum thyroxine (T4) levels of *Slc26a4*$^{+/-}$ and *Slc26a4*$^{-/-}$ mice over a developmental time course. All tested methods of RNA amplification were suitable for gene array application and demonstrated high internal consistency. Intermethod comparisons revealed variations in data, suggesting that a single amplification method ought to be used within a given experiment. Markers of free radical stress were increased in the stria vascularis of *Slc26a4*$^{-/-}$ mice before the onset of hearing. Progressive loss of Kcnj10 expression was seen in *Slc26a4*$^{-/-}$ mice at the onset of hearing. Furthermore, free radical stress modulated the expression of Kcnj10 in cultured stria vascularis and in a heterologous expression system. The *Slc26a4* mRNA expression was marginal in the thyroid and did not correlate with serum T4 levels. Further, absence of *Slc26a4* did not affect free radical stress markers in the thyroid. These data suggest that free radical stress-mediated loss of Kcnj10 expression in stria vascularis contributes to deafness in the Pendred syndrome mouse model and that pendrin is not essential for the function of mouse thyroid gland.

THE ROLE OF FREE RADICAL STRESS IN THE ETIOLOGY OF PENDRED SYNDROME

IN A MOUSE MODEL.

by

RUCHIRA SINGH

B.Tech., Jawaharlal Nehru Technological University, Hyderabad, India, 2001

A DISSERTATION

submitted in partial fulfillment of the requirements for the degree

DOCTOR OF PHILOSOPHY

Department of Anatomy & Physiology
College of Veterinary Medicine

KANSAS STATE UNIVERSITY
Manhattan, Kansas

2008

Approved by:

Major Professor
Dr. Philine Wangemann

Abstract

Pendred syndrome is characterized by sensorineural deafness and post-pubertal goiter. It is caused by mutations in the anion exchanger, pendrin (*SLC26A4*). The purpose of this study was to understand the etiology of Pendred syndrome using a mouse model. Different methods of amplification from nanogram amounts of starting RNA were evaluated for gene array application. Gene arrays were performed and free radical stress markers were compared between the stria vascularis and the thyroid of the $Slc26a4^{+/-}$ and $Slc26a4^{-/-}$ mice. Hearing loss in $Slc26a4^{-/-}$ mice is linked to the loss of Kcnj10 protein expression and consequently the loss of endocochlear potential. To understand the mechanism of hearing loss in $Slc26a4^{-/-}$ mice, progressive loss of Kcnj10 protein expression in stria vascularis of $Slc26a4^{-/-}$ mice was assessed, the modulation of Kcnj10 protein expression by free radical stress in cultured stria vascularis and in an heterologous expression system was evaluated. To characterize the thyroid pathology, pendrin expression in the thyroid of $Slc26a4^{+/-}$ mice was measured in a developmental study and correlated with serum thyroxine (T4) levels of $Slc26a4^{+/-}$ and $Slc26a4^{-/-}$ mice over a developmental time course. All tested methods of RNA amplification were suitable for gene array application and demonstrated high internal consistency. Intermethod comparisons revealed variations in data, suggesting that a single amplification method ought to be used within a given experiment. Markers of free radical stress were increased in the stria vascularis of $Slc26a4^{-/-}$ mice before the onset of hearing. Progressive loss of Kcnj10 expression was seen in $Slc26a4^{-/-}$ mice at the onset of hearing. Furthermore, free radical stress modulated the expression of Kcnj10 in cultured stria vascularis and in a heterologous expression system. The pendrin mRNA expression was marginal in the thyroid and did not correlate with serum T4 levels. Further, absence of pendrin did not affect free radical stress markers in the thyroid. These data suggest that free radical stress-mediated loss of Kcnj10 expression in stria vascularis contributes to deafness in the Pendred syndrome mouse model and that pendrin is not essential for the function of mouse thyroid gland.

TABLE OF CONTENTS

List of Figures

List of Tables

Acknowledgements

CHAPTER 1 - Introduction

Organization of this chapter

This chapter begins with an overview of the ear and of the mechanisms involved in hearing, followed by a brief summary of the different types of hearing loss. The mechanisms involved in several genetic and non-genetic forms of sensorineural deafness (defects in cochlea) are provided, with a particular emphasis on Pendred syndrome, the subject of this dissertation. The clinical features of this disease and the current knowledge about the pathology of this disease as obtained from studies on the animal model are summarized. Then, a description of the expression and function of pendrin in the pendrin-expressing tissues, stria vascularis and thyroid, is provided. The components and mechanisms of free radical stress, which plays a role in many forms of sensoineural deafness, are described. Because gene arrays have been a major tool in formulating the hypothesis for this dissertation, a brief section on the use and methodology of gene arrays is included. Finally, the approaches to be used in achieving the goal of this dissertation are outlined.

Hearing

Humans are capable of hearing in the frequency range of 20 to 20,000 Hz. Perception of sound is a complex process that is performed by the auditory apparatus. The auditory system consists of the outer ear, middle ear, inner ear and the auditory cortex in the brain. Sound waves enter the outer ear and are transmitted to the middle ear, where the pressure of the sound waves on the tympanic membrane is converted into mechanical vibrations. The cochlea then converts the mechanical vibrations into electrical signals in the inner ear. These electrical signals are transmitted to the auditory cortex, where they are interpreted by the brain (Fig. 1.1).
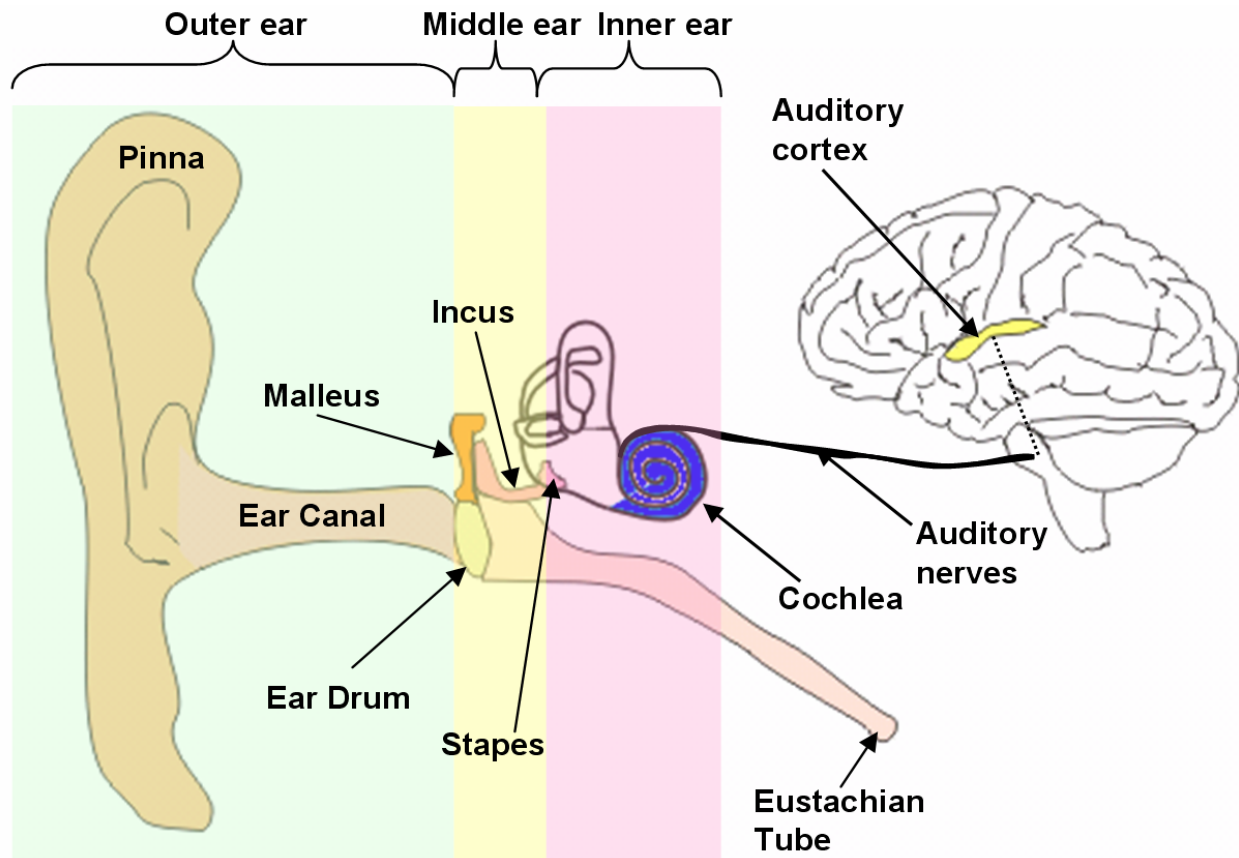
Figure 1.1: Schematic diagram of the auditory apparatus
The auditory apparatus consisting of outer ear, middle ear, inner ear and the auditory cortex is shown. (For a brief description of the sound transduction mechanism, see text).

The outer ear consists of the pinna (or auricle) and the outer ear canal and is key to the localization of sound. Sound is collected by the pinna, the visible external ear. In humans, the pinna is required for comprehension of directionality of sound but is not essential for hearing. However, in some animals with a flexible external ear (like the horse), the pinna is indispensable for sound localization and amplification. The outer ear canal channels sound waves to the tympanic membrane (ear drum) of the middle ear. The outer ear canal also produces cerumin (natural wax) that provides a protection from external irritants.

The middle ear consists of an air-filled tympanic cavity, the tympanic membrane, three bony ossicles (malleus, incus and stapes), middle ear muscles and the Eustachian tube. The tympanic membrane is a thin, but extremely strong, membrane that is connected to the malleus. The incus joins the malleus and the stapes together, forming a chain of levers. Movement of the tympanic membrane by sound wave pressure leads to successive movement of the malleus, the

incus and the stapes. The stapes contacts the oval window of the cochlea in the inner ear. When the stapes moves as a result of sound pressure, it causes fluid movement in the cochlea, which subsequently drives sensory transduction. The Eustachian tube joins the tympanic cavity of the middle ear to the nasal pharynx and equilibrates the air pressure between the tympanic cavity and the external environment. The middle ear plays a key role in the efficient transmission of sound energy. In the absence of this complex architecture, most of the sound-associated vibrational energy received at the external ear would be dissipated before reaching the inner ear. The tympanic membrane has an extremely large surface area compared to the stapes (the smallest bone in the body) and this helps in concentrating the energy of the sound waves. Furthermore, the lever arrangement of the ossicles leads to an increase in the force applied to the stapes and thereby to the fluid spaces in the inner ear.

The inner ear is encased in the temporal bone and consists of the cochlea (the organ of hearing) and the vestibular system (the organ of balance). The cochlea is a snail-shaped structure of two and three-quarter turns that spirals around a central bony core (the modiolous). The cochlea contains three parallel fluid-filled comparments: scala vestibuli, scala media and scala tympani. The scala media forms the cochlear duct, which separates the scala vestibuli from the scala tympani and contains the sensory epithelium (Fig. 1.2). The scala vestibuli and the scala tympani are filled with perilymph, which resembles most extracelluar fluids with high Na^+ (~150 mM) and low K^+ (~5 mM) concentrations. The scala media is filled with endolymph, a unique extracellular fluid with an ionic composition similar to intracellular fluid, with high K^+ (~150 mM) and low Na^+ (~1.3 mM) concentrations. On one side of the cochlear duct is the stria vascularis, which is responsible for the maintainence of the ionic composition and the highly positive potential (endocochlear potential, +80mV) of the endolymph. The endocochlear potential is the driving force for sensory transduction and is required for the sensitivity of hearing. The scala media is separated from the scala vestibuli by the Reissner's membrane and from the scala tympani by the basilar membrane. The organ of Corti contains the sensory receptor cells (hair cells), faces the scala media and resides on the basilar membrane. The hair cells are essentially sandwiched between two extracellular matrices, the tectorial membrane (on top) and the basilar membrane (on bottom). The major sensory receptor cells involved in the detection of sound are the inner hair cells. The outer hair cells, in conjunction with the tectorial

membrane, play a role in the amplification of the movements of the basilar membrane. Fluid displacement caused by the vibration of the stapes leads to the oscillatory movement of the flexible basilar membrane and alternating depolarization-hyperpolarization of the inner hair cells. The basilar membrane decreases in rigidity from the base to the apex of the cochlea, so different parts of the cochlea respond to different sound frequencies. High frequency is detected at the base of the cochlea whereas low frequency sound is detected at the apex. When the basilar membrane oscillates, mechanically gated channels are opened by the displacement of stereocilia on top of each inner hair cell, which, with the driving force provided by the endocochlear potential, causes an influx of K^+ into the inner hair cells. This movement of K^+ depolarizes the hair cells, consequently opening voltage-gated Ca^{2+} channels that mediate Ca^{2+} influx and ultimately the release of neurotransmitter from the basal pole of the hair cells. When neurotransmitter is released from the inner hair cells, afferent nerves initiate an action potential that is sent to the brainstem, where the auditory nerve synapses in the cochlear nucleus. Auditory information from the cochlear nucleus is divided into two pathways. First, auditory nerve fibers from the ventral cochlear nuclei terminate at the superior olivary nucleus where differences in the timing and loudness of sound from each ear is compared to infer the directionality of sound. Auditory fibers from the superior olivary nucleus then passes upward to the lateral lemniscus and from there project to the inferior colliculus. The second auditory pathway includes auditory nerve fibers from the dorsal cochlear nuclei that directly go to the lateral leminscus and from there pass to the inferior colliculus. The auditory pathway from the inferior colliculus proceeds to the auditory nucleus (medial geniculate nucleus) in the sensory thalamus, and from there is projected to the auditory cortex, enabling the perception of sounds.
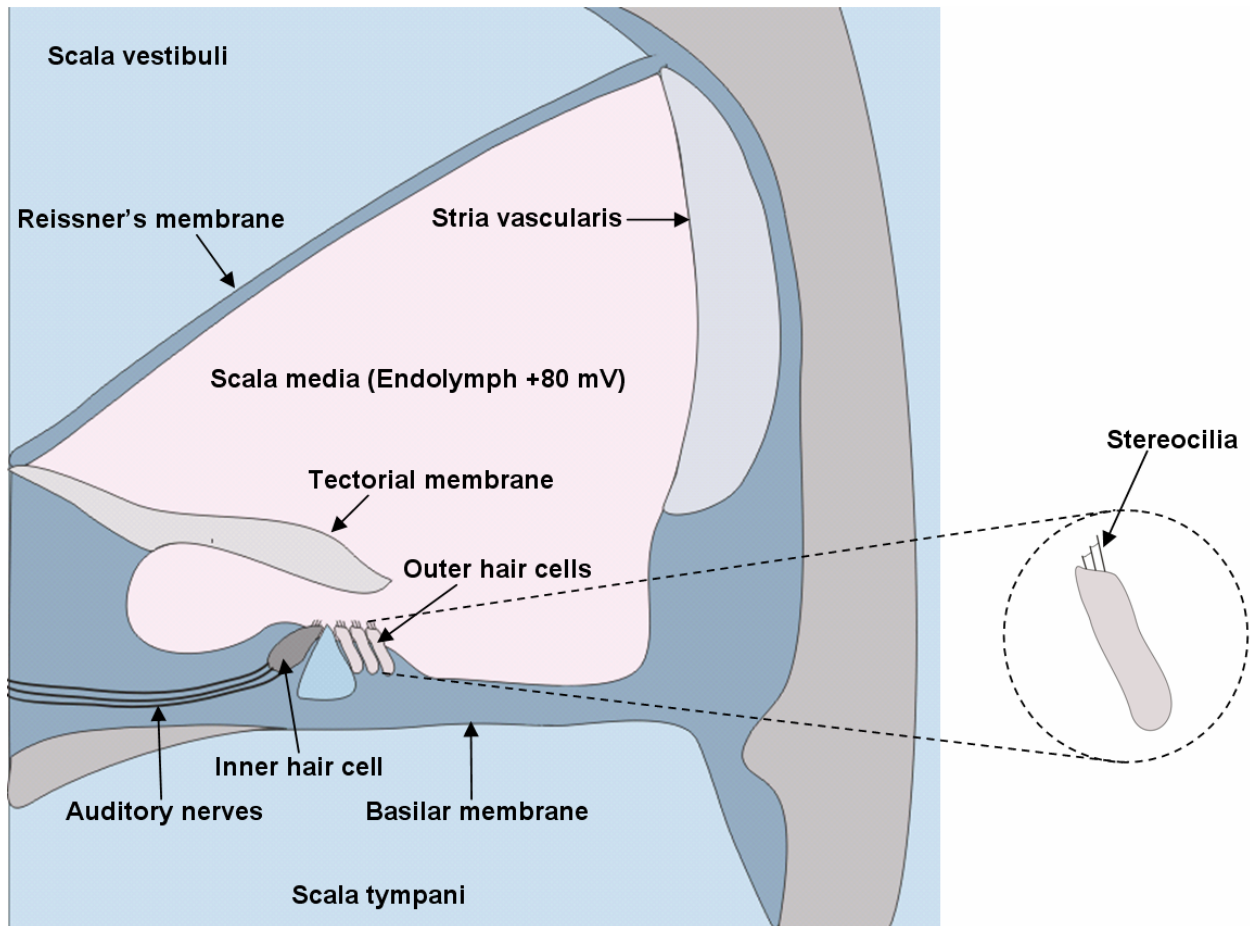
Figure 1.2: Schematic diagram showing the major components of the cochlea that are involved in sensory transduction.
Left: A cross section of the cochlear duct. The perilymph fluid spaces, scala vestibuli and scala tympani (blue) are separated by the scala media (cochlear duct, pink). Also labeled in the diagram are the Reissner's membrane, stria vascularis, sensory hair cells (inner hair cell and outer hair cells), sterocilia on the inner hair cell, afferent auditory nerve fibers, the tectorial and the basilar membrane. Right: Magnified view of the hair cell showing the stereocila. (For a brief description on the cochlear function, see text).

Hearing loss

Deafness is defined as the impaired or complete loss of hearing and affects approximately 1-5 newborns per 1000 births (34). The onset of deafness can be variable, affecting patients either at birth, prelingually or later in adult life. Furthermore, hearing loss can have a sudden onset or deteriorate progressively. Hearing loss can be broadly classified into different categories depending on the threshold intensity: mild (20-40 dB), moderate (40-70 dB), severe (70-90 dB), and profound (> 90 dB).

The three major forms of hearing loss are conductive hearing loss, sensorineural hearing loss and mixed hearing loss. Conductive hearing loss is due to problems in the outer and middle ear that interfere with the efficiency of sound transmission to the cochlea. This type of hearing loss can generally be treated without surgery. Sensorineural hearing loss is due to defects in the cochlea or the auditory nerve pathway and accounts for approximately 90% of individuals affected by deafness worldwide. Mixed hearing loss, as the name implies, is due to a combination of conductive and sensorineural defects.

Inner ear disease mechanisms

Sensorineural hearing loss due to defects in the cochlea can be caused by genetic mutations and/or environmental factors. Genetic forms of hearing loss can be linked to either a syndromic disease or can be non-syndromic in presentation, affecting only the cochlea (60). Examples of syndromic hearing loss include Usher syndrome (deafness and retinitis pigmentosa), Pendred syndrome (deafness and goiter), Jervell and Lange-Nielsen syndrome (deafness and long QT intervals), and Alport syndrome (deafness and renal anomalies). Examples of genes that are mutated in non-syndromic forms of hearing loss include *CX26*, *CX30*, *CDH23*, *TECTA*, *THRB* and *COCH* (46). Non-genetic hearing loss results from a variety of causes including noise exposure, contact with organic solvents, drug-induced ototoxicity, viral infections, and trauma (9; 18; 20; 21; 51). The risk of acquired hearing loss due to environmental exposure may be increased in humans with a genetic mutation. For example, people with mutations in 12S rRNA are more likely to develop hearing loss from the use of ototoxic drugs than individuals in the general population (17). Apart from factors that affect the inner ear directly, sensorineural deafness can also result from congenital systemic hypothyroidism (41; 65).

Mouse models for genetic, as well as environmentally-acquired, hearing loss have been critical to the understanding of cochlear pathology in sensorineural hearing loss (19; 43). In most cases of sensorineural hearing loss, the primary effect is either sensory (affecting the hair cells), metabolic (affecting the stria vascularis), mechanical (affecting the basilar and tectorial membrane) or neural (affecting the auditory nerve). Brief descriptions of several common forms

of sensorineural hearing loss, and the associated cochlear pathology are presented in the following paragraphs.

Genetic forms of sensorineural hearing loss

Ushers syndrome type 1 (USH1): USH1 is an autosomally inherited disease with profound congenital hearing loss, vestibular dysfunction and adult onset of retinitis pigmentosa. To date, mutations leading to USH1 have been identified in 5 genes: *MYO7A*, *CDH23*, *PCDH15*, *USH1C* and *USH1G*, (29). Mouse models defective in each of these genes display hearing impairment but do not develop retinitis pigmentosa (2). Proteins encoded by these genes, myosin VIIa, cadherin 23, protocadherin 15, harmonin and SANS, localize primarily in the hair cell sterocilia. Experimental evidence suggest that loss of hearing results from lack of sterocilliary links and disorganized hair cell bundles (12).

Deafness due to mutations in connexins: Connexins form the functional unit of intercellular channels, gap junctions that electrically couple neighboring cells and provide a conduit for metabolite transport. The murine cochlea has an extensive gap junction network with prominent expression of five connexin genes: *Cx26*, *Cx30*, *Cx31*, *Cx29* and *Cx45* (1). Mutations in *CX26* account for almost 50% of cases of non-syndromic hearing loss in childhood (10; 27). Cx26 and Cx30 are highly expressed in the cochlea in cells of the organ of Corti and the lateral wall (stria vascularis and spiral ligament) (33). Absence of *Cx26* and *Cx30* in knockout mouse models is associated with deafness (7; 64). Hearing loss in the $Cx26^{-/-}$ and $Cx30^{-/-}$ mice may be a consequence of cellular death in the organ of Corti and loss of endocochlear potential. $Cx30^{-/-}$ mice fail to develop endocochlear potential, whereas $Cx26^{-/-}$ mice lose the endocochlear potential soon after the onset of hearing.

Environmentally acquired/ non-genetic hearing loss

Noise-induced hearing loss (NIHL): NIHL is one of the primary causes of non-genetic sensorineural hearing loss (9). Traumatic or constant high level exposure to noise leads to increased production of free radical species in the cochlea, necrosis and apoptosis of sensory hair cells, reduction in endocochlear potential and damage to cellular structures in both the organ of Corti and stria vascularis (22). It has been suggested that free radical stress instigates the

observed cochlear pathology in NIHL. This hypothesis is supported by studies in animal models that successfully demonstrate protection against NIHL by antioxidant treatment (42). Apart from NIHL, free radical stress has been shown to be involved in the mechanisms of hearing loss due to drug-induced ototoxicity and aging (51). In both drug-induced ototoxicity (from drugs like aminoglycosides or cisplatin) and aging, the primarily affected tissues are either sensory hair cells or stria vascularis. Further, antioxidant treatment has also been shown to ameliorate aminoglycoside and cisplatin-induced ototoxicity (50; 52).

Neonatal hypothyroidism: Thyroid hormones are critical for cochlear development, and the lack of thyroid hormone due to either genetic or environmental factors during prenatal and early postnatal development leads to deafness (28; 58). Cochlear sensitivity to thyroid hormone is demonstrated by the fact that maturation of sensory cell-containing organ of Corti is dependent on the availability of thyroid hormone (66). Moreover, the tectorial membrane is distended during hypothyroidism in mice and the levels of tectorial membrane-specific protein Tectb are altered, indicating a role of extracellular matrix in the pathophysiology of deafness (28). In this context, it is important to note that loss of another tectorial membrane-specific protein, TECTA, leads to deafness in humans (40). The impact of thyroid hormone deficiency in the cochlea is not limited to the organ of Corti region. Studies show loss of endocochlear potential, loss of Na^+-K^+ ATPase in stria vascularis and degeneration of stria vascularis under thyroid hormone deficiency (39; 73)

Menière's disease: The symptoms of this disease include fluctuating hearing loss, vertigo, tinnitus and sensation of fullness in the ear (38). The cause of Menière's disease is unknown, but emotional as well as physical stress is known to trigger the episodic attacks of vertigo and hearing loss in affected persons (57; 63). Menière's disease patients consistently show enlargement of the endolymphatic space, leading to the distention of Reissner's membrane (44). The speculated origins of Menière's disease include: disturbed fluid homeostasis of the endolymph, oxidative stress, hair cell apoptosis, autoimmunity and excitotoxicity (55).

Tremendous progress has been made toward understanding the causes and pathologies for various types of sensorineural hearing loss. However, we numerous genes (eg.,: OTOA,

DFNA5) associated with deafness remain incompletely understood due in part to the lack of adequate models. As a result, their role in the cochlea remains undefined. (19).

Pendred syndrome

Pendred syndrome was first described by Dr. Vaughn Pendred in 1896 (45). It is an autosomal recessive disease that affects the inner ear and the thyroid and is caused by loss-of-function mutations in an anion exchanger, pendrin, (*SLC26A4*) (15).

Clinical features

The clinical features of Pendred syndrome include deafness, enlarged vestibular aqueduct, goiter and positive perchlorate discharge test (8). Hearing loss, the most consistent pathology of Pendred syndrome, can either be manifested at birth or can develop progressively, affecting most patients prelingually (8; 61). In a few cases, hearing loss was documented to have been triggered by a slight head injury or mild infection (35). In contrast to deafness, the thyroid pathology in Pendred syndrome is variable in nature. Goiter affects most patients after puberty and can be either hypothyroid or euthyroid. Clinical tests to evaluate thyroid function include measurement of triiodothyronine (T3), thyroxine (T4) and thyroid stimulating hormone (TSH). Patients with Pendred syndrome generally show serum TSH, T4 and T3 within normal ranges. However, affected members of a family have significantly higher levels of TSH and T3/T4 ratio in the serum and significantly lower levels of serum T4 when compared to their unaffected siblings (56). Increased levels of serum thyroglobulin have also been reported in patients with Pendred syndrome, suggesting that the integrity of the thyroid epithelium may be compromised (56). Although Pendred syndrome patients do not have overt balance problems, detailed testing in a few clinical studies has revealed vestibular defects (61).

Animal models

Investigations of the mechanisms involved in the etiology of Pendred syndrome have been greatly assisted by the creation of a mouse model. Wild-type mice as well as *Slc26a4*$^{+/-}$ mice begin hearing at postnatal day 12 (P12) (31; 69). The *Slc26a4*$^{+/-}$ mice show no symptoms of vestibular dysfunction and were used in our study as controls. However, *Slc26a4*$^{-/-}$ mice never

develop hearing and display severe symptoms of vestibular dysfunction by 3 weeks of age (14; 69). Studies on adult $Slc26a4^{-/-}$ mice have not revealed any thyroid pathology (14). The loss of endocochlear potential has been suggested as the primary cause of deafness in the Pendred syndrome mouse model (68).

Stria vascularis and endocochlear potential

The stria vascularis is a double-layered epithelium consisting of marginal cells, intermediate cells and basal cells. Tight junctions in the marginal cell layer form the barrier between the endolymph and the intrastrial fluid, whereas the tight junctions of the basal cell layer form the barrier between the intrastrial fluid and the extracellular fluid in the spiral ligament (Fig. 1.3). Gap junctions connect basal cells to the spiral ligament fibrocytes and the intermediate cells in the stria vascularis. The tight junctions in both layers of the epithelium isolate the stria vascularis from the surrounding tissue. This double-layered system is required for the generation and maintainence of the endocochlear potential, since the vestibular system, which has only a single marginal cell layer, fails to produce an endovestibular potential.

The endocochlear potential is created by a very low K^+ concentration (~1.3 mM) in the intrastrial fluid and a high K^+ concentration in the cytosol of the intermediate cells. The marginal cells contribute to the formation of endocochlear potential by pumping K^+ from the interstrial space into scala media, thereby maintaining low K^+ in the intrastrial fluid. Basal cells help in the generation of endocochlear potential by providing K^+ to the intermediate cells {reviewed in (67)}.

The K^+ channel Kcnj10 is expressed in the intermediate cells of stria vascularis and is necessary for the generation of the endocochlear potential. The indispensable role of Kcnj10 in the development of endocochlear potential is evident from the observation that $Kcnj10^{-/-}$ mice fail to develop an endocochlear potential (37).

Pendrin expression and function

Pendrin is primarily expressed in the inner ear, thyroid and kidney (16; 48; 49). *Slc26a4* mRNA expression has also been shown in the mammary gland, testes, endometrium and placenta

(4; 32; 47; 62). In heterologous expression systems, pendrin has been characterized as an anion exchanger capable of transporting Cl^-, HCO_3^-, I^-, and formate (53; 54; 59).

Pendrin in the inner ear

Pendrin expression has been shown in the cochlea, the vestibular labyrinth and the endolymphatic sac (16). In the cochlea, pendrin is expressed in the outer sulcus cells, root cells, spiral prominence epithelium and the spindle cells of stria vascularis (Fig. 1.3A) (68). The absence of pendrin leads to a more acidic endolymph in the Pendred syndrome mouse model, suggesting a role of pendrin in bicarbonate secretion and cochlear pH homeostasis (69). Pendrin is reportedly involved in bicarbonate transport in the renal collecting duct (49), which supports the hypothesis that pendrin contributes to the cochlea pH regulation.

Although normal K^+ concentration has been observed in the endolymph of adult *Slc26a4$^{-/-}$* mice, the endolymphatic spaces were enlarged prenatally, suggesting an increased rate of K^+ secretion from the stria vascularis (14; 68). Further, the endocochlear potential that is generated by stria vascularis and is required for the sensitivity of hearing is progressively lost in *Slc26a4$^{-/-}$* mice (69). In the stria vascularis, Kcnj10 protein expression is greatly reduced at P15 (69) (Fig. 1.3B). Although pendrin is only marginally expressed in stria vascularis, the cochlear pathology in *Slc26a4$^{-/-}$* mice indicates that the loss of stria vascularis function may underly deafness in the Pendred syndrome mouse model. However, the mechanism by which loss of pendrin can affect Kcnj10 protein expression in stria vascularis and thereby endocochlear potential has not yet been established.
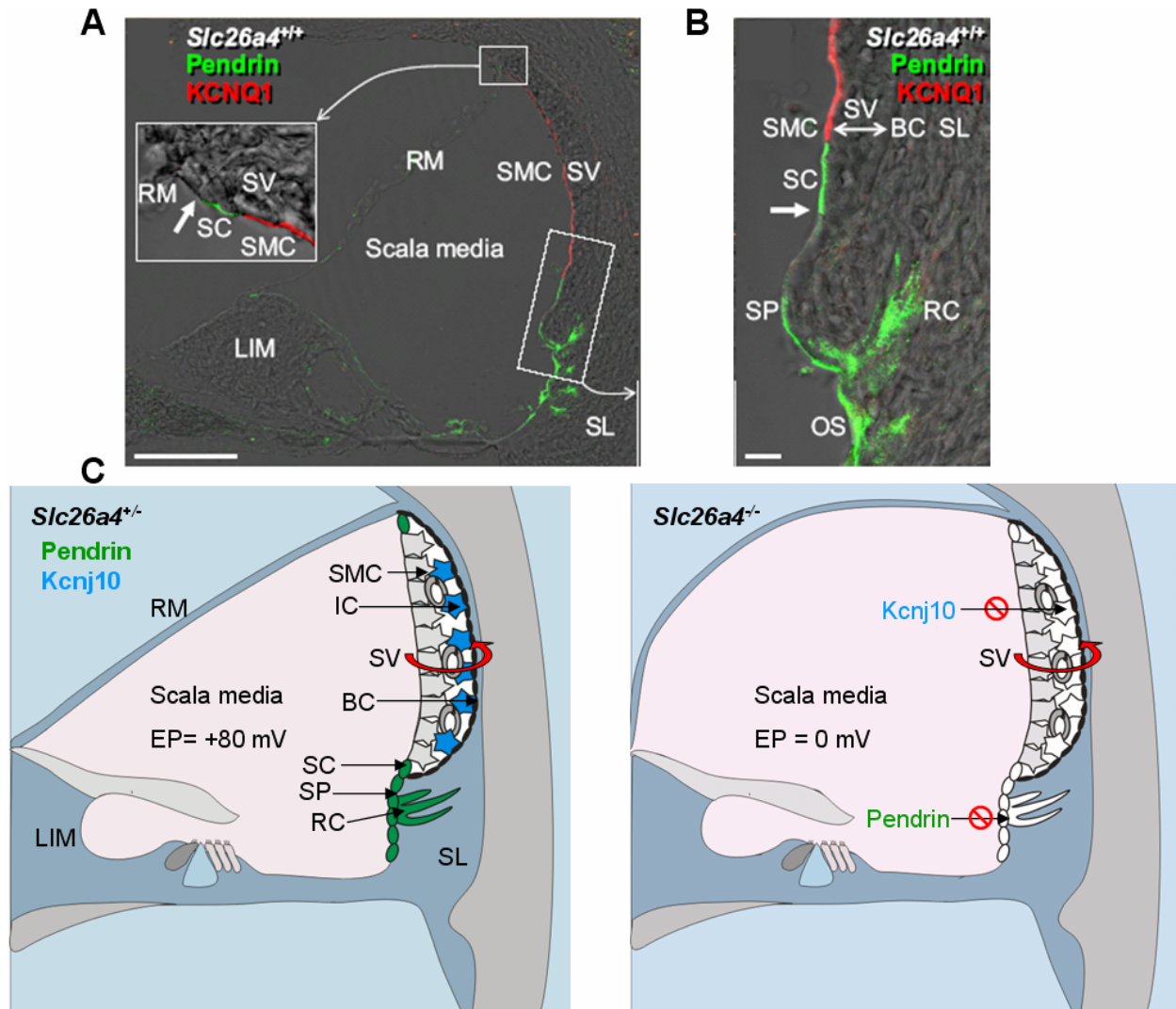
Figure 1.3: Localization of pendrin and Kcnj10 *in Slc26a4$^{+/-}$* and *Slc26a4$^{-/-}$ mice.*

A, B) Pendrin expression in the cochlea. Pendrin is mainly expressed in spiral prominence epithelial cells (SP), root cells (RC) and in outer sulcus epithelial cells (OS) and spindle cells (SC) (green). Figure was adapted from Wangemann et al., 2004. C) Kcnj10 protein expression is lost in the cochlea of Slc26a4$^{-/-}$ mice. Schematic diagram showing the different cellular localization of pendrin (green) and Kcnj10 (blue) in the cochlea of Slc26a4$^{+/-}$ mice (left). In the Slc26a4$^{-/-}$ mice that lack pendrin, expression of Kcnj10 is lost in the stria vascularis (right). Moreover, the Slc26a4$^{-/-}$ mice have an enlarged endolymphatic space and no endocochlear potential. Also note that in the stria vascularis (SV), the strial marginal cells (SMC) and the basal cell (BC) are interconnected between themselves by tight junctions thereby forming two barriers. (Other abbreviations used in the figure: LIM: Spiral limbus, RM: Reissner's membrane, SL: Spiral ligament)

Pendrin in the thyroid

In the thyroid, pendrin is expressed in the apical membrane of thyrocytes (5). Pendrin has been shown to mediate iodide efflux *in vitro* in mammalian cells (71). Iodide organification defects observed in patients with Pendred syndrome strongly suggest that pendrin is the apical iodide transporter in the thyroid (48). A schematic diagram depicting organification of iodide in the thyroid gland is shown (Fig. 1.4). However, the thyroid likely has alternative pathways for apical iodide transport, since the absence of pendrin leads to only partial defects in iodide organification. In adult mice, no differences in the serum T3, T4 and TSH levels were observed between $Slc26a4^{+/+}$ and $Slc26a4^{-/-}$ mice, indicating that pendrin is not necessary for thyroid hormone production (14).
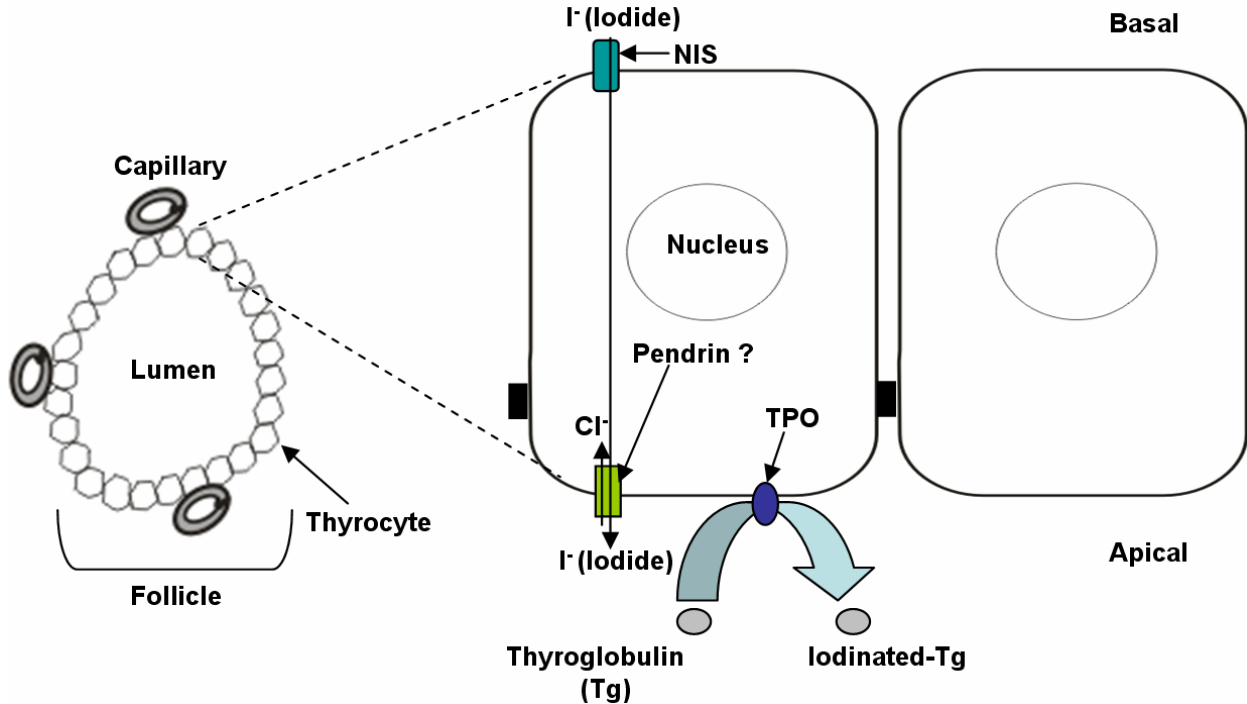
Figure 1.4: Schematic diagram showing iodide organification in the thyroid.
Pendrin is expressed in the apical membrane of the thyroid follicular cells and may be the apical iodide efflux pathway. (Note: TPO indicates the thyroid peroxidase).

Thyroid gland function

The thyroid consists of two lobes that are located on either side of the trachea. The functional unit of the thyroid gland and site of production of thyroid hormone is the follicle, a protein-rich colloid (predominantly made up of thyroglobulin) surrounded by follicular cells.

The process of thyroid hormone production is shown in Fig. 1.4 and Fig. 1.5. Iodide is taken up from the blood into the follicular cells of the thyroid gland by the basolatarally located transporter, Na^+/I^- symporter, NIS. Iodide is then transported across the apical membrane of the follicular cell by a yet-to-be-identified transporter (pendrin is a candidate protein for this role). At the apical membrane of the follicular cells, iodide is oxidized by hydrogen peroxide, H_2O_2, in a reaction that is catalyzed by the thyroid peroxidase (*Tpo*). Oxidation of iodide leads to the formation of various intermediate species: hypoiodate (OI^-), hypoiodous acid (HOI) or iodinium (I^+). These species are incorporated into the tyrosine residues of the thyroid hormone precursor thyroglobulin to form mono-iodotyrosine (MIT) and di-iodotyrosine (DIT). The MIT and DIT thyroglobulin complexes are taken up into the colloid where T4 thyroglobulin and T3 thyroglobulin complexes are formed. The major coupling reaction is between two DIT molecules, which combine to form the T4 thyroglobulin complex. Coupling can also take place between a DIT and a MIT molecule to form the T3 thyroglobulin complex. The T3 and T4 thyroglobulin complexes are taken up into the follicular cells by pinocytosis. Within the follicular cells, hydrolysis of T3 and T4 thyroglobulin complexes in the lysosomes releases unbound T3 and T4. A small amount of T4 is further converted into T3 in the follicular cells by the action of cellular deiodinases (*Dio1* and *Dio2*). Finally, the thyroid hormones (T3 and T4) are released into the blood.

The primary form of thyroid hormone produced and secreted by the thyroid gland is T4 whereas the biologically active form of thyroid hormone that is utilized in cells is T3. Target cell membranes have thyroid hormone transporters that mediate the cellular uptake of thyroid hormone from the blood (Fig. 1.5). Once within the cell cytosol, T4 is converted by the cellular enzymes *Dio1* and *Dio2* to T3, which is the the biologically active form of thyroid hormone (T3) (3; 24; 70).

14
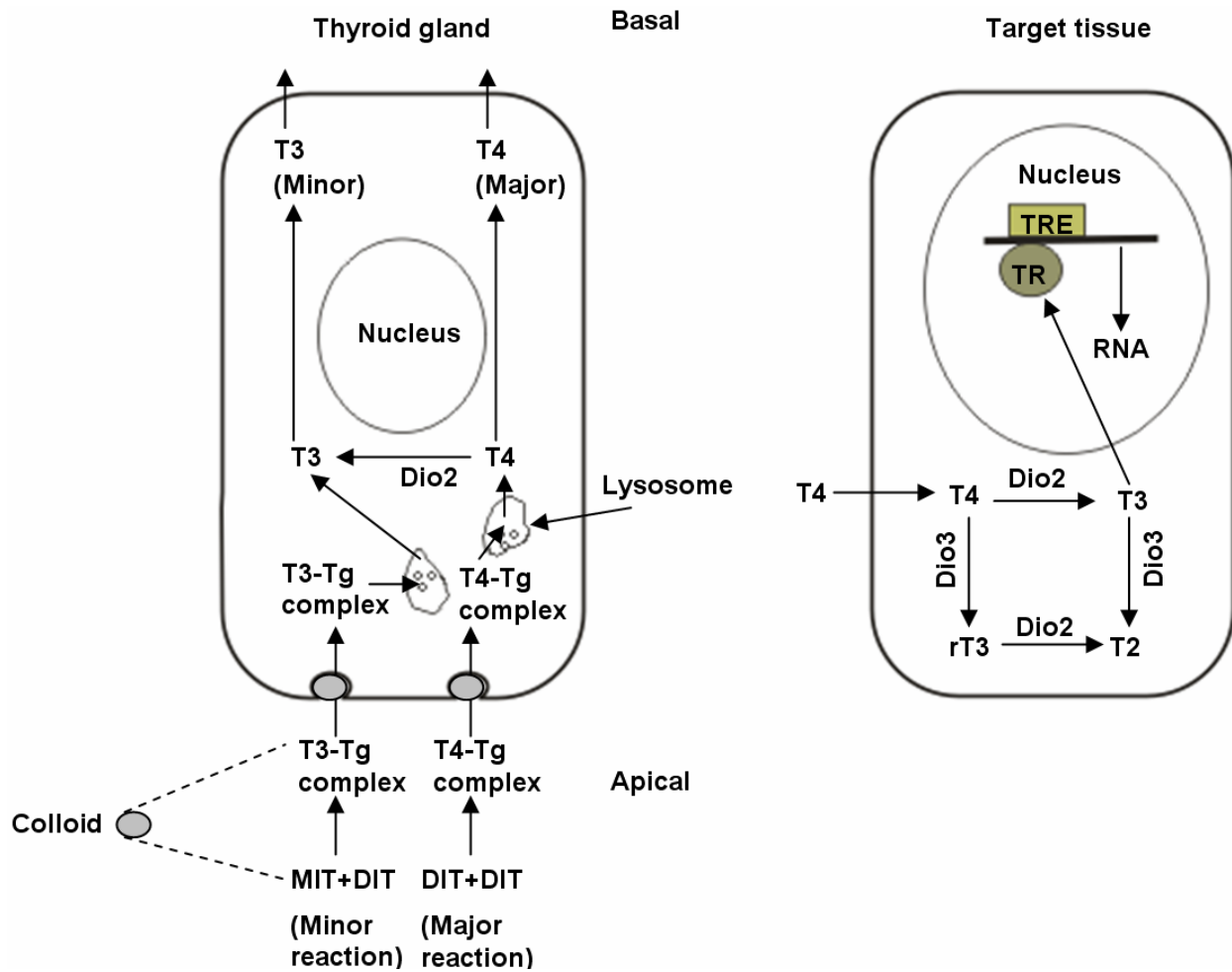
Figure 1.5: Schematic diagram showing production, secretion and cellular metabolism of thyroid hormone.
Left: *The thyroid hormones, T4 and T3, are produced in the follicular cells of the thyroid gland and released into the blood. **Right**: T4 is taken up by a cell within the target tissue and converted to the biologically active form, T3. (Abbreviations used: DIT, diiodotyrosine, MIT: monoiodotyrosine, Tg: thyroglobulin, TRE: thyroid hormone responsive element, TR: thyroid hormone receptor)*

The metabolic activity of virtually every cell in the body is governed by thyroid hormones. Thus, the strict control of their production and availability is indispensable to body function. The maturation and development of a number of tissues, including the cochlea, requires thyroid hormones during a specific time frame. In rats, the crucial time period in which the cochlea is sensitive to thyroid hormone begins embryonically with the onset of thyroid gland function at embryonic day 17 (~ E17) and continues until the onset of hearing at ~P12. Unlike hypothyroidism acquired in adulthood, the symptoms of which are reversible after treatment, the

lack of thyroid hormone during early development results in permanent deafness. Correcting thyroid hormone levels after the period of thyroid hormone sensitivity does not restore hearing (11; 66).

The production and secretion of thyroid hormone by the thyroid gland varies during development. In the mouse, the levels of T4 in the serum peak between P10 and P15, then decrease gradually until P21 (weaning) before peaking again to reach adult levels around puberty (6).

While evaluating thyroid gland function in Pendred syndrome, it would be important to consider the time points of maximal thyroid hormone requirement in the cochlea and the time points of maximal thyroid hormone production by the thyroid gland. It is possible that the absence of pendrin during developmentally critical time points leads to transient hypothyroidism in the Pendred syndrome mouse model.

Free radical stress

Free radicals are highly reactive molecules due to the presence of an unpaired electron. The term 'free radical stress' refers to levels of reactive oxygen and nitrogen species, either radicals or non-radicals, in excess of those compatible with health. The majority of free radical production occurs during mitochondrial energy metabolism. Free radicals have important functions under physiological conditions. They can act as cell signaling molecules. Macrophages and phagocytes utilize free radicals to defend against bacterial invasion. In health, a balance exists between the production of free radicals and their removal by antioxidant defenses. In disease, either the level of production of free radicals is increased or the function of the antioxidant defense system is compromised. Either disruption thus leads to elevated levels of free radicals and free radical stress {reviewed in (13)}.

Free radical stress can be extremely damaging to tissues. Free radicals can promote tissue injury, inflammation and increased cellular death, each of which in turn can increase the production of free radicals. Left uncontrolled, a vicious circle that can lead to tissue destruction results (72). As mentioned previously in the section on inner ear disease mechanisms, free radical stress has been implicated as the cause of hearing loss in drug-induced ototoxicity and

noise-induced hearing loss. Increased levels of reactive oxygen species have also been linked to the pathology of thyroid tumorigenesis and goiter formation (22; 30; 52; 26). Moreover, oxidative stress has been associated with reduced Kcnj10 expression in other systems including ischemia-reperfusion injury to the retina and spinal cord of SOD1-G93A mutant mice (23; 25). It is concievable that loss of pendrin leads to increased oxidative stress in the stria vascularis and the thyroid. Furthermore, increased levels of free radical stress in stria vascularis of $Slc26a4^{-/-}$ mice could be responsible for the observed loss of Kcnj10 protein expression (Fig. 1.3B).

Gene array

The development of the gene array technology has provided scientists with the ability to study the concurrent expression of a large number of genes in a genome at the same time. The evaluation of differential gene expression between stria vascularis of $Slc26a4^{+/-}$ and $Slc26a4^{-/-}$ mice would facilitate identification of the biochemical pathway that leads to hearing loss in Pendred syndrome.

A typical gene array platform (gene chip) consists of cDNA or gene-specific oligonucleotides attached in extremely high density to a glass microscope slide or silicon wafer. cRNA or cDNA from a sample is hybridized on the chip and the amount of cDNA bound to each oligonucleotide probe is evaluated. The amount of binding detected is taken as representative of the level of gene expression in the original sample. Tissue samples that are obtained by microdissection (example: stria vascularis and mouse thyroid), laser capture microscopy and needle biopsy do not yield sufficient RNA to be used directly in a gene array experiment. RNA amplification methods are generally used for producing microgram amounts of RNA from these samples before they are hybridized on the gene chip. The quality of the starting RNA and the reliability of the amplification method in truly representing the original sample determine the quality of the gene array data.

Current study

To understand the etiology of Pendred syndrome in a mouse model we took the following 3 experimental approaches (illustrated in Fig. 1.6 and Fig. 1.8):

1) Different RNA amplification methods were evaluated for application in gene array analyses. The ability to obtain robust amplification of array-caliber RNA from nanogram amounts of starting material allowed the production of gene arrays yielding excellent data quality. Gene arrays were performed on RNA isolated from stria vascularis of $Slc26a4^{+/-}$ and $Slc26a4^{-/-}$ mice before the onset of hearing at P10 as well from stria vascularis of $Slc26a4^{+/-}$ and $Slc26a4^{-/-}$ adult mice. The data obtained from the gene array experiments were submitted to the Gene Expression Omnibus (GEO) database (GSE10587 and GSE4749). Analogous analyses were also carried out on thyroid gene arrays obtained from $Slc26a4^{+/-}$ and $Slc26a4^{-/-}$ mice at P15, the time of maximal thyroid gland activity (GSE10589). Gene expression changes were evaluated between the stria vascularis and thyroid of $Slc26a4^{+/-}$ and $Slc26a4^{-/-}$ mice and the results were used to guide further studies.
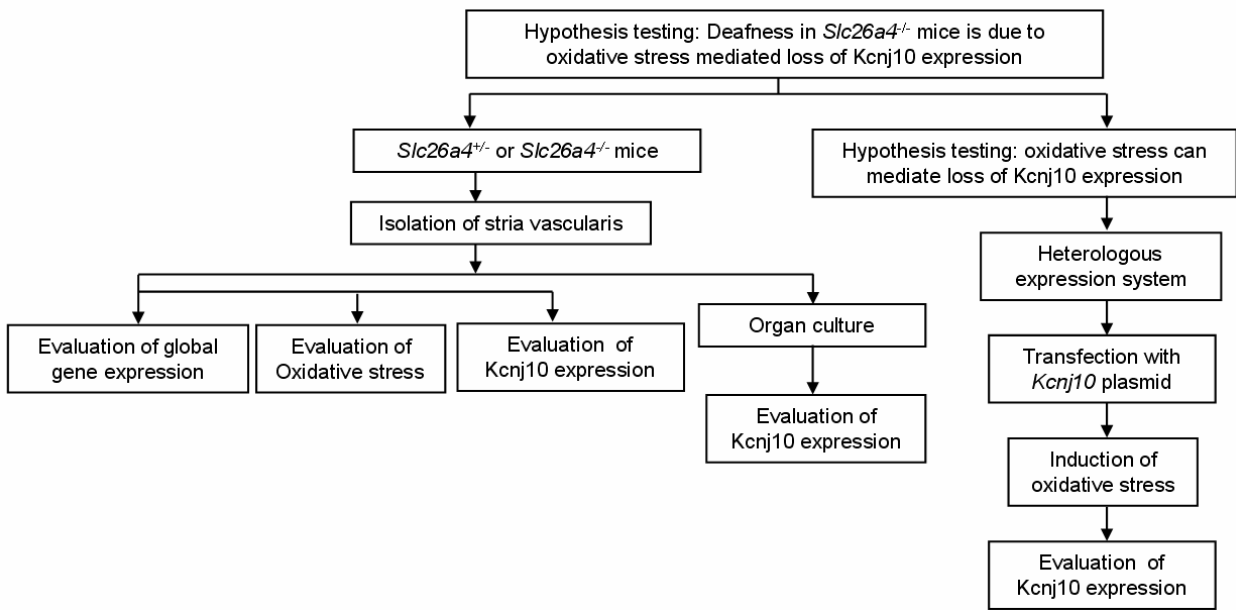
Figure 1.6: Flow chart illustrating the experimental approach used to evaluate a cause of deafness in Pendred syndrome mouse model.

2) Markers of free radical stress were compared between the stria vascularis of $Slc26a4^{+/-}$ and $Slc26a4^{-/-}$ mice in a developmental study of the following ages: P10 (before the onset of hearing), P15 (after the onset of hearing), P35 (adolescence) and P80 (young adults). The levels of Kcnj10 protein expression were compared between P10 and P15 in $Slc26a4^{+/-}$ and $Slc26a4^{-/-}$ mice to correlate the levels of Kcnj10 protein with the onset of hearing. We also

investigated the ability of free radical stress-inducing agents to modulate the expression of Kcnj10 protein in organ cultures of stria vascularis and in a heterologous expression system.

Because pendrin and Kcnj10 are expressed in different cells (Fig. 1.3), the decreased expression of the latter can not be the direct result of the lack of pendrin. A previous study from our laboratory demonstrated an increased pigmentation in the stria vascularis of adult *Slc26a4*$^{-/-}$ mice, suggesting free radical stress. In our present data from gene arrays on mouse stria vascularis, we found increased levels of *Trf* expression and decreased levels of *Tfrc* expression which is consistent with the presence of iron-mediated oxidative stress in the stria vascularis of *Slc26a4*$^{-/-}$ mice.

The enlarged endolymph in the *Slc26a4*$^{-/-}$ mice maintains the typical K$^+$ concentration. This might require increased rate of K$^+$ secretion from stria vascularis. An increased rate of ion transport has been correlated with energy metabolism in the stria vascularis (36). Higher metabolism could serve as a source of free radical stress. Free radical stress could also be a consequence of reduced intracellular pH of strial marginal cells, an implicit consequence of endolymph acidification. In *Slc26a4*$^{-/-}$ mice, increased oxidative stress could diminish Kcnj10 expression and thereby dissipate the endocochlear potential, resulting in deafness. We hypothesized that free radical stress could link the absence of pendrin with the loss of Kcnj10 in the Pendred syndrome mouse model (Fig. 1.7).
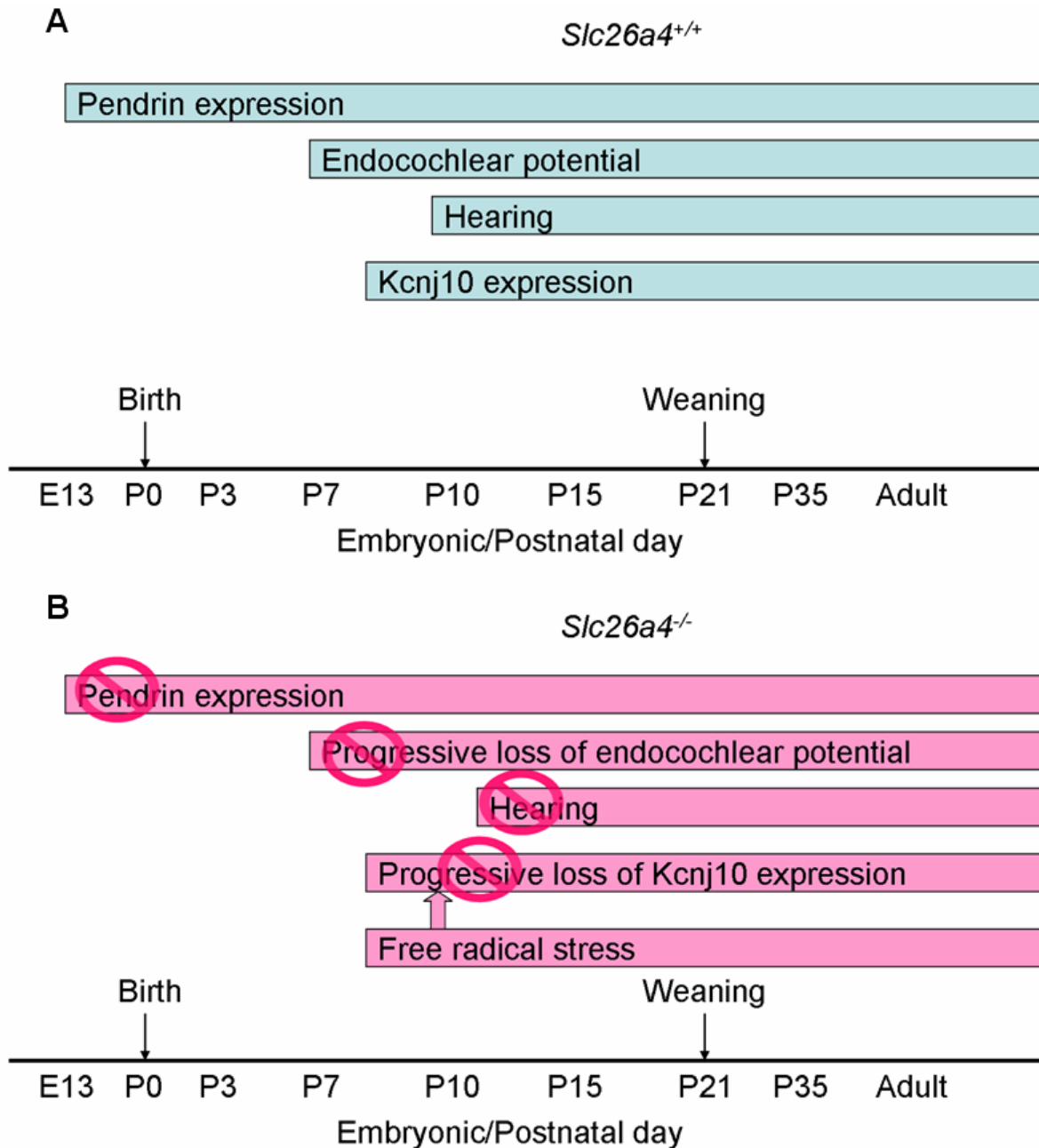
Figure 1.7: Hypothesis
A graphical depiction of the sequence of events in the cochlea during development of A) Slc26a4^{+/+} mice and B) Slc26a4^{-/-} mice. Pendrin expression that begins at embryonic day 13 (E13) in Slc26a4^{+/+} mice is absent in Slc26a4^{-/-} mice. Development of endochlear potential and Kcnj10 expression does not parallel the wild-type mice and is progressively lost before the onset of hearing at P12 . The Slc26a4^{-/-} mice never develop hearing. We hypothesize that increased free radical stress in the stria vascularis depicted in B leads to loss of Kcnj10 protein expression and consequently leads to the failure of maintainence of endocochlear potential. In the absence of endocochlear potential Slc26a4^{-/-} mice are deaf.

3) To determine whether transient systemic hypothyroidism was present in *Slc26a4*$^{-/-}$ mice, the serum T4 levels were measured at various ages and the expression of genes involved in thyroid hormone synthesis were evaluated. In order to know if pendrin expression in the thyroid is correlated to the serum T4 levels, particularly during the adolescent peak in serum T4 levels around P15, we performed a developmental study on thyroids from *Slc26a4*$^{+/-}$ mice. Furthermore, certain markers of free radical stress were compared between the thyroids of *Slc26a4*$^{+/-}$ and *Slc26a4*$^{-/-}$ mice (Fig. 1.8).

Everett and co-workers reported normal thyroid gland function and histology in adult *Slc26a4*$^{-/-}$ mice. However, the thyroid gland activity in mice peaks at approximately P15, raising the possibility of transient hypothyroidism early in development. Moreover, the fact that thyroid hormone synthesis requires the production of H_2O_2, a reactive oxygen species, taken together with our measurements indicating increased levels of free radical stress in the stria vascularis, led us to test for the presence of oxidative stress in the thyroid of *Slc26a4*$^{-/-}$ mice.
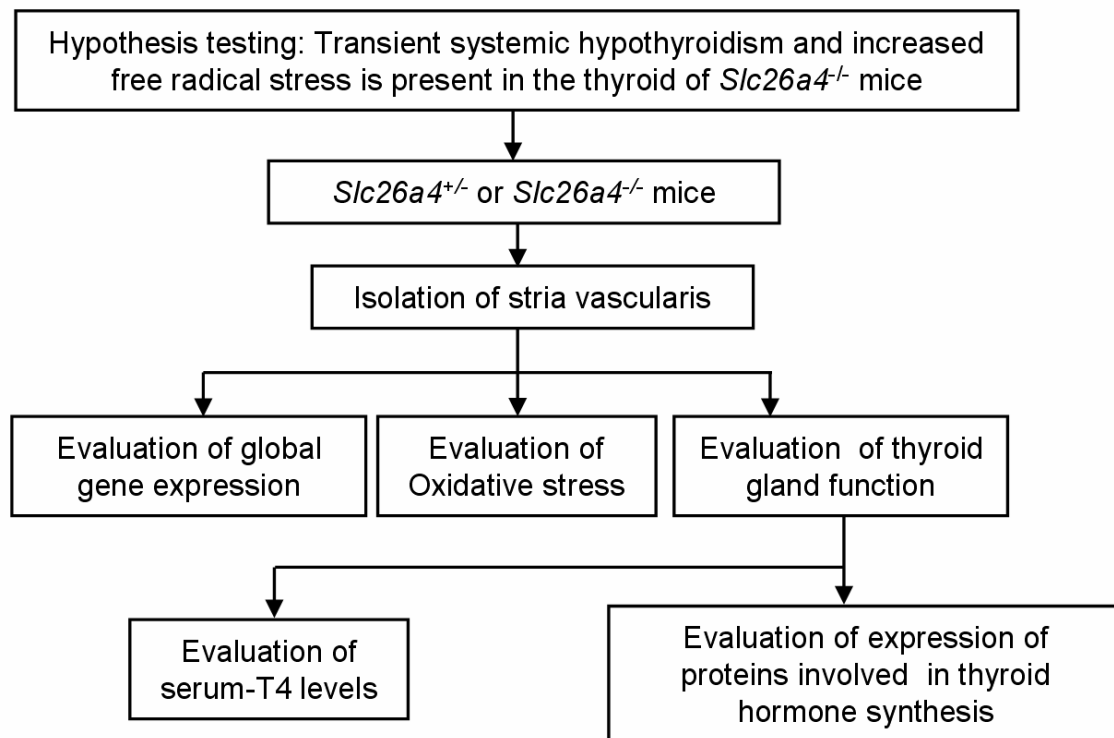
Figure 1.8: Flow chart illustrating the experimental approach used to evaluate the thyroid pathology in the Pendred syndrome mouse model.

References

1. **Ahmad S, Chen S, Sun J and Lin X**. Connexins 26 and 30 are co-assembled to form gap junctions in the cochlea of mice. *Biochem Biophys Res Commun* 307: 362-368, 2003.

2. **Ahmed ZM, Riazuddin S, Riazuddin S and Wilcox ER**. The molecular genetics of Usher syndrome. *Clin Genet* 63: 431-444, 2003.

3. **Bianco AC, Salvatore D, Gereben B, Berry MJ and Larsen PR**. Biochemistry, cellular and molecular biology, and physiological roles of the iodothyronine selenodeiodinases. *Endocr Rev* 23: 38-89, 2002.

4. **Bidart JM, Lacroix L, Evain-Brion D, Caillou B, Lazar V, Frydman R, Bellet D, Filetti S and Schlumberger M**. Expression of Na^+/I^- symporter and Pendred syndrome genes in trophoblast cells. *J Clin Endocrinol Metab* 85: 4367-4372, 2000.

5. **Bidart JM, Mian C, Lazar V, Russo D, Filetti S, Caillou B and Schlumberger M**. Expression of pendrin and the Pendred syndrome (*PDS*) gene in human thyroid tissues. *J Clin Endocrinol Metab* 85: 2028-2033, 2000.

6. **Campos-Barros A, Amma LL, Faris JS, Shailam R, Kelley MW and Forrest D**. Type 2 iodothyronine deiodinase expression in the cochlea before the onset of hearing. *Proc Natl Acad Sci U S A* 97: 1287-1292, 2000.

7. **Cohen-Salmon M, Ott T, Michel V, Hardelin JP, Perfettini I, Eybalin M, Wu T, Marcus DC, Wangemann P, Willecke K and Petit C**. Targeted ablation of connexin26 in the inner ear epithelial gap junction network causes hearing impairment and cell death. *Curr Biol* 12: 1106-1111, 2002.

8. **Cremers CW, Admiraal RJ, Huygen PL, Bolder C, Everett LA, Joosten FB, Green ED, van Camp G and Otten BJ**. Progressive hearing loss, hypoplasia of the cochlea and widened vestibular aqueducts are very common features in Pendred's syndrome. *Int J Pediatr Otorhinolaryngol* 45: 113-123, 1998.

9. **Daniel E**. Noise and hearing loss: a review. *J Sch Health* 77: 225-231, 2007.

10. **Del C, I, Moreno-Pelayo MA, Del Castillo FJ, Brownstein Z, Marlin S, Adina Q, Cockburn DJ, Pandya A, Siemering KR, Chamberlin GP, Ballana E, Wuyts W, Maciel-Guerra AT, Alvarez A, Villamar M, Shohat M, Abeliovich D, Dahl HH, Estivill X, Gasparini P, Hutchin T, Nance WE, Sartorato EL, Smith RJ, van Camp G, Avraham KB, Petit C and Moreno F**. Prevalence and evolutionary origins of the del(GJB6-D13S1830) mutation in the *DFNB1* locus in hearing-impaired subjects: a multicenter study. *Am J Hum Genet* 73: 1452-1458, 2003.

11. **Deol MS**. An experimental approach to the understanding and treatment of hereditary syndromes with congenital deafness and hypothyroidism. *J Med Genet* 10: 235-242, 1973.

12. **El Amraoui A and Petit C**. Usher I syndrome: unravelling the mechanisms that underlie the cohesion of the growing hair bundle in inner ear sensory cells. *J Cell Sci* 118: 4593-4603, 2005.

13. **Evans P and Halliwell B**. Free radicals and hearing. Cause, consequence, and criteria. *Ann N Y Acad Sci* 884: 19-40, 1999.

14. **Everett LA, Belyantseva IA, Noben-Trauth K, Cantos R, Chen A, Thakkar SI, Hoogstraten-Miller SL, Kachar B, Wu DK and Green ED**. Targeted disruption of mouse *Pds* provides insight about the inner-ear defects encountered in Pendred syndrome. *Hum Mol Genet* 10: 153-161, 2001.

15. **Everett LA, Glaser B, Beck JC, Idol JR, Buchs A, Heyman M, Adawi F, Hazani E, Nassir E, Baxevanis AD, Sheffield VC and Green ED**. Pendred syndrome is caused by mutations in a putative sulphate transporter gene (*PDS*). *Nat Genet* 17: 411-422, 1997.

16. **Everett LA, Morsli H, Wu DK and Green ED**. Expression pattern of the mouse ortholog of the Pendred's syndrome gene (*Pds*) suggests a key role for pendrin in the inner ear. *Proc Natl Acad Sci U S A* 96: 9727-9732, 1999.

17. **Fischel-Ghodsian N**. Genetic factors in aminoglycoside toxicity. *Ann N Y Acad Sci* 884: 99-109, 1999.

18. **Fowler KB and Boppana SB**. Congenital cytomegalovirus (CMV) infection and hearing deficit. *J Clin Virol* 35: 226-231, 2006.

19. **Friedman LM, Dror AA and Avraham KB**. Mouse models to study inner ear development and hereditary hearing loss. *Int J Dev Biol* 51: 609-631, 2007.

20. **Fuente A and McPherson B**. Organic solvents and hearing loss: The challenge for audiology. *Int J Audiol* 45: 367-381, 2006.

21. **Gratton MA and Vazquez AE**. Age-related hearing loss: current research. *Curr Opin Otolaryngol Head Neck Surg* 11: 367-371, 2003.

22. **Henderson D, Bielefeld EC, Harris KC and Hu BH**. The role of oxidative stress in noise-induced hearing loss. *Ear Hear* 27: 1-19, 2006.

23. **Iandiev I, Tenckhoff S, Pannicke T, Biedermann B, Hollborn M, Wiedemann P, Reichenbach A and Bringmann A**. Differential regulation of Kir4.1 and Kir2.1 expression in the ischemic rat retina. *Neurosci Lett* 396: 97-101, 2006.

24. **Jansen J, Friesema EC, Milici C and Visser TJ**. Thyroid hormone transporters in health and disease. *Thyroid* 15: 757-768, 2005.

25. **Kaiser M, Maletzki I, Hulsmann S, Holtmann B, Schulz-Schaeffer W, Kirchhoff F, Bahr M and Neusch C**. Progressive loss of a glial potassium channel (KCNJ10) in the spinal cord of the SOD1 (G93A) transgenic mouse model of amyotrophic lateral sclerosis. *J Neurochem* 99: 900-912, 2006.

26. **Karbownik M and Lewinski A**. The role of oxidative stress in physiological and pathological processes in the thyroid gland; possible involvement in pineal-thyroid interactions. *Neuro Endocrinol Lett* 24: 293-303, 2003.

27. **Kelsell DP, Dunlop J, Stevens HP, Lench NJ, Liang JN, Parry G, Mueller RF and Leigh IM**. Connexin 26 mutations in hereditary non-syndromic sensorineural deafness. *Nature* 387: 80-83, 1997.

28. **Knipper M, Richardson G, Mack A, Muller M, Goodyear R, Limberger A, Rohbock K, Kopschall I, Zenner HP and Zimmermann U**. Thyroid hormone-deficient period prior to the onset of hearing is associated with reduced levels of beta-tectorin protein in the tectorial membrane: implication for hearing loss. *J Biol Chem* 276: 39046-39052, 2001.

29. **Kremer H, van Wijk E, Marker T, Wolfrum U and Roepman R**. Usher syndrome: molecular links of pathogenesis, proteins and pathways. *Hum Mol Genet* 15 Spec No 2: R262-R270, 2006.

30. **Krohn K, Maier J and Paschke R**. Mechanisms of disease: hydrogen peroxide, DNA damage and mutagenesis in the development of thyroid tumors. *Nat Clin Pract Endocrinol Metab* 3: 713-720, 2007.

31. **Kros CJ, Ruppersberg JP and Rusch A**. Expression of a potassium current in inner hair cells during development of hearing in mice. *Nature* 394: 281-284, 1998.

32. **Lacroix L, Mian C, Caillou B, Talbot M, Filetti S, Schlumberger M and Bidart JM**. Na(+)/I(-) symporter and Pendred syndrome gene and protein expressions in human extra-thyroidal tissues. *Eur J Endocrinol* 144: 297-302, 2001.

33. **Lautermann J, ten Cate WJ, Altenhoff P, Grummer R, Traub O, Frank H, Jahnke K and Winterhager E**. Expression of the gap-junction connexins 26 and 30 in the rat cochlea. *Cell Tissue Res* 294: 415-420, 1998.

34. **Low WK, Pang KY, Ho LY, Lim SB and Joseph R**. Universal newborn hearing screening in Singapore: the need, implementation and challenges. *Ann Acad Med Singapore* 34: 301-306, 2005.

35. **Luxon LM, Cohen M, Coffey RA, Phelps PD, Britton KE, Jan H, Trembath RC and Reardon W**. Neuro-otological findings in Pendred syndrome. *Int J Audiol* 42: 82-88, 2003.

36. **Marcus DC, Thalmann R and Marcus NY**. Respiratory rate and ATP content of stria vascularis of guinea pig in vitro. *Laryngoscope* 88: 1825-1835, 1978.

37. **Marcus DC, Wu T, Wangemann P and Kofuji P**. KCNJ10 (*Kir4.1*) potassium channel knockout abolishes endocochlear potential. *Am J Physiol Cell Physiol* 282: C403-C407, 2002.

38. **Ménière P**. Mémoire sur des lésions de l'orielle interne donnant lieu à des symptômes de cogestion cérébrale apoplectiforme. *Gaz Med Paris* 16: 597-601, 1861.

39. **Meyerhoff WL**. Hypothyroidism and the ear: electrophysiological, morphological, and chemical considerations. *Laryngoscope* 89: 1-25, 1979.

40. **Mustapha M, Weil D, Chardenoux S, Elias S, El Zir E, Beckmann JS, Loiselet J and Petit C**. An alpha-tectorin gene defect causes a newly identified autosomal recessive form of sensorineural pre-lingual non-syndromic deafness, DFNB21. *Hum Mol Genet* 8: 409-412, 1999.

41. **O'Malley BW, Jr., Li D and Turner DS**. Hearing loss and cochlear abnormalities in the congenital hypothyroid (hyt/hyt) mouse. *Hear Res* 88: 181-189, 1995.

42. **Ohinata Y, Yamasoba T, Schacht J and Miller JM**. Glutathione limits noise-induced hearing loss. *Hear Res* 146: 28-34, 2000.

43. **Ohlemiller KK**. Contributions of mouse models to understanding of age- and noise-related hearing loss. *Brain Res* 1091: 89-102, 2006.

44. **Paparella MM and Djalilian HR**. Etiology, pathophysiology of symptoms, and pathogenesis of Meniere's disease. *Otolaryngol Clin North Am* 35: 529-45, vi, 2002.

45. **Pendred V.** Deaf-mutism and goitre. *Lancet* 11: 532, 1896.

46. **Petit C, Levilliers J and Hardelin JP**. Molecular genetics of hearing loss. *Annu Rev Genet* 35: 589-646, 2001.

47. **Rillema JA and Hill MA**. Prolactin regulation of the pendrin-iodide transporter in the mammary gland. *Am J Physiol Endocrinol Metab* 284: E25-E28, 2003.

48. **Royaux IE, Suzuki K, Mori A, Katoh R, Everett LA, Kohn LD and Green ED**. Pendrin, the protein encoded by the Pendred syndrome gene (*PDS*), is an apical porter of iodide in the thyroid and is regulated by thyroglobulin in FRTL-5 cells. *Endocrinology* 141: 839-845, 2000.

49. **Royaux IE, Wall SM, Karniski LP, Everett LA, Suzuki K, Knepper MA and Green ED**. Pendrin, encoded by the Pendred syndrome gene, resides in the apical region of renal intercalated cells and mediates bicarbonate secretion. *Proc Natl Acad Sci U S A* 98: 4221-4226, 2001.

50. **Rybak LP, Husain K, Whitworth C and Somani SM**. Dose dependent protection by lipoic acid against cisplatin-induced ototoxicity in rats: antioxidant defense system. *Toxicol Sci* 47: 195-202, 1999.

51. **Rybak LP and Ramkumar V**. Ototoxicity. *Kidney Int* 72: 931-935, 2007.

52. **Rybak LP and Whitworth CA**. Ototoxicity: therapeutic opportunities. *Drug Discov Today* 10: 1313-1321, 2005.

53. **Scott DA and Karniski LP**. Human pendrin expressed in *Xenopus laevis* oocytes mediates chloride/formate exchange. *Am J Physiol Cell Physiol* 278: C207-C211, 2000.

54. **Scott DA, Wang R, Kreman TM, Sheffield VC and Karniski LP**. The Pendred syndrome gene encodes a chloride-iodide transport protein. *Nat Genet* 21: 440-443, 1999.

55. **Semaan MT, Alagramam KN and Megerian CA**. The basic science of Meniere's disease and endolymphatic hydrops. *Curr Opin Otolaryngol Head Neck Surg* 13: 301-307, 2005.

56. **Sheffield VC, Kraiem Z, Beck JC, Nishimura D, Stone EM, Salameh M, Sadeh O and Glaser B**. Pendred syndrome maps to chromosome 7q21-34 and is caused by an intrinsic defect in thyroid iodine organification. *Nat Genet* 12: 424-426, 1996.

57. **Soderman AC, Moller J, Bagger-Sjoback D, Bergenius J and Hallqvist J**. Stress as a trigger of attacks in Meniere's disease. A case-crossover study. *Laryngoscope* 114: 1843-1848, 2004.

58. **Sohmer H and Freeman S**. The importance of thyroid hormone for auditory development in the fetus and neonate. *Audiol Neurootol* 1: 137-147, 1996.

59. **Soleimani M, Greeley T, Petrovic S, Wang Z, Amlal H, Kopp P and Burnham CE**. Pendrin: an apical Cl^-/OH^-. *Am J Physiol Renal Physiol* 280: F356-F364, 2001.

60. **Spillmann T**. Genetic diseases of hearing. *Curr Opin Neurol* 7: 81-87, 1994.

61. **Stinckens C, Huygen PL, Joosten FB, van Camp G, Otten B and Cremers CW**. Fluctuant, progressive hearing loss associated with Meniere like vertigo in three patients with the Pendred syndrome. *Int J Pediatr Otorhinolaryngol* 61: 207-215, 2001.

62. **Suzuki K, Royaux IE, Everett LA, Mori-Aoki A, Suzuki S, Nakamura K, Sakai T, Katoh R, Toda S, Green ED and Kohn LD**. Expression of *PDS/Pds*, the Pendred syndrome gene, in endometrium. *J Clin Endocrinol Metab* 87: 938, 2002.

63. **Takahashi M, Odagiri K, Sato R, Wada R and Onuki J**. Personal factors involved in onset or progression of Meniere's disease and low-tone sensorineural hearing loss. *ORL J Otorhinolaryngol Relat Spec* 67: 300-304, 2005.

64. **Teubner B, Michel V, Pesch J, Lautermann J, Cohen-Salmon M, Sohl G, Jahnke K, Winterhager E, Herberhold C, Hardelin JP, Petit C and Willecke K**. Connexin30 (*Gjb6*)-deficiency causes severe hearing impairment and lack of endocochlear potential. *Hum Mol Genet* 12: 13-21, 2003.

65. **Trotter WR**. The association of deafness with thyroid dysfunction. *Br Med Bull* 16: 92-98, 1960.

66. **Uziel A**. Periods of sensitivity to thyroid hormone during the development of the organ of Corti. *Acta Otolaryngol Suppl* 429: 23-27, 1986.

67. **Wangemann P**. Supporting sensory transduction: cochlear fluid homeostasis and the endocochlear potential. *J Physiol* 576: 11-21, 2006.

68. **Wangemann P, Itza EM, Albrecht B, Wu T, Jabba SV, Maganti RJ, Lee JH, Everett LA, Wall SM, Royaux IE, Green ED and Marcus DC**. Loss of KCNJ10 protein expression abolishes endocochlear potential and causes deafness in Pendred syndrome mouse model. *BMC Med* 2: 30, 2004.

69. **Wangemann P, Nakaya K, Wu T, Maganti RJ, Itza EM, Sanneman JD, Harbidge DG, Billings S and Marcus DC**. Loss of cochlear HCO_3^- secretion causes deafness via endolymphatic acidification and inhibition of Ca^{2+} reabsorption in a Pendred syndrome mouse model. *Am J Physiol Renal Physiol* 292: F1345-F1353, 2007.

70. **Yen PM**. Physiological and molecular basis of thyroid hormone action. *Physiol Rev* 81: 1097-1142, 2001.

71. **Yoshida A, Taniguchi S, Hisatome I, Royaux IE, Green ED, Kohn LD and Suzuki K**. Pendrin is an iodide-specific apical porter responsible for iodide efflux from thyroid cells. *J Clin Endocrinol Metab* 87: 3356-3361, 2002.

72. **Zorov DB, Juhaszova M and Sollott SJ**. Mitochondrial ROS-induced ROS release: an update and review. *Biochim Biophys Acta* 1757: 509-517, 2006.

73. **Zuo J and Rarey KE**. Responsiveness of alpha 1 and beta 1 cochlear Na, K-ATPase isoforms to thyroid hormone. *Acta Otolaryngol* 116: 422-428, 1996.

CHAPTER 2 - Microarray-based comparison of three amplification methods for nanogram amounts of total RNA

These data have been published in the following refereed journal article:

Abstract

Gene expression profiling using microarrays requires microgram amounts of RNA, which limits its direct application for the study of nanogram RNA samples available from microdissection, laser-capture microscopy or needle biopsies. A novel system, based on Ribo-SPIA™ technology, has recently been introduced (RS, Ovation-Biotin amplification and labeling system, NuGEN Technologies, San Carlos, CA). The utility of the RS system, an optimized prototype system for picogram RNA samples (pRS, NuGEN Technologies), and two T7-based systems involving one or two rounds of amplification (OneRA, Standard Protocol, Affymetrix, Santa Clara, CA or TwoRA, Small Sample Prototcol, Version II, Affymetrix) were evaluated. Mouse kidney (MK) and universal reference (MUR) RNA samples, 0.3 ng to 10 μg, were analyzed by high-density Affymetrix Mouse 430 2.0 GeneChip® arrays. Call concordance between replicates, correlations of signal intensity, signal intensity ratios, and minimal fold-increase necessary for significance, were determined. All systems amplified partially overlapping sets of genes with similar signal intensity correlations. pRS amplified the highest number of genes from 10-ng RNA samples. 24 of 26 genes verified by RT-PCR were detected in samples prepared by pRS. TwoRA yielded somewhat higher call concordances than RS and pRS (91.8% versus 89.3% and 88.1%, respectively). In conclusion, although all target preparation methods were found suitable, pRS amplified the highest number of targets and was found to be suitable for amplification of as little as 0.3 ng total RNA. In addition, RS and pRS were faster and simpler than the T7-based methods and resulted in the generation of cDNA, which is more stable than cRNA.

Keywords

Gene expression microarray analysis; microdissection; nucleic acid amplification techniques

Introduction

Microarrays provide a widely accepted method for gene expression profiling on a genome wide scale. Affymetrix GeneChip® microarrays consist of oligonucleotide probes presented on a chip for hybridization to biotin-labeled cDNA or cRNA targets prepared from

sample RNA (11). Hybridization is detected as fluorescence after binding to labeled streptavidin. Gene expression profiling using GeneChip arrays require amplification of sample RNA irrespective of the available amounts of RNA. The Affymetrix Standard Protocol, which is well-established for the preparation of cRNA targets from microgram amounts of total RNA, consists of one round of T7 amplification (OneRA) to generate biotin-labeled targets. Gene expression profiling of small tissue samples obtained by micro-dissection, laser-capture microscopy or needle biopsy that yield mere nanograms of RNA requires amplification either of the hybridization signal (8; 20) or of the starting material. Methods for amplification of the starting material consist of exponential amplification by PCR (7; 13; 16; 22) and linear amplification with multiple rounds of T7 polymerase (1; 3; 4; 9; 15; 21). T7-based linear amplification systems have been used widely for amplification and production of cRNA targets. The Affymetrix Small Sample Protocol consists of two rounds of amplification (TwoRA) including biotin-labeling and is a well-established T7-based method for the preparation of cRNA targets from nanogram amounts of RNA (4). A novel linear amplification method, Ribo-SPIA™, which enables mRNA amplification in a simple and rapid procedure, has been introduced recently (NuGEN Technologies, San Carlos CA) (2; 5). Two systems based on this novel amplification technology, the Ovation Biotin System (RS) and a prototype system designed for target preparation from subnanogram level total RNA samples (picogram Ribo-SPIA™ prototype system, or pRS), were evaluated and compared with the T7-based single and two round amplification systems. The Ribo-SPIA systems have several advantages. Sample preparation can be performed within one day, which is much faster than the twenty-plus hrs required for TwoRA. Further, RS and pRS yield cDNA, which is more stable than cRNA and eliminates biases in microarray results due to RNA degradation (19). The present study was designed to evaluate target populations generated by the Ribo-SPIA™ based systems and the T7-based systems. Targets were analyzed by high-density Affymetrix Mouse 430 2 GeneChip®. Evaluation was based on direct comparisons and differential gene expression and included call concordances, signal correlations and sensitivities. Detection of a limited set of targets was verified by RT-PCR.

Materials and Methods

Target preparation

Mouse kidney (MK) total RNA (Ambion, Austin, TX) and mouse universal reference (MUR) total RNA (Stratagen, La Jolla, CA) were chosen as sources for RNA to minimize biological variation and inter-experimental differences. Targets were prepared by four different methods: 1) one round of amplification (OneRA), 2) two rounds of amplification (TwoRA), 3) Ribo-SPIA linear amplification with the Ovation biotin system (RS), and 4) Ribo-SPIA linear amplification with the pictogram Ribo-SPIA prototype system (pRS).

One Round of Amplification

Starting with 10 μg of total RNA, cRNA targets were prepared by OneRA (Standard Protocol, Version-VII, https://www.affymetrix.com/support/downloads/manuals/expression_s2_manual.pdf, Affymetrix, Santa Clara, CA; Fig. 2.1). Briefly, RNA was transcribed into cDNA by reverse transcriptase using a T7-primer that contains a promoter for DNA-dependent RNA polymerase (3; 21). Following RNase H-mediated second-strand cDNA synthesis, the double-stranded cDNA is purified and serves as a template in the subsequent in vitro transcription (IVT) reaction. The IVT reaction is carried out in the presence of T7 RNA polymerase and a biotinylated nucleotide analog/ribonucleotide mix for cRNA amplification and biotin labeling. The biotinylated cRNA targets are then cleaned up, fragmented, and hybridized to GeneChip expression arrays.

Two Round of Amplification

Starting with 10 ng of total RNA, cRNA targets were generated by TwoRA (Small SampleProtocol, Version II, Affymetrix; Fig. 2.1). Briefly, in vitro transcribed cRNA, generated by the first round of amplification (see above) was subjected to a second round of amplification. cRNA was transcribed into cDNA using random primers and subsequently removed by heat-induced fragmentation. A second cDNA strand was synthesized using a T7-primer. A second cDNA strand was synthesized using a T7-primer to generate a dscDNA template containing the

T7 promoter sequence. The resulting dscDNA was then amplified and labeled using a biotinylated nucleotide analog/ribonucleotide mix in the second IVT reaction. The labeled cRNA was then cleaned up, fragmented, and hybridized to GeneChip expression arrays.
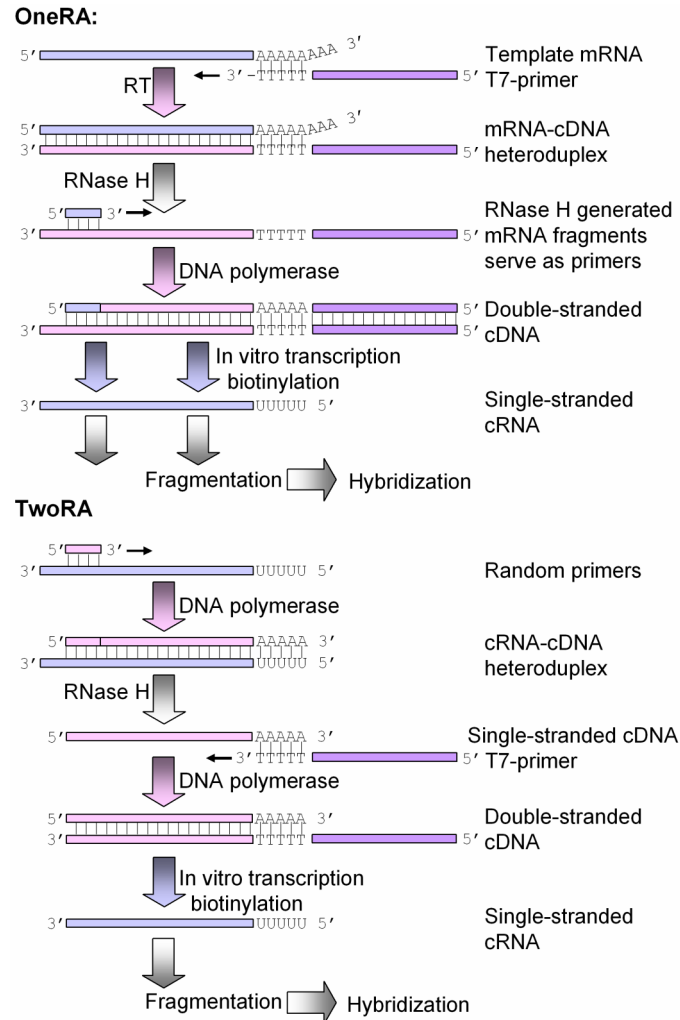
Figure 2.1: Schematic representation of target preparation using one (OneRA) and two (TwoRA) rounds of amplification. *RNA is shown in blue and DNA is shown in pink.*

Ribo-SPIA™ Linear Amplification

Ribo-SPIA™-based RNA amplifications and target preparations were carried out according to manufacturer's instructions (picogram Ribo-SPIA™ prototype system, pRS and OvationTM Biotin System, RS, see http://www.nugeninc.com/technology/index.shtml, Nugen, San Carlos, CA; Fig. 2.2). Briefly, RNA was reverse transcribed into cDNA by reverse transcriptase using a DNA/RNA chimeric primer that is part DNA and part RNA. RNA was

degraded by heat and fragments served as primers for second strand synthesis, yielding a double stranded cDNA with an RNA/DNA heteroduplex at one end. The RNA portion of the heteroduplex portion of the dscDNA, were digested by RNAse H added to the reaction mixture together with a DNA polymerase and a second chimeric cDNA/cRNA primer (amplification primer). Amplification proceeds by primer extension, strand displacement and degradation of the RNA portion of the primer extension product hybridized to the target to reveal part of the priming site for subsequent primer hybridization and extension by strand displacement DNA synthesis. Accumulated cDNA amplification products were fragmented and labeled to generate biotinylated cDNA targets. cDNA targets were prepared by RS starting with 100, 30, 10 or 3 ng of total RNA or by pRS starting from 10, 3 or 0.3 ng of total RNA.
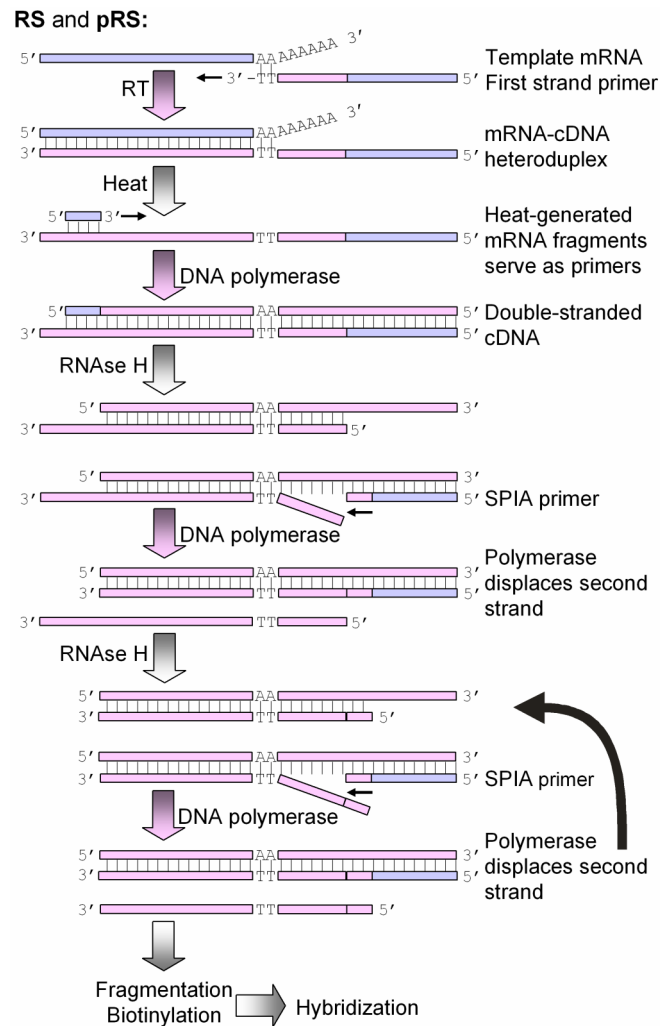
Figure 2.2: Schematic representation of target preparation using Ribo-SPIA™ linear amplification (RS, Ovation-Biotin amplification and labeling system; and pRS, picogram RNA samples). *RNA is shown in blue and DNA is shown in pink.*

Table 2.1: GeneChip array quality metrics (Averge ± SD).

Values are averages ± SD. OneRA, one round of amplification; TwoRA, two rounds of amplification; RS, Ribo-SPIA technology; pRS, pictogram RNA samples.

Method	Number of Chips	Scale Factor	Average Call All	Percent Present Call	Background Intensity	Noise	Raw Q
OneRA	6	3.5 ± 0.6	696.5 ± 7.8	45.4 ± 4.0	42.6 ± 2.0	2.6 ± 0.2	1.4 ± 0.1
TwoRA	6	2.4 ± 0.2	698.0 ± 7.8	46.7 ± 2.5	47.2 ± 2.8	3.0 ± 0.2	1.5 ± 0.1
RS	15	4.1 ± 0.7	685.7 ± 19.8	43.6 ± 2.0	46.0 ± 5.5	2.9 ± 0.7	1.5 ± 0.2
pRS	12	2.0 ± 0.3	712.1 ± 27.9	51.3 ± 3.8	74.4 ±12.7	3.9 ± 0.6	2.5 ± 0.3

Table 2.2: Verification of GeneChip array data obtained from MUR RNA.

Targets were selected according to a set of criteria to ensure fair comparison between TwoRA and RS (see MATERIALS AND METHODS). Targets called present or absent in all three replicates are marked P or A, respectively. Targets variably called present or absent are marked with asterisk.

Gene Symbol Affymetrix #	Average Intensity OneRA	Average Intensity TwoRA	Average Intensity RS	Average Intensity pRS	Left Primer Right Primer	Expected Product Size	Observed Product Size	RT-PCR Result
Cdkn1a 1421679_a_at	128 A	1252 P	302 A	1415 P	ccgtggacagtgagcagtt gagtgcaagacagcgacaag	286	279	P
Nck1 1421487_a_at	584 A	826 P	117 A	205 P	tttggaaccatctcctccac gcccaatgcagtaaacagtc	254	248	P
Nme3 1448905_at	262 A	531 P	7 A	165 P	aagctggtggcactgaagctag cgagtcgctgccatgaattac	266	270	P
Cpsf1 1417665_a_at	3330 P	3990 P	184 A	827 P	gcccatgcaagaaaagacat ggtctgtctccagccaagtc	267	275	P
Ruvbl2 1422482_at	2858 P	2752 P	166 A	478 P	ggaccgcttgctcattgtat gtactgtgtggagcgggatt	275	276	P
Hrmt1l1 1416844_at	1833 P	2311 P	48 A	243 *	acccactgtgacatccacac gcatcaaggacaccactgac	262	269	P
Tce2 1421971_a_at	1980 P	1974 P	207 A	387 P	atgtaccacgattggcgttt cacaggacctctctgccagt	283	275	P
Prkcsh 1416339_a_at	2563 P	1828 P	162 A	764 P	gacgagctgtagcctgaacc tcatccatttatctcccacca	287	279	P
1110035H23Rik 1416315_at	1210 P	1273 P	99 A	191 P	agcaaaggtgattcctggtg cactggagagagctgatgga	271	268	P
Pold1 1448187_at	1480 P	1238 P	108 A	260 P	ctgcccatcgacactcagta gtcttgcatcgtgtgtggtc	146	137	P
Nxph3 1419710_at	900 P	1082 P	136 A	68 A	actgaggctgaaatggcaac aggtggttagggcagaggat	257	256	P
Nsd1 1420882_a_at	1132 P	882 P	111 A	438 P	ggagttccagtgctccttca gcccatgtgtcctctgctat	273	271	P
Slc22a5 1450395_at	677 P	667 P	101 A	180 P	ggggagtttgtttgtttgtca caccgatgtgacacgactg	291	298	P
Lmnb2 1448531_at	334 A	313 A	1092 P	636 P	aacctccagaacccaccag cactccgggtaaccatctca	251	243	P
Hspa4 1416147_at	343 A	146 A	1081 P	170 P	cagttgggtgtaggcatggt gtcggcaatgaggtgttctt	299	293	P

35

Gene Symbol Affymetrix #	Average Intensity OneRA	Average Intensity TwoRA	Average Intensity RS	Average Intensity pRS	Left Primer Right Primer	Expected Product Size	Observed Product Size	RT-PCR Result
Neu3 1419339_at	83 A	22 A	536 P	539 P	gcccttatc cttccaataatgc cagtgttagaatgtccccctgg	294	297	P
Foxc2 1416693_at	898 P	355 A	3582 P	4382 P	gggacccctaatgacttctg ttaaaggctctgggcaagaa	124	123	P
Hoxc4 1422870_at	357 A	275 A	2844 P	942 P	ccccatctctttccttaggc taaccacgatgagggtaggg	271	259	P
Tle3 1419654_at	382 P	42 A	2146 P	1998 P	acagcgaggattttctgtgg aaaagcacccacaccagttg	300	293	P
Max 1423501_at	215 A	151 A	2001 P	2268 P	tcctccctcacctctgtttg ctgcaaatctgtccccactt	197	185	P
Dusp10 1417163_at	204 A	93 A	1889 P	2339 P	gacctggaactgactgcaca tagcctgtctccccagagaa	138	138	P
Tcp1-rs1 1425195_a_at	1051 P	326 A	1340 P	1110 P	atcctctgggagcatctgg ggtcctctggtttcctttc	214	217	P
Akt3 1422078_at	369 P	65 A	1304 P	795 P	attgcctgcgtttttctttg cctctcacatccatcccttg	220	220	P
Hspa4 1416147_at	343 A	146 A	1081 P	170 P	cagttgggtgtaggcatggt gtcggcaatgaggtgttctt	299	294	P
Zfp235 1449329_at	70 A	66 A	889 P	645 P	agctggtgattggcagaac tgggtagcactatgcctcaa	255	59	P
Pik3r1 1425515_at	309 P	43 A	677 P	1289 P	tcatgtgtcagaaggcagga cccaaccctcccacttctat	287	290	P

Quantification and quality assessment of RNA, cRNA and cDNA

Quantities of total RNA, cRNA and cDNA were determined by absorbance spectrophotometry (ND-1000 Spectrophotometer, Nanodrop Technologies, Rockland, DE). For total RNA and for cRNA the conventional conversion, 1 OD260 = 40 ng/μl, was used. For cDNA the manufacturer's recommended conversion, 1 OD260 = 33 ng/μl, was used (Nugen). Quality of total RNA (eukaryotic total RNA nano assay) and of cRNA and cDNA (mRNA smear nano assay) was determined by microfluidic electrophoresis (Bioanalyzer, Agilent Technologies, Palo Alto, CA).

Microarray analysis

Hybridizations of cRNA and cDNA targets were carried out according to manufacturer's recommended procedures on high-density oligo-nucleotide gene chips (Mouse 430 2 expression array, see http://www.affymetrix.com/support/technical/datasheets/mogarrays_datasheet.pdf, Affymetrix). A total of 39 target preparations were performed and each preparation was analyzed by one GeneChip® array. Data were scaled to a target intensity of 500 (GCOS software, Affymetrix). Normalization quality controls including scaling factors, average intensities, present

calls, background intensities, noise and raw Q values were all within acceptable limits (Table 2.1). Hybridization controls, BioB, BioC, BioD and CreX, were called present on all chips and yielded the expected increases in intensities. Analyses of target populations were supported by GeneSpring (Silicon Genetics, Redwood City, CA), Excel (Microsoft, CA) and Origin 6.0 (OriginLab, Northampton, MA). Microarray data were deposited at NCBI GEO accession number #GSE1435 and #GSE2019.

Call concordance

Probe sets are either called present (P), absent (A) or marginal (M) based on detection p-values (P: p-value < 0.05, M: p-value 0.05-0.065, A: p-value > 0.065). Nine field P/A/M matrices comparing data from two chips were constructed (Origin 6.0). Call concordance was the sum of the three concordant fields (P-P, A-A and M-M) and call discordance was the sum of the other six fields (P-A, A-P, P-M, M-P, A-M, M-A). Data were expressed as percentage of the total number of probe sets (n = 45,101). Call concordance within a set of triplicate data was computed as average ± SD of three pair-wise comparisons. Call concordance between two sets of triplicates was computed as average ± SD of all nine pair wise comparisons.

Signal correlation

Signal intensities without regard to present, absent or marginal calls were correlated and linear correlation coefficients (r) were determined (Origin, version 6.0). Correlations r values within a set of triplicates were reported as average ± SD of the three possible correlations. Correlations r values between two sets of triplicates were based on averaged intensities and reported as a simple r value.

Sensitivity

Sensitivity was evaluated from the estimated fold-change necessary for significance ($Fold_{sig}$). $Fold_{sig}$ was obtained according to $Fold_{sig} = (Avg + 2.776 \times \sqrt{(2/3 \times SD^2)}) / Avg$ where Avg and SD are the average and standard deviation of the signal intensity of genes that are called present in all replicates, 2.776 is the t-value at p=0.05, assuming 4 degrees of freedom.

Differential gene expression

Signal intensity ratios of genes detected present in all targets prepared from 10 μg and 10 ng MK and MUR RNA by OneRA, TwoRA, RS and pRS were calculated from averages of triplicates. Ratios were correlated between amplification systems and correlations coefficients were obtained.

Verification of microarray data

A small number of gene targets amplified from MUR RNA and detected by microarray were verified by performing RT-PCR (Table 2. 2). Targets were chosen based on gene array data obtained from 10 ng MUR RNA amplified by either TwoRA or RS. For each method, 13 targets were selected based on a set of six criteria established to assure fair selection between these two methods: 1) Targets must be called present in three replicates of the considered amplification method (TwoRA or RS). 2) Targets must be called absent in three replicates of the other amplification method. 3) Hybridization intensities of the three replicates of the considered amplification method must be >100. 4) Targets of the considered amplification method must be annotated by Affymetrix as full-length mRNA and not as expressed sequence tag. 5) Hybridization intensities must be comparable between sets of chosen targets. 6) Fold-differences between called present by one amplification method and absent by the other method must be comparable between sets of chosen targets. Average intensities and calls for the 26 selected genes are given in Table 2.2 not only for TwoRA and RS but also for OneRA and pRS.

Real time RT-PCR was performed in the presence of 0.2x SYBR green I (Molecular Probes) using MUR RNA and gene-specific primers (Tables 2.2) (23). RT was performed for 30 min at 50°C and 15 min at 95°C. PCR consisted of 50 cycles of 1 min at 60°C, 1 min at 72°C, 7s heating to hot-measurement temperature, 13-s hot-measurement at 78°C below product melting temperature, and 1 min at 94°C. Hot-measurements were performed to eliminate the detection of primer-dimers that tend to have melting temperatures between 72°C and 75°C. PCR was followed by melting (60°C to 95°C). Targets were considered present when a single product of the appropriate size was obtained. Target sizes were determined by microfluidic electrophoresis

(Agilent BioAnalyzer). The average difference between observed and expected product size was 5.6 ± 3.8 bp (n=25).

Statistics

Gene array experiments were performed in triplicate. RT-PCR experiments were performed at least in duplicate, mostly in quadruplicate. Data, including quality control values, are expressed as average $\pm$ SD. The significance of continuous data was determined using One-way ANOVA with Bonferroni post hoc test. Significance was assumed at $p < 0.05$.

Results

Target yields and amplification

Samples of total RNA ranging from 0.3 ng to 10 μg were used as starting materials. Quantities were verified spectrophotometrically. RNA qualities were evaluated by microfluidic electrophoresis (Fig. 2.3). MUR RNA was of slightly higher quality than MK RNA as evident from the larger ratio between the 28S and 18S peak. cRNA targets were prepared by OneRA or TwoRA starting with 10 μg or 10 ng RNA, respectively. Alternatively, cDNA targets were prepared by RS starting with 3, 10, 30 or 100 ng RNA and by pRS starting with 0.3, 3 and 10 ng RNA. Fig. 2.4 summarizes cRNA and cDNA target yields obtained after amplification. Yields for cRNA and cDNA targets were significantly different but each was sufficient for preparation of the hybridization cocktail (Affymetrix). The size distribution of amplified products and of biotinylated and fragmented targets are shown in Fig. 2.5.
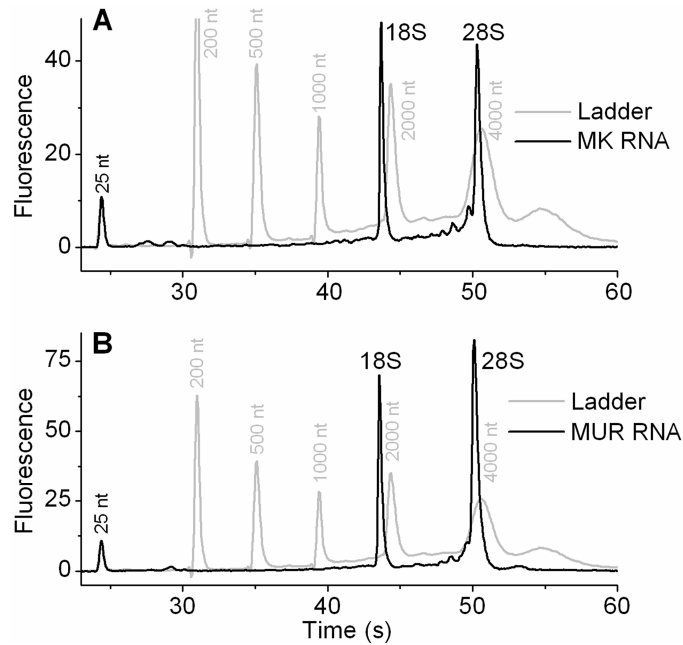
Figure 2.3: Quality of RNA used as starting material.
Electropherograms (BioAnalyzer, Agilent) of (A) mouse kidney (MK) total RNA and (B) mouse universal reference (MUR) total RNA. Sharp peaks representing 18S and 28S rRNA demonstrate good quality (solid lines), although the mass ratio for the two rRNA species was lower for MK RNA. Each sample was spiked with a 25 nt marker to aid alignment of traces with a ladder consisting of 200, 500, 1000, 2000 and 4000 nt fragments (shaded traces).
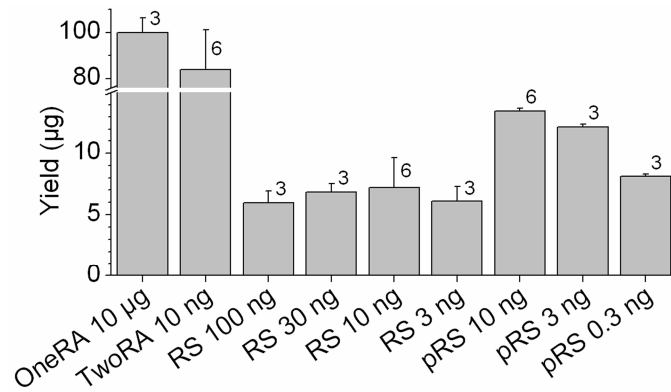
Figure 2.4: Amplification yields.
cRNA was obtained from 10 μg total RNA using OneRA and from 10 ng using TwoRA. cDNA was obtained from 0.3, 3, 10, 30 or 100 ng total RNA using RS and pRS. Numbers next to error bars represent the numbers of experiments conducted.
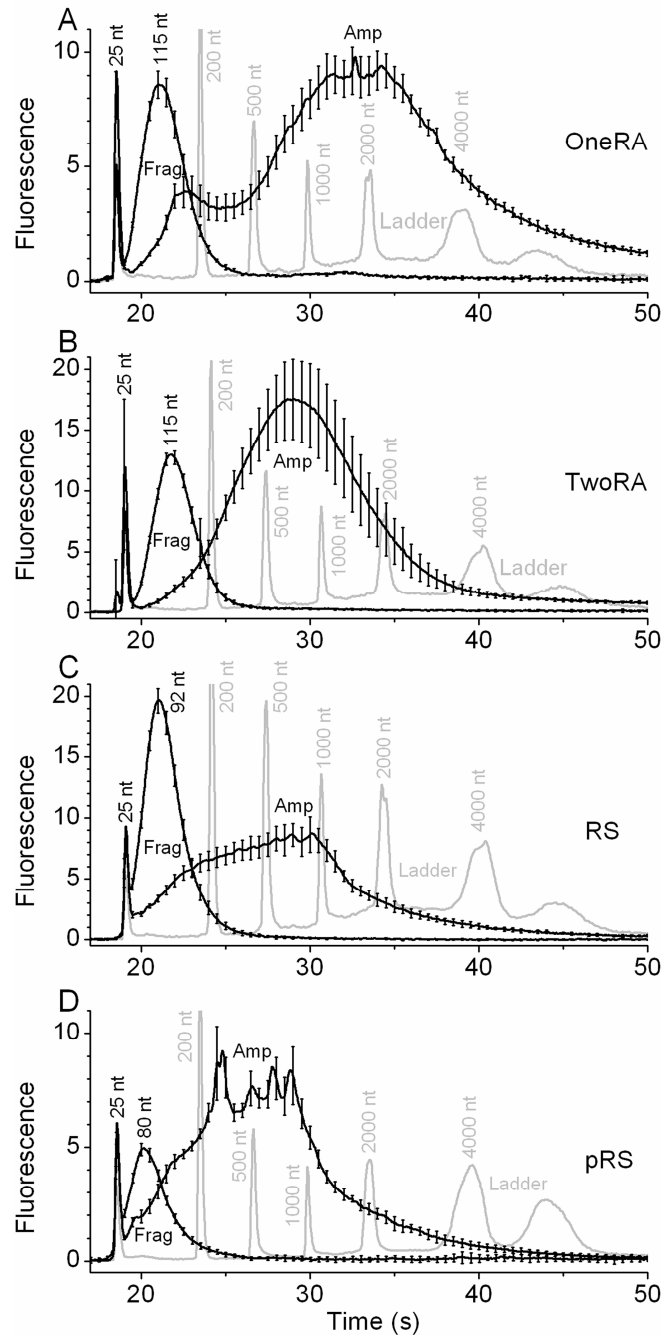
Figure 2.5: Quality of cRNA and cDNA targets obtained after amplification (Amp) and fragmentation (Frag).
(A) Averaged electropherograms of cRNA targets were prepared using OneRA from 10 µg of total RNA (n=3). (B) cRNA targets were prepared using TwoRA from 10 ng of total RNA (n=3). (C) cDNA targets were prepared by using RS from 3, 10, 30 or 100 ng of total RNA (n=1 each). (D) cDNA targets were prepared using pRS from 10 ng of total RNA (n=2). Each sample was spiked with a 25 nt marker to aid alignment of traces with a ladder consisting of 200, 500, 1000, 2000 and 4000 nt fragments (shaded traces).

These target preparation methods, OneRA, TwoRA, RS and pRS, are designed to amplify mRNA, priming at the poly-A tail. Adherence to this design goal was evaluated by gene array analysis. Poly-A tail independent amplification was evaluated by probes for 18S rRNA, which is thought not to contain a poly-A tail and therefore should not be amplified and consequently not called present. Probe sets for 18S hybridized with targets prepared by OneRA yielded low signal intensities and were not consistently called present (see Fig. 2.6). In contrast, 18S probe sets hybridized with targets prepared by TwoRA, RS or pRS were consistently called present. Hybridization with targets prepared by TwoRA, RS or pRS yielded high signal intensities.
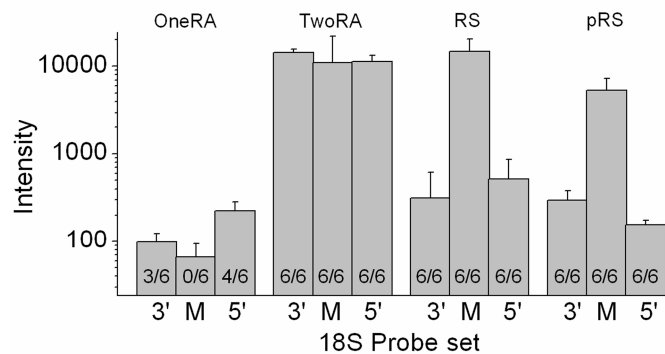
Figure 2.6: Amplification of 18S rRNA.
Signal intensity of the 3', M and 5' probes sets. Probe sets were consistently called present for six target preparations prepared using TwoRA or using RS or pRS (each 6/6) but not for targets prepared using OneRA.

Bias toward amplification of the 3′ end of targets was evaluated by probes located toward the 3′ and 5′ ends and in the middle of GAPDH, β-actin and transferrin receptor. Signal intensity ratios, 3′-5′ and 3′-M, were calculated (Table 2.3). Ratios should ideally be unity. Ratios for targets prepared by OneRA were closest to unity. Increase 3′-5′ ratios were noted for all other target preparation methods from the lower input total RNA samples. This observation is similar to that noted by others and likely does not affect the quality of expression profiling with the GeneChip arrays, as the probe design for these arrays is 3′ biased (12). 3′ biases for targets prepared by RS and pRS were similar regardless of the amount of starting material.

Table 2.3: Amplification induced 3′ bias, as measured by signal intensity on GeneChip arrays.

Values are averages ± SD. Ratios were obtained for targets that were prepared from MUR RNA (each n=3) by one (OneRA), two (TwoRA) rounds of amplification or by Ribo-SPIA™ linear amplification (RS and pRS). OneRA was taken as standard and significantly different data were marked with an asterisk.

Gene	Ratio	Distances from 3'	OneRA (10 µg)	TwoRA (10 ng)	RS (10 ng)	pRS (10 ng)
GAPDH	3'/M	387 / 770	0.87 ± 0.03	1.09 ± 0.04 *	1.6 ± 0.1 *	1.12 ± 0.02 *
GAPDH	3'/5'	387 / 1138	0.80 ± 0.03	1.7 ± 0.1*	1.5 ± 0.1 *	1.12 ± 0.03 *
β-Actin	3'/M	972 / 1298	1.09 ± 0.05	1.2 ± 0.1	2.9 ± 0.2 *	2.5 ± 0.1 *
β-Actin	3'/5'	972 / 1665	1.17 ± 0.06	1.5 ± 0.1 *	3.1 ± 0.1 *	3.8 ± 0.2 *
Transferrin Receptor	3'/5'	528 / 2225	3.4 ± 0.2	-	-	-

The numbers of probe sets that were called present, absent or marginal were tabulated (Table 2.4). pRS had the highest number of present calls followed by OneRA, TwoRA and RS, respectively. More genes were consistently (in all three replicates) called present after pRS than after TwoRA or RS (Fig. 2.7). A sizable number of targets (13,539, based on MUR RNA) was amplified by all three methods. Similar observations were made for MK RNA. For targets prepared by RS and pRS, present calls decreased and absent calls increased with decreasing amounts of starting material (Table 2.4). Sensitivity was computed as average fold-change necessary for significance (Table 2.4). Fold$_{sig}$ was found to be intensity dependent (Fig. 2.8).
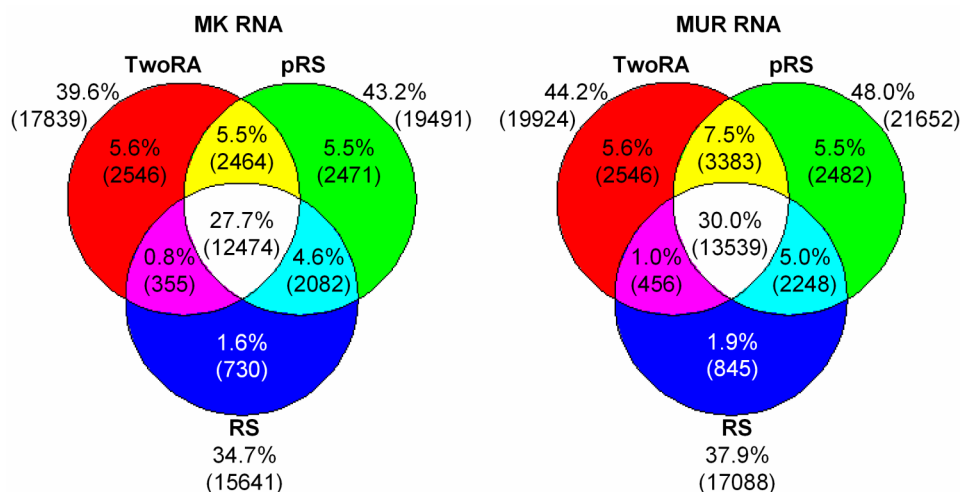
Figure 2.7: Venn diagrams of genes consistently called present.
Target populations were prepared from 10 ng MK or MUR RNA using TwoRA or using RS or pRS. 100% is the total of 45,101 probe sets.

Table 2.4: Call distribution, call concordance, signal correlation and estimated average fold-change necessary for significance.
Call distributions and call concordances are relative to the total number of 45,101 probe sets. Call concordances and signal correlations are based on the three possible comparisons within triplicate samples. Estimated average fold-changes necessary for significance (Foldsig) were based on average intensity and standard deviation for present genes. Targets were prepared from mouse kidney (MK) or mouse universal reference (MUR) RNA using OneRA or TwoRA or Ribo-SPIA linear amplification (RS or pRS). Targets prepared using OneRA from 10 µg RNA were taken as standard and significantly different data were marked with an asterisk.

Method	RNA	P (%)	A (%)	M (%)	Concordance (%)	Correlation (R)	$Fold_{sig}$
OneRA	10 µgMK	42.0 ± 2.1	56.1 ± 2.1	1.94 ± 0.06	90.8 ± 0.6	0.991 ± 0.005	1.27 ± 0.20
TwoRA	10 ngMK	44.5 ± 1.3	53.5 ± 1.2	1.96 ± 0.06	91.4 ± 0.4	0.99562 ± 0.00004	1.26 ± 0.19*
RS	100 ngMK	45.8 ± 0.5 *	52.4 ± 0.5 *	1.81 ± 0.11	89.7 ± 0.3 *	0.991 ± 0.001	1.33 ± 0.22*
RS	30 ngMK	45.2 ± 0.7 *	53.0 ± 0.7 *	1.75 ± 0.02	90.0 ± 0.3	0.995 ± 0.001	1.29 ± 0.21*
RS	10 ngMK	41.7 ± 1.0	56.5 ± 1.0	1.78 ± 0.05	88.4 ± 0.6 *	0.981 ± 0.010	1.44 ± 0.28*
RS	3 ngMK	41.2 ± 0.2	57.1 ± 0.3	1.77 ± 0.14	88.5 ± 0.2 *	0.990 ± 0.001	1.43 ± 0.30*
pRS	10 ngMK	50.4 ± 0.7	48.2 ± 0.7	1.37 ± 0.06	88.4 ± 0.04 *	0.9957 ± 0.0002	1.39 ± 0.34*
OneRA	10 µgMUR	48.8 ± 0.6	49.3 ± 0.6	1.87 ± 0.03	92.2 ± 0.1	0.9978 ± 0.0002	1.20 ± 0.17
TwoRA	10 ngMUR	48.8 ± 0.5	49.2 ± 0.5	1.97 ± 0.04	91.8 ± 0.2	0.9964 ± 0.0003	1.24 ± 0.18*
RS	10 ngMUR	44.2 ± 0.7 *	53.8 ± 0.7 *	1.91 ± 0.06	89.3 ± 0.3 *	0.995 ± 0.001	1.29 ± 0.21*
pRS	10 ngMUR	54.8 ± 1.1	43.7 ± 1.0	1.43 ± 0.12	88.1 ± 0.1 *	0.991 ± 0.005	1.40 ± 0.30*
pRS	3 ngMUR	53.2 ± 0.9	45.3 ± 0.9	1.43 ± 0.12	87.0 ± 0.3 *	0.990 ± 0.003	1.50 ± 0.39*
pRS	0.3 ngMUR	45.9 ± 1.2	52.9 ± 1.2	1.27 ± 0.06	83.6 ± 0.8 *	0.966 ± 0.005 *	1.91 ± 0.64*

Verification of amplification

A sizable number of targets (13,995 = 13,539 + 456, based on MUR RNA) were amplified from 10 ng RNA by both TwoRA and RS (Fig. 2.7). An additional 5,929 (= 2,546 + 3,383) targets were TwoRA-specific since they were amplified by TwoRA and not by RS and an additional 3,093 (= 845 + 2,248) targets were RS-specific since they were amplified by RS and not by TwoRA. TwoRA- and RS-specific targets had similar distributions of hybridization intensities and of fold-differences between hybridization intensities that were called present and called absent. TwoRA- and RS-specific target populations were sampled according to a set of criteria (see Methods) that ensured fair comparison between these two systems. All 13 TwoRA-

specific and all 13 RS-specific targets could be verified in MUR RNA (Tables 2.1) consistent with equal fidelity of TwoRA and RS. Of the 26 selected targets 15 were called present by OneRA and 24 were called present by pRS. Quantitative comparisons other than between TwoRA and RS are not warranted given that unbiased selection was ensured only for TwoRA and RS. Taken together, these data demonstrate equal fidelity of TwoRA and RS and suggest that each amplification system amplifies a unique set of targets, in addition to the overlapping target sets.
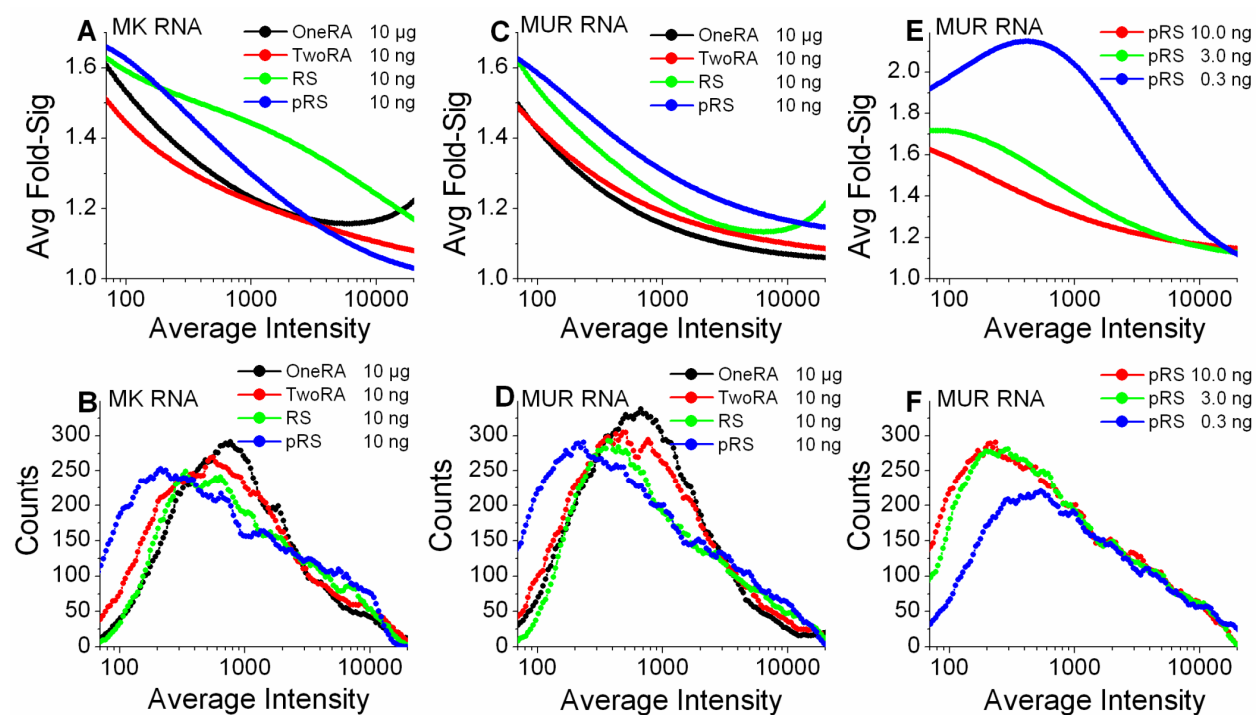
Figure 2.8: Intensity dependence of estimated fold-change necessary for significance. *Fold-changes for significance were computed on the basis of averages and standard deviations. Traces represent smoothed averages. A, C, E: Estimated fold-changes for significance computed from target populations amplified from different amounts of MK RNA or MUR RNA. B, D, F: Smoothed frequency distributions of intensities are provided for comparison. Target populations were prepared using OneRA or TwoRA or using RS or pRS.*

Reproducibility between replicates

Call concordances and correlation coefficients within triplicate samples were calculated to evaluate reproducibility between replicates (Table 2.4, best examples are shown in Figs. 9A-D and 10). Between replicates call concordances were similar for targets prepared by OneRA or

TwoRA and somewhat lower for RS and pRS (92.2%, 91.8%, 89.3% and 88.1%, respectively, for target prepared from 10 μg and 10 ng MUR RNA). Signal correlations were similar for targets prepared by all amplification systems.
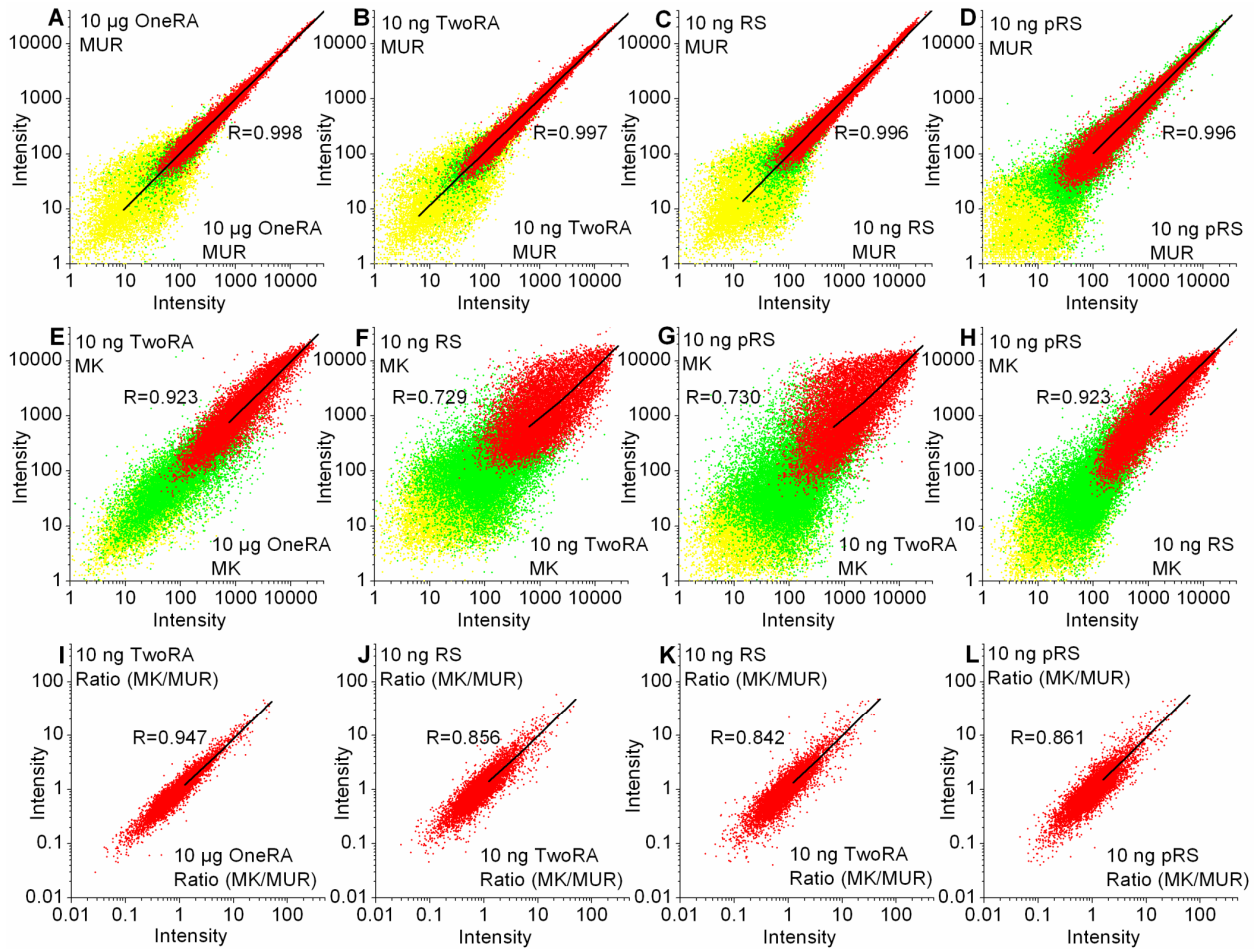
Figure 2.9: Correlation of signal intensities and ratios.
(A-D) Best examples of correlations of individual data sets (replicates) prepared using OneRA or TwoRA or using RS or pRS from MUR RNA. (E-H) Correlation of averaged data sets prepared by OneRA, TwoRA, RS or pRS from MK RNA. (I-L) Correlation of ratios computed from averaged data sets (MK/MUR) that originated from samples prepared using OneRA, TwoRA, RS or pRS.
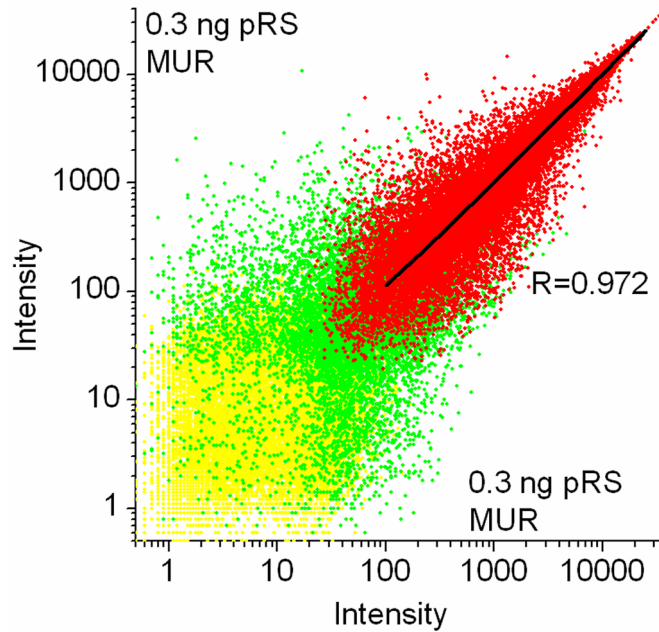
Figure 2.10: Correlation of signal intensity for 0.3 ng total RNA.
Best example of correlations of individual data sets (replicates) prepared using pRS from mouse MUR RNA.

Fidelity of amplification systems

Direct comparison

Call concordances were obtained from comparisons of samples prepared from 10 µg RNA by OneRA and from 10 ng by TwoRA, RS or pRS (Table 2.5). Call concordances between OneRA and TwoRA were higher than for any other comparison. Observations were similar for MK and MUR RNA. Signal intensities were correlated between amplification systems (Fig. 2.9 E-H). Correlations coefficients were better between OneRA and TwoRA and between RS and pRS most likely due to the greater similarities between these amplification systems. Low call concordances and signal correlations between T7- and Ribo-SPIA™ -based systems suggests that the two amplification methods may introduce different biases or that cDNA and cRNA perform differently on GeneChip® arrays. Indeed, cDNA/DNA hybridizations may be more reliable than cRNA/DNA hybridization due to the lesser complexity of cDNA/DNA interactions (17; 18; 24), which may affect both Present/Absent calls and signal intensities.

Differential gene expression

Amplification-induced bias in signal intensity can be canceled by computing differential gene expression. Signal intensity ratios of data originating from MK and MUR RNA were calculated from averages of triplicates. Ratios of samples that were prepared by different amplification systems were compared. Correlations coefficients were obtained for probes that were called present in all sets of triplicates prepared by OneRA, TwoRA, RS and pRS (Fig. 2.9 I-L). Correlation between TwoRA and OneRA was considerably better than between other amplification systems.

Table 2.5: Call concordances and signal intensity correlations between systems.
Call concordances are calculated between target populations generated from 10 μg RNA using one (OneRA) or from 10 ng RNA by two (TwoRA) rounds of amplification or Ribo-SPIA linear amplification (RS or pRS). Call concordances are averages ± SD of the nine possible comparisons between two sets of triplicates. Signal correlation coefficients were obtained from correlation of averaged triplicates.

MK RNA	RNA	Concordance (%)	P–P (%)	A–A (%)	A–P (%)	P–A (%)	Correlation (R)
OneRA – TwoRA	K	86.7 ± 0.8	37.6 ± 1.3	49.0 ± 0.9	5.9 ± 1.3	3.7 ± 0.6	0.923
OneRA – RS	K	76.5 ± 1.0	31.2 ± 1.0	45.3 ± 1.1	9.8 ± 1.1	10.1 ± 0.9	0.693
OneRA – pRS	K	60.7 ± 0.3	27.4 ± 1.0	33.2 ± 0.9	22.0 ± 1.1	14.1 ± 0.8	0.702
TwoRA – RS	K	77.5 ± 0.4	32.9 ± 0.6	44.5 ± 0.8	8.1 ± 0.7	10.8 ± 0.6	0.729
TwoRA – pRS	K	60.6 ± 0.2	28.6 ± 0.7	31.9 ± 0.6	20.8 ± 0.7	15.3 ± 0.6	0.730
RS – pRS	K	60.0 ± 0.3	26.9 ± 0.5	33.1 ± 0.7	22.6 ± 0.5	14.3 ± 0.6	0.923

MUR RNA	RNA	Concordance (%)	P–P (%)	A–A (%)	A–P (%)	P–A (%)	Correlation (R)
OneRA – TwoRA	UR	87.6 ± 0.2	43.5 ± 0.3	43.9 ± 0.4	4.4 ± 0.3	4.5 ± 0.3	0.930
OneRA – RS	UR	74.0 ± 0.3	34.6 ± 0.4	39.3 ± 0.4	8.9 ± 0.3	13.4 ± 0.5	0.685
OneRA – pRS	UR	59.3 ± 0.1	32.6 ± 0.3	26.7 ± 0.2	21.8 ± 0.3	15.6 ± 0.3	0.734
TwoRA – RS	UR	75.3 ± 0.3	35.3 ± 0.5	40.0 ± 0.3	8.3 ± 0.3	12.7 ± 0.5	0.701
TwoRA – pRS	UR	58.7 ± 0.2	32.3 ± 0.3	26.4 ± 0.2	22.0 ± 0.2	15.9 ± 0.2	0.741
RS – pRS	UR	56.6 ± 0.2	28.9 ± 0.4	27.6 ± 0.3	25.4 ± 0.4	14.8 ± 0.2	0.907

Discussion

Microarray-based gene expression profiling of microdissected tissue samples and needle biopsies is often limited due to insufficient amounts of RNA. Methods devised to overcome this limitation include signal amplification (8; 20) and sample amplification including exponential

amplification by PCR (7; 9; 13; 16; 22) and linear amplification by T7 polymerase (1; 4; 15; 21). T7-based linear amplification methods including TwoRA are commonly used for preparation of targets from nanogram amounts of RNA (3; 21). RS and pRS are novel systems that are based on Ribo-SPIA™ technology that was recently introduced as an alternative to TwoRA. The goal of the present study was to compare RS, pRS, TwoRA and OneRA. Target yields and qualities, amplification biases, call concordances, correlation coefficients and sensitivities were determined. Evaluations were based on direct comparisons and on differential gene expression. OneRA was taken as baseline, mostly for historical reasons (11). Although, OneRA is the major linear amplification protocol used on the Affymetrix platform, it should not be assumed to generate a 'true' or 'standard' gene expression profile as implied by its commercial name.

RS and pRS generated significantly smaller amounts of cDNA than TwoRA generated cRNA (Fig. 2.4), although all systems produced sufficient amounts of targets given that 15 μg of cRNA and only 2 μg of cDNA are needed for array hybridization. Yields of cDNA targets prepared by RS and pRS were independent of the amount of starting material, which is similar to the pattern observed with PCR.

Probe sets for 18S rRNA were low in signal intensity and inconsistently called present in targets prepared by OneRA. However, 18S rRNA was consistently called present with high signal intensities in target preparations prepared by TwoRA, RS and pRS (Fig. 2.6). This observation may indicate that both T7- and Ribo-SPIA™- based amplification systems prime at internal poly-A sites. Alternatively, it is conceivable that poly-adenylated forms 18S rRNA may be present as has recently been observed in yeast (10). Thus, it is possible that the higher sensitivity afforded by RNA amplification enables the detection of small amounts of poly-adenylated rRNA on the arrays. The majority of amplified transcripts generated by RS and pRS were up to 1,000 nt in length (Fig. 2.5). A similar length distribution was found for TwoRA. In contrast, the majority of amplified transcripts generated by OneRA were up to 2,500 nt in length. These differences are not likely to be important on Affymetrix arrays in which >98% of the probe sets are located less than 600 nt from the 3′ end.

3′ bias was further determined for three genes with probe sets that varied in their distances from the 3′ end of the mRNA (Table 2.3). 3′/M and 3'/5' ratios for GAPDH are best

suited to predict fidelity of expression profiling given that >98% of probe sets on Affymetrix mouse 430 2 chips are specific for sequences within 600 nt from the 3′ end. The observation that 3′/M and 3'/5' ratios for GAPDH were close to unity is consistent with the view that TwoRA, RS and pRS amplify targets with high fidelity. The observation that 3'/5' ratios for the transferrin receptor, which are based on probe sets located 528 and 2,225 nt from the 3' end, could only be obtained for OneRA is consistent with the finding that OneRA yielded longer transcripts than TwoRA, RS or pRS.

The RNA starting material for MK and MUR differed notably in quality (Fig. 2.3). Consistently, significant differences between MK and MUR RNA were found for probe sets that are located 972 and 1665 nt from the 3′ end (3′-5′ ratio for β-actin, Fig. 2.11). However, no significant differences were found for ratios of probes set that are located 387 and 770 nt from the 3′ end (3′/M ratio for GAPDH, Fig. 2.11). Given that >98% of probes are located within 600 nt of the 3′ end, the difference in RNA quality was not expected to have a major effect on the gene array data. Consistently, analyses of GeneChip array data from both RNA gave similar results.

A sizable number of targets (13,539 in 10 ng MUR RNA) were detected by TwoRA, RS and pRS. The highest number of genes (21,652 in 10 ng MUR RNA) was consistently called present in targets prepared by pRS compared to RS and TwoRA (Fig. 2.7). pRS consistently amplified 15,179 targets from 0.3 ng of total RNA with acceptable reproducibility as measured by call concordance, signal correlation and sensitivity (Table 2.4, Fig. 2.8 and 2.10). Verification of 13 TwoRA- and 13 RS-specific targets by RT-PCR (Table 2.2) demonstrate that TwoRA and RS amplify partially unique sets of targets.

Reproducibility between replicates was based on call concordance and estimated fold-changes necessary for significance (Table 2.4, Fig. 2.8). Reproducibility for targets that were prepared from 10 ng RNA by TwoRA was higher than for targets that were prepared from 10 ng RNA by RS or pRS. Fold-changes necessary for significance, however, were well below 2 for all amplification systems. A fold change of 2 is sometimes used as an arbitrary lower limit for significance.
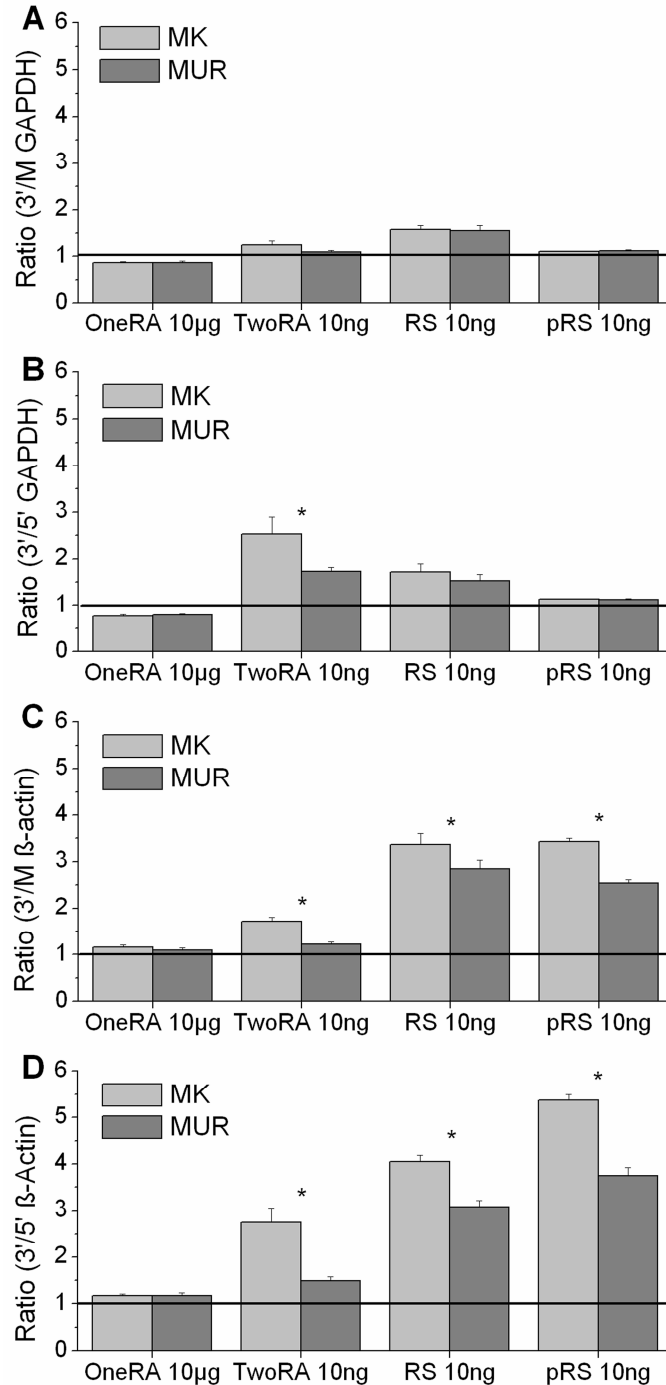
Figure 2.11: 3′ bias as a function of the quality of the RNA starting material.
MK RNA was of slightly lesser quality than MUR RNA as evident from the lesser ratio of the 18S and the 28S peaks, (see Fig. 3). Targets were prepared using OneRA from 10 μg RNA, TwoRA from 10 ng RNA or RS or pRS from 10 ng RNA. A-D: 3′/M and 3′/5′ ratios for GAPDH and β-actin, n=3 for each ratio. *Significant differences between MK and MUR RNA. Note that no significant differences are found for OneRA and for ratios that span short distances.

As expected, comparisons of targets populations prepared by different amplification methods yielded poorer call concordances and signal intensity correlations than comparisons of targets populations prepared by the same method (9; 14). This difference illustrates the presence of system-specific biases.

Call concordances were higher between the two T7-based systems, OneRA and TwoRA, than between T7- and Ribo-SPIA™-based systems (Table 2.5), most likely due to the greater similarity of the methods and the similar number of present calls. Although RS and pRS are similar methods, they differed greatly in the number of present calls, which resulted in a poorer call concordance. Signal correlation coefficients within the two T7-based (OneRA and TwoRA) or within the two Ribo-SPIA™-based methods (RS and pRS) were significantly higher than any comparison between these methods (Table 2.5, Fig. 2.9 E-H). The observation that A-P calls between OneRA and TwoRA or between OneRA and pRS were significantly larger than P-A calls is consistent with amplification of rare messages by TwoRA and pRS. Amplification is likely to raise signal intensities of rare genes above the noise level (6).

Differential gene expression was computed in an attempt to cancel system-dependent biases. Nevertheless, correlation between ratios of targets prepared by T7-based systems, TwoRA and OneRA, was considerably better than between ratios of T7- and Ribo-SPIA™-based methods (Fig. 2.9 G-I). This observation underscores the presence of system specific biases.

All nanogram amplification methods, TwoRA, RS and pRS, yielded sufficient material for gene array work, although TwoRA yielded quantitatively more cRNA than RS or pRS yielded cDNA. The RS and pRS target preparation methods produced results comparable to those observed using more traditional T7-based methods and will enable studies of smaller RNA samples because the required input level is lower and the time and effort required for amplification are lower. pRS reproducibly amplified the highest number of targets and was found to be suitable for amplification of total RNA from amounts as low as 0.3 ng. Reproducibility and sensitivity of TwoRA, relative to OneRA, were higher than those of RS or pRS. All amplification systems, OneRA, TwoRA, RS and pRS, amplified large overlapping sets of targets. Target preparations using RS and pRS were faster and produced cDNA, which is more stable than cRNA and thus can be banked for additional studies. The presence of system-specific

biases prompts the recommendation that changes in amplification methodology within a study be avoided. Indeed, in the anticipation of future refined studies on nanogram amounts RNA, investigators may want to choose a nanogram amplification system for a pilot study even if microgram amounts of RNA are available.

Acknowledgments

Grants

Disclosures

J. D. Heath and N. Kurn are employees of NuGEN Technologies, Inc. M. Wang and G. Deng were employees of NuGEN at the time this study was conducted. NuGEN has patents and patents pending on some of the products and processes described in this article.

References

1. **Baugh LR, Hill AA, Brown EL and Hunter CP**. Quantitative analysis of mRNA amplification by in vitro transcription. *Nucleic Acids Res* 29: E29, 2001.

2. **Deng G, Dafforn A, Wang M, Chen P, Purohit S, Wang S, Pillarisetty S, Iglehart D, Koritala S, Lato S, Herrler M, Heath J, Stanchfield J and Kurn N.A**. A new method for amplification and labeling of RNA from small clinical samples for use with the Affymetrix eneChip platform. *Am Soc Human Genetics* 53: 1507, 2003.

3. **Eberwine J**. Amplification of mRNA populations using aRNA generated from immobilized oligo(dT)-T7 primed cDNA. *Biotechniques* 20: 584-591, 1996.

4. **Feldman AL, Costouros NG, Wang E, Qian M, Marincola FM, Alexander HR and Libutti SK**. Advantages of mRNA amplification for microarray analysis. *Biotechniques* 33: 906-12, 914, 2002.

5. **Heath J, Brooks A, Richfield E, Thiruchelvam M, Cory-Slechta D, Wang M, Chen P, Dafforn A, Deng G, Iglehart D, Koritala S, Lato S, Pillarisetty S, Rurohit R, Herrler M, Stanchfield J and Kurn N**. Comparative gene expression analysis of microdissected brain tissues in a mouse model of idiopathic Parkinsons disease using a novel RNA amplification system. *Am Soc Human Genetics* 53: 1553, 2003.

6. **Hu L, Wang J, Baggerly K, Wang H, Fuller GN, Hamilton SR, Coombes KR and Zhang W**. Obtaining reliable information from minute amounts of RNA using cDNA microarrays. *BMC Genomics* 3: 16, 2002.

7. **Iscove NN, Barbara M, Gu M, Gibson M, Modi C and Winegarden N**. Representation is faithfully preserved in global cDNA amplified exponentially from sub-picogram quantities of mRNA. *Nat Biotechnol* 20: 940-943, 2002.

8. **Karsten SL, Van Deerlin VM, Sabatti C, Gill LH and Geschwind DH**. An evaluation of tyramide signal amplification and archived fixed and frozen tissue in microarray gene expression analysis. *Nucleic Acids Res* 30: E4, 2002.

9. **Kenzelmann M, Klaren R, Hergenhahn M, Bonrouhi M, Grone HJ, Schmid W and Schutz G**. High-accuracy amplification of nanogram total RNA amounts for gene profiling. *Genomics* 83: 550-558, 2004.

10. **Kuai L, Fang F, Butler JS and Sherman F**. Polyadenylation of rRNA in Saccharomyces cerevisiae. *Proc Natl Acad Sci U S A* 101: 8581-8586, 2004.

11. **Lockhart DJ, Dong H, Byrne MC, Follettie MT, Gallo MV, Chee MS, Mittmann M, Wang C, Kobayashi M, Horton H and Brown EL**. Expression monitoring by hybridization to high-density oligonucleotide arrays. *Nat Biotechnol* 14: 1675-1680, 1996.

12. **Luzzi V, Mahadevappa M, Raja R, Warrington JA and Watson MA**. Accurate and reproducible gene expression profiles from laser capture microdissection, transcript amplification, and high density oligonucleotide microarray analysis. *J Mol Diagn* 5: 9-14, 2003.

13. **Makrigiorgos GM, Chakrabarti S, Zhang Y, Kaur M and Price BD**. A PCR-based amplification method retaining the quantitative difference between two complex genomes. *Nat Biotechnol* 20: 936-939, 2002.

14. **McClintick JN, Jerome RE, Nicholson CR, Crabb DW and Edenberg HJ**. Reproducibility of oligonucleotide arrays using small samples. *BMC Genomics* 4: 4, 2003.

15. **Pabon C, Modrusan Z, Ruvolo MV, Coleman IM, Daniel S, Yue H and Arnold LJ, Jr.** Optimized T7 amplification system for microarray analysis. *Biotechniques* 31: 874-879, 2001.

16. **Puskas LG, Zvara A, Hackler L, Jr. and van Hummelen P**. RNA amplification results in reproducible microarray data with slight ratio bias. *Biotechniques* 32: 1330-4, 1336, 1338, 1340, 2002.

17. **Rosenow C, Saxena RM, Durst M and Gingeras TR**. Prokaryotic RNA preparation methods useful for high density array analysis: comparison of two approaches. *Nucleic Acids Res* 29: E112, 2001.

18. **Schwille P, Oehlenschlager F and Walter NG**. Quantitative hybridization kinetics of DNA probes to RNA in solution followed by diffusional fluorescence correlation analysis. *Biochemistry* 35: 10182-10193, 1996.

19. **Spiess AN, Mueller N and Ivell R**. Amplified RNA degradation in T7-amplification methods results in biased microarray hybridizations. *BMC Genomics* 4: 44, 2003.

20. **Stears RL, Getts RC and Gullans SR**. A novel, sensitive detection system for high-density microarrays using dendrimer technology. *Physiol Genomics* 3: 93-99, 2000.

21. **Van Gelder RN, von Zastrow ME, Yool A, Dement WC, Barchas JD and Eberwine JH**. Amplified RNA synthesized from limited quantities of heterogeneous cDNA. *Proc Natl Acad Sci U S A* 87: 1663-1667, 1990.

22. **Wang E, Miller LD, Ohnmacht GA, Liu ET and Marincola FM**. High-fidelity mRNA amplification for gene profiling. *Nat Biotechnol* 18: 457-459, 2000.

23. **Wangemann P, Itza EM, Albrecht B, Wu T, Jabba SV, Maganti RJLJH, Everett LA, Wall SM, Royaux IE, Green ED and Marcus DC**. Loss of KCNJ10 protein expression abolishes endocochlear potential and causes deafness in Pendred syndrome mouse model. *BMC Medicine* 2: 30, 2004.

24. **Wu P, Nakano S and Sugimoto N**. Temperature dependence of thermodynamic properties for DNA/DNA and RNA/DNA duplex formation. *Eur J Biochem* 269: 2821-2830, 2002.

CHAPTER 3 - Free radical stress-mediated loss of Kcnj10 protein expression in stria vascularis contributes to deafness in Pendred syndrome mouse model

Abstract

Pendred syndrome is due to loss-of-function mutations of *Slc26a4*, which codes for the HCO_3^- transporter pendrin. Loss of pendrin function causes deafness via a loss of the K^+ channel Kcnj10 in stria vascularis and consequent loss of the endocochlear potential. Pendrin and Kcnj10 are expressed in different cell types. Here we report that free radical stress provides a link between the loss of Kcnj10 and the loss of pendrin. Studies were performed using native and cultured stria vascularis from *Slc26a4*^{+/-} and *Slc26a4*^{-/-} mice as well as CHO-K1 cells. Kcnj10, oxidized proteins and proteins involved in iron metabolism were quantified by Western blotting. Nitrated proteins were quantified by ELISA. Total iron was measured by ferrozine spectrophotometry and gene expression was quantified by qRT-PCR. At postnatal day 10 (P10), stria vascularis from *Slc26a4*^{+/-} and *Slc26a4*^{-/-} mice expressed similar amounts of Kcnj10. *Slc26a4*^{-/-} mice lost Kcnj10 expression during the next 5 days of development. In contrast, stria vascularis, obtained from P10 *Slc26a4*^{-/-} mice and kept in culture for 5 days, maintained Kcnj10 expression. Stria vascularis from *Slc26a4*^{-/-} mice was found to suffer from free radical stress evident by elevated amounts of oxidized and nitrated proteins and other changes in protein and gene expression. Free radical stress induced by 3-morpholinosydnonimine-N-ethylcarbamide (SIN-1) was found to be sufficient to reduce Kcnj10 expression in CHO-K1 cells. These data demonstrate that free radical stress provides a link between loss of pendrin and loss of Kcnj10 in *Slc26a4*^{-/-} mice and possibly in human patients suffering from Pendred syndrome.

Keywords

Cochlea; pendrin; oxidation; nitration

Introduction

Pendred syndrome, the most frequent hereditary form of syndromic deafness, is an autosomal recessive disease that affects the inner ear and the thyroid and causes childhood deafness and post puberty goiter (9; 21; 29). It is caused by loss-of-function mutations of the gene *SLC26A4*, which encodes the anion exchanger pendrin (13; 16; 32). Pendrin has been

characterized in heterologous expression systems to be an anion exchanger that accepts Cl^-, $HCO3^-$, I^-, and formate (37).

Investigations of the cause of deafness in Pendred syndrome have recently been facilitated by the creation of mouse model (12). The following observations have been made in the Pendred syndrome mouse model: 1) Enlargement of endolymphatic spaces prenatally. 2) Acidification of endolymph at P10. 3) Increased Ca^{2+} concentration in the endolymph at P10. 4) Reduction in endocochlear potential at P10. 5) Loss of Kcnj10 protein expression at P15; 6) Macrophage invasion in stria vascularis at ~P35. 7) No changes in endolymphatic K^+ concentration in adult mice. 8) Degeneration of strial marginal cells in adult mice (12; 20; 42; 44).

In the cochlea, pendrin is mainly expressed in the apical membrane of outer sulcus and spiral prominence epithelial cells that border endolymph (Fig. 3.1) (14; 42). The observation that loss of pendrin leads to acidification of endolymph suggests that pendrin mediates HCO_3^- secretion (28; 44).

Sensory transduction in the cochlea depends on the endocochlear potential, which is generated by the K^+ channel Kcnj10 in stria vascularis (26; 41). The generation of a small endocochlear potential at P10 is consistent with the expression of K^+ channel Kcnj10. Both Kcnj10 expression and endocochlear potential are lost during further development and consequently *Slc26a4*$^{-/-}$ mice never develop hearing (42; 44).

Loss of pendrin cannot directly affect Kcnj10 protein expression, since Kcnj10 and pendrin are expressed in different cells in the cochlear lateral wall (Fig. 3.1A) (42; 44). In this study we hypothesize that free radical stress could be the link between loss of pendrin and reduction of Kcnj10 protein expression.

Increased oxidative stress in the Pendred Syndrome mouse model may be a consequence of enlarged endolymphatic spaces and/or the acidic endolymph. The K^+ concentration is maintained at normal levels in the enlarged *Slc26a4*$^{-/-}$ endolymph volume, which implies increased rates of K^+ secretion by stria vascularis to compensate for K^+ leakage (42). The rate of ion transport correlates with ATP production and metabolism in stria vascularis (23; 25).

Elevated rates of K^+ secretion in the stria vascularis of *Slc26a4*$^{-/-}$ mice could enhance free radical stress as a result of increased energy metabolism, which is a major source of oxygen free radicals. Oxidative stress in stria vascularis may also be a consequence of endolymph acidification. The acidic pH of endolymph could reduce the cytosolic pH in strial marginal cells that border endolymph. Cytosolic acidification is a condition favorable to release of iron from proteins and in the presence of superoxide anion ($O_2^{\bullet-}$), nitric oxide radical ($\bullet NO$) leads to the formation of peroxynitrite ($ONOO^-$) and hydroxyl radical ($^{\bullet}OH^-$) (4; 10).
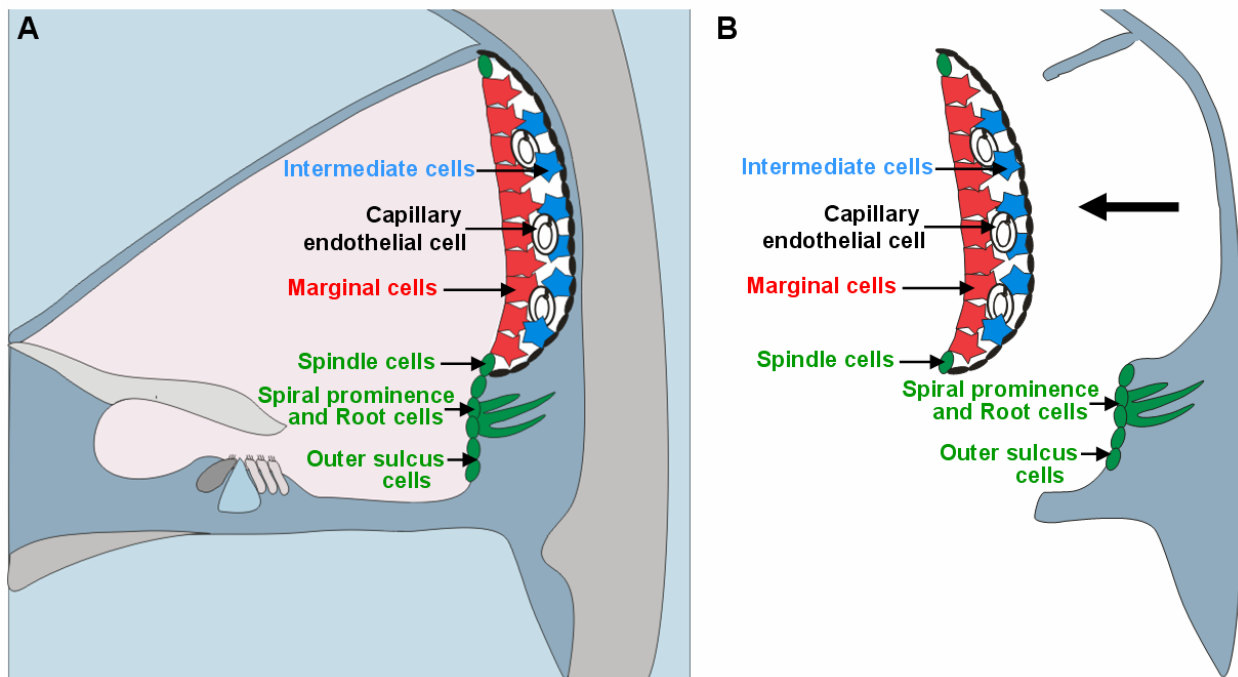
Figure 3.1: Schematic diagram for Kcnj10 and pendrin expression in the cochlea.
(A) Kcnj10 *is expressed in intermediate cells (blue) inside stria vascularis and pendrin is mainly expressed in spiral prominence epithelial cells, root cells and in outer sulcus epithelial cells (green). (B) Two preparations were obtained from the lateral wall of the cochlea. The preparation of stria vascularis contained the K^+ channel* Kcnj10 *and the preparation of spiral ligament contained pendrin in cells located in spiral prominence epithelial cells, root cells and in outer sulcus epithelial cells. Both* Kcnj10 *and pendrin are lost in Slc26a4*$^{-/-}$ *mice. The preparation of spiral ligament also contained remnants of Reissner's membrane in addition to the spiral ligament.*

Oxygen free radicals can originate from a leaky electron transfer in the mitochondrial electron transport chain during production of ATP. Incomplete reduction of O_2 during metabolism generates the free radical ($O_2^{\bullet-}$), which spontaneously dismutates to hydrogen peroxide (H_2O_2). These two reactive oxygen species can be involved in further reactions that

generate more aggressive, damaging radicals. In the presence of Fe^{2+}, H_2O_2 can enter into the Fenton reaction that yields the extremely aggressive $^{\bullet}OH^-$. $\bullet NO$ synthesized by nitric oxide synthase can react with $\bullet O_2^-$ to yield peroxynitrite ($ONOO^-$) which decomposes to form $\bullet OH^-$ and nitrate radical ($\bullet NO_2$) (5; 40). Transition metal ions bound to lipids and proteins can react with H_2O_2, $^{\bullet}OH^-$ and $\bullet NO_2$ to generate intermediates that subsequently cause oxidation and nitration of proteins and lipids, impairing the ability of the cell to function normally (30; 38).

Defense mechanisms against free radical stress entail sequestration of catalysts that promote the formation of free radicals and detoxification by chemical conversion. The free radical $\bullet O_2^-$ can be converted to O_2 and H_2O by superoxide dismutase in conjunction with catalase or glutathione peroxidase. Catalysts that generate free radicals, such as Fe, Zn and Cu, are sequestered by ferritin, metallothionein, and ceruloplasmin (34; 36; 46). The cellular availability of the catalyst Fe is controlled via transcriptional and translational mechanisms. The expression of the Fe chelator transferrin (*Trf*) and the uptake mechanism transferrin receptor (*Tfrc*) are controlled by an iron-response protein, aconitase (*Aco1*) (8; 11). When the cytosolic free Fe concentration is high, retardation of *Tfrc* mRNA degradation is lifted and translation of *Trf* is promoted leading to an increased expression of the chelator *Trf* and a decreased expression of the Fe uptake mechanism *Tfrc*. Together, these changes in the expression of Fe related proteins can mediate a reduction in the cytosolic free Fe concentration. Decreases in *Tfrc* transcript and increases in *Trf* protein expression, however, are often not sufficient to control oxidative stress and can be taken as an indication for the presence of Fe-mediated oxidative stress.

In the present study, we obtained direct and indirect measures of oxidative and nitrative stress before and after the onset of hearing in stria vascularis and a preparation of spiral ligament that included pendrin-expressing outer sulcus and spiral prominence epithelial cells. The levels of oxidized and nitrated proteins in conjunction with the mRNA expression of genes involved in antioxidant defenses were used to assess oxidative and nitrative stress. We evaluated the impact of oxidative and nitrative stress on the protein levels of Kcnj10 using an expression system model. To ascertain whether the loss of Kcnj10 was a consequence of the conditions prevalent in the stria vascularis of *Slc26a4$^{-/-}$*mice, stria vascularis from P10 organ cultures and the corresponding time points *in vivo* were compared for the protein level expression of Kcnj10.

Methods

Animal use and tissue preparations

The *Slc26a4*^{-/-} mouse strain was created in the laboratory of Dr.Eric Green at the National Institute of Health (12). *Slc26a4*^{-/-} and *Slc26a4*^{+/-} mice were raised in a colony at Kansas State University that was established with breeders kindly provided by Dr. Susan Wall (Emory University). Mice were deeply anesthetized with tribromoethanol (560 mg/kg, i.p.) and sacrificed by transcardial perfusion with Cl⁻ free solution. Cl⁻ free solution contained (in mM) 150 Na-gluconate, 1.6 K_2HPO_4, 0.4 KH_2PO_4, 4 Ca^{2+}-gluconate, 1 $MgSO_4$ and 5 glucose, pH 7.4. Temporal bones housing the cochleae were removed and separate fractions of stria vascularis and spiral ligament were obtained by microdissection (Fig. 3.1B). All procedures concerning animals were approved by the Institutional Animal Care and Use Committee of Kansas State University.

Quantitative RT-PCR

Real time RT-PCR in presence of SYBR green (Molecular Probes, Eugene, OR) was carried out in 96-well plates (OneStep RT-PCR Kit, Qiagen Valencia, CA; iCycler, BioRad, Hercules,CA) using gene specific primers (Table 3.1). Transcripts were quantified in paired experiments using one master mix and total RNA isolated from pairs of age and sex matched *Slc26a4*^{-/-} and *Slc26a4*^{+/-} mice. RT was performed for 30 min at 50°C and terminated by heating to 95°C for 15 min. PCR consisted of 40 cycles of 1 min annealing at 60°C, 1 min elongation at 72°C, 20s hot-measurement at 78°C, and 1 min denaturation at 94°C. Amplification of a single product was verified by gel electrophoresis and identity of the product was verified once by sequencing. The number of template molecules (T) was calculated according to T = 10^ log (number of molecules at C_t) / (PCR efficiency^C_t). C_t was defined as the cycle at which the fluorescence of the product molecules reached a set threshold. The number of molecules at C_t was calibrated by amplifying known numbers of 18S rRNA molecules. The content of 18S in total RNA was estimated under the assumption that total RNA consists of 100% of 18S and 28S rRNA. PCR efficiency was obtained from the slope of the log-linear phase of the growth curve (31).

Table 3.1: Gene specific primers

Gene	Primers	Product size
Superoxide dismutase (*Sod2*)	aca agc aca gcc tcc cag a (*sense*) tag cct cca gca act ctc ct (*antisense*)	291 bp
Metallothionein 3 (*Mt3*)	gga tat gga ccc tga gac (*sense*) gac acc cag cac tat tta c (*antisense*)	260 bp
Aconitase (*Aco1*)	cag gat gga tgc tac tac c (*sense*) gga ggt gct tgg taa tgg (*antisense*)	232 bp
Transferrin (*Trf*)	act gct ctg cct tga caa tac (*sense*) cac gcc ttc ctg ctg att c (*antisense*)	319 bp
Transferrin receptor (*Trfr*)	ttc cgc cat ctc agt cat cag (*sense*) tgg act tcg ccg caa cac (*antisense*)	300 bp
Ferritin (*Ftl1*)	agc gtc tcc tcg agt ttc ag (*sense*) agg ttg gtc aga tgg ttg c (*antisense*)	200 bp

Isolation of protein

Tissue fractions were transferred from the dissection dish into 0.5 ml microcentrifuge tubes and Cl⁻ free solution was removed after a pulse spin. Four different methods for protein isolation were used. Method 1: Proteins were extracted by first adding 20 µl protein extraction buffer 1 (ReadyPrep Sequential Extraction Kit, Cat# 163-2101 and 163-2102, BioRad) and vortexing for 3 min. The homogenized tissue was centrifuged at 16,000 rpm for 10 min at RT. Subsequently extraction buffer 2 was added and the process was repeated. Proteins in the supernatant were transferred into a new tube and either used immediately or stored at -80°C. Method 2: Proteins were extracted by adding 30 µl of Tris-Triton buffer (50 mM Tris, 150 mM NaCl, 1% Triton-X) and incubating for 30 min in a sonicating water bath at 0°C (Fisher Scientific FS20). Proteins in the supernatant were transferred to a new tube and either used immediately or stored at -80°C. Method 3: Proteins were extracted by adding 30 µl of Tris-SDS buffer (50 mM Tris, 150 mM NaCl, 0.5% SDS) and incubating for 30 min in a sonicating water bath at 0°C. Proteins in the supernatant were transferred to a new tube and either used immediately or stored at -80°C. Method 4: The tissue was fixed in 0.6 N trichloroacetic acid on ice, centrifuged at 15,000 rpm for 10 min at 4°C and the supernatant was removed. The proteins were extracted by adding 30 µl of Urea buffer (9 M Urea, 0.065 mM DTT, 2% Triton-X) and incubating for 30 min in a sonicating water bath at 0°C. The protein containing solution was neutralized by adding 1 M Tris. To this solution 5 µl of 1% SDS was added and resulting

mixture was incubated for 30 min in a sonicating water bath at 0°C. Proteins in the supernatant were transferred to a new tube and either used immediately or stored at -80°C.

Detection of oxidized proteins

Carbonyl groups of oxidized proteins were derivatized with dinitrophenylhydrazine (Oxyblot Kit, Cat# S7150, Millipore, Billerica) to form denitrophenylhydrazone (DNP). DNP-labeled proteins were separated by SDS gel electrophoresis (5µl/lane) and detected in Western blots. Procedures were carried out according to manufacturer's recommendations. Differences in the presence of oxidized proteins were evaluated by comparison to the expression of *actin* or tubulin.

Quantitation of nitrotyrosine by ELISA

Protein was isolated using the Tris-Triton method (method 2) and the level of nitrotyrosine was quantified by two different immunoabsorbent assays (Cat# HK501, Cell sciences, Canton, MA; Cat#17-376, Millipore) according to manufacturer's recommendation. The total protein content of the sample was measured. (NanoOrange protein quantitation kit, Cat # N666, Invitrogen, Carlsbad, CA). Differences in the amount of nitrotyrosine was evaluated by comparison of nitrated protein content to the total protein content.

Quantitative western blotting

An equal volume of Laemelli buffer containing 5% β-mercaptoethanol was added to the protein samples and incubated at 75°C for 10 min. Protein samples (15 µl) were separated by SDS-PAGE gel electrophoresis (4-15% Tris-SDS Polyacrylamide Precast Gels, BioRad). After separation, proteins were transferred to either nitrocellulose or PVDF membranes (0.2 µm pore size, BioRad), blocked with 5% dry milk in TBS-Tween (137 mM NaCl, 20 mM Tris-Cl, 0.1% Tween-20, pH 7.6) and probed with primary antibodies (rabbit anti-Kcnj10, 1:1000, Cat# APC-035, Alomone labs, Jerusalam, Israel; mouse anti-Kcnj10, Cat# H00003766-M01, Novus Biologicals, Littleton, CO; rabbit anti-*trf*, 1:750, Cat #A76, Biomeda, Foster City, CA; mouse anti-*tfrc* 1:2,000, Cat #13-6800, Zymed, San Francisco, CA; rabbit anti-actin, 1:1000, Cat# A2066, Sigma, St. Louis, MO; rabbit anti-tubulin, 1:500, Cat# ab6046, Cambridge, MA).

Membranes were washed 4x for 15 min in TBS-Tween and incubated with HRP-conjugated secondary antibodies (anti-rabbit, 1:100,000, Cat# 1858415; anti-mouse, 1:100,000, Cat# 1858416, Pierce, Rockford, IL). After washing, 4x for 15 min in TBS-Tween, HRP was detected by chemiluminescence (SuperSignal West Femto Maximum Sensitivity Substrate, Cat# 34095, Pierce) using a camera based imaging workstation (4000MM, Kodak). Quantification of oxidized proteins and of Kcnj10 protein was carried out by integration of signals arising from specific staining (Fig. 3.2). Differences in Kcnj10 expression was evaluated by comparison to the expression of actin or tubulin.
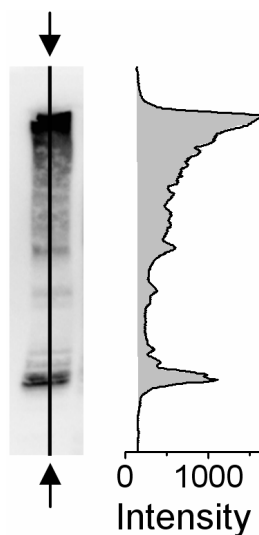
Figure 3.2: Illustration of the method used for the quantification of oxidized proteins and of Kcnj10 protein expression.
Chemiluminescence was detected a digital format using a camera-based system (Kodak 4000 MM). Staining, consisting of both smears and bands, was observed for oxidized proteins as well as for Kcnj10 protein. The specificity of smears and bands was confirmed in independent experiments. The intensity of staining was integrated over the entire length of the blot.

Immunoprecipitation

Protein was isolated using the Tris-Triton method (method 2). An equal volume of sepharose protein G beads (Cat#P3296, Sigma) was added to protein lysate followed by incubation on ice for 60 min. This mixture was spun at 10000 x g for 10 min at 4°C and the supernatant (precleared lysate) was transferred to a fresh microcentrifuge tube. 10 μg of mouse monoclonal antibody for Kcnj10 was added to the cold precleared lysate and the mixture was incubated at 4°C for 1 hr. 50 μl of protein G beads washed in Tris-Triton buffer was added to the antibody-lysate mixture followed by incubation for 3 hr at 4°C on a shaker. The supernatant

was removed after a quick spin (10000 x g for 30 sec) and the beads were washed 4x in Tris-Triton buffer. 50 µl of 1x Laemelli buffer was added to the bead pellet and this mixture was vortexed and heated at 95°C for 15 min followed by centrifugation at 10000 x g for 5 min. The supernatant was collected in a fresh microcentrifuge tube and used as the sample for Western blotting.

Quantification of total tissue Fe content

Total tissue Fe content (*tissue-Fe*) was measured using a modified ferrozine-based assay (15). Freshly isolated tissue fractions of stria vascularis and spiral ligament were transferred into microcentrifuge tubes and Cl^--free solution was removed. Guanidine hydrochloride (2 µl) was added to the tissue and mixing was facilitated by a pulse spin. After incubation for 45 min at 60°C, 2 µl of FAT solution was added. FAT solution contained 0.5 M ferrozine, 0.5 M ascorbic acid and 1 M Tris-Cl, pH 7. Mixing was facilitated by a pulse spin and the tissue was incubated for 45 min at 60°C. Absorbance at 562 nm was measured in the supernatant of the 4 µl sample (ND1000, Nanodrop Technologies) and standards containing $FeCl_2$ that were processed in parallel. Following *Tissue-Fe* measurements, the total protein content of samples was determined (NanoOrange Protein Quantitation Kit). Measurements of the *Tissue-Fe* are reported per mg protein.

Organ culture

Freshly microdissected stria vascularis from P10 *Slc26a4$^{-/-}$* and *Slc26a4$^{+/-}$* mice was cultured in 35 mm flat bottom culture dishes (Cat# 08-757-100A, Fisher) containing 2 ml media for 1, 3 and 5 days. The media consisted of DMEM (Cat# 30-2002, ATCC) supplemented with 10 % fetal bovine serum (FBS, Cat# 30-2020, ATCC)FBS, 500 µM furosemide (Cat# F4381, Sigma-Aldrich) in) and 1% pencillin-streptomycin antibiotic mixture. The media was changed every day. Cultured stria vascularis at the end of 1, 3 and 5 days was transferred from the culture dish to a 0.5 ml microcentrifuge tube and washed twice with Cl^- free solution to remove excess media. Protein was isolated using the Tris-Triton buffer (method 3). Protein was either used immediately or stored at -80°C.

Cell culture

Chinese hamster ovary cells, CHO-K1 (Cat# CRL-9618, ATCC, Manassas, VA) were cultured as monolayers in Dulbecco's minimal essential medium (DMEM) supplemented with 10% FBS and 1% pencillin-streptomycin antibiotic mixture (Cat# 30-2300, ATCC) in a cell culture incubator maintained at 37°C and 5% CO_2. The CHO-K1 cells were transfected in a T25 flask (Cat # 10-126-39, Fisher, St. Louis, MO) with a GFP-*Kcnj10*-Export sequence plasmid (a generous gift from Dr. Nikolaj Klocker, Dept of Physiology, University of Freiburg, Germany) using Lipofectamine 2000™ (Cat# 11668-019, Invitrogen) according to manufacture's instructions. The CHO-K1 cells containing the GFP-*Kcnj10*-Export plasmid were split 24 hrs post transfection and seeded in three wells. To replicate the conditions of organ culture, 500 µM furosemide was added to each well 48 hours post transfection and wells were subjected to different levels of oxidative and nitrative stress. The first of the three wells was exposed to oxidative stress by adding 10 µM H_2O_2 (Cat# H1009, Sigma-Aldrich, St. Louis, MO). The second well was exposed to oxidative and nitrative stress by adding 1 mM SIN-1 hydrochloride (Cat# M5793, Sigma-Aldrich). The third well served as a control. This protocol was devised to ensure that differences in transfection efficiency did not impact the results. After twelve hours, cells were lysed and protein was extracted using the Tris-Triton buffer. Protein was either used immediately or stored at -80°C.

Statistical Analysis

Data are expressed as averages ± SE. Data were compared by paired and unpaired t-test as appropriate. Significance was assumed at $P < 0.05$.

Results

Stria vascularis contains elevated levels of nitrated proteins

The amount of nitrated proteins in relationship to the total protein was quantified at ages P15 and P35 in stria vascularis and the spiral ligament preparation of *Slc26a4*^{-/-} and *Slc26a4*^{+/-} mice (Fig. 3.3A). Increased levels of nitration were observed in stria vascularis but not in the

spiral ligament preparation of *Slc26a4⁻/⁻* compared to *Slc26a4⁺/⁻* mice. The increased levels of nitrated proteins suggest that stria vascularis of *Slc26a4⁻/⁻* mice is under increased nitrative stress.

A   Nitrated proteins
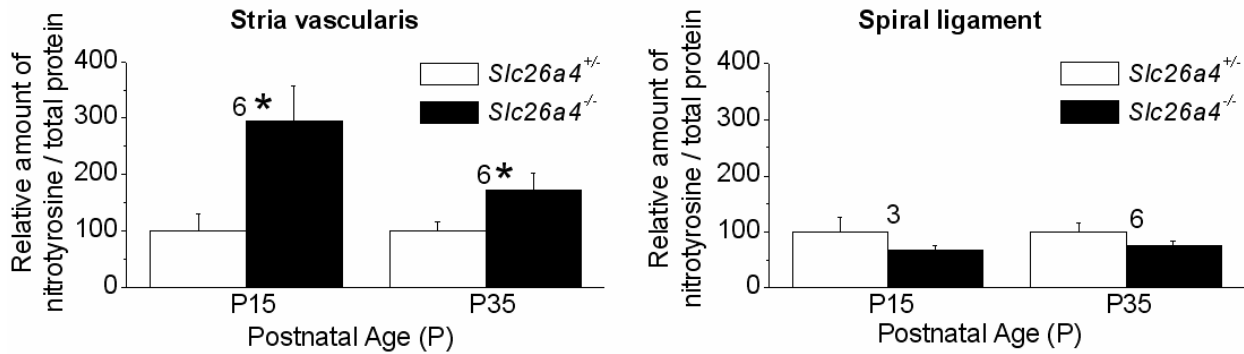
B   Oxidized proteins
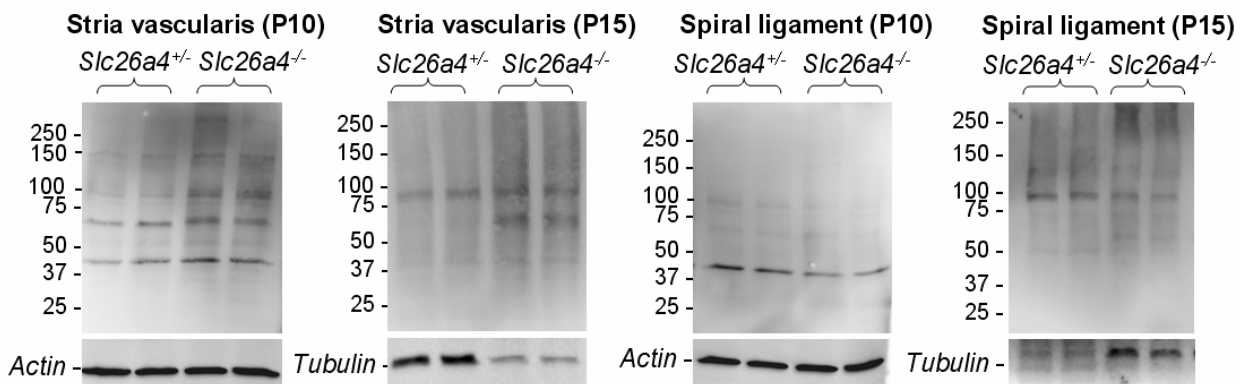
Figure 3.3: Quantification of nitrated and oxidized proteins.
(A) Nitrated proteins were quantified against total protein in stria vascularis and in the preparation of spiral ligament in Slc26a4⁺/⁻ and Slc26a4⁻/⁻ mice at ages P15 and P35. Data are presented as percent of nitrated protein in stria vascularis of Slc26a4⁺/⁻ mice. Significant changes are marked (*) and numbers next to the bars represent the number of experiments. (B) Oxidized proteins were quantified against actin *or* tubulin *in stria vascularis and in the preparation of spiral ligament in Slc26a4⁺/⁻ and Slc26a4⁻/⁻ mice at ages P10 and P15. Representative examples of three experiments are shown. Increased amounts of nitrated and oxidized proteins were found in stria vascularis but not in the preparation of spiral ligament of Slc26a4⁻/⁻ mice. The presence of nitrated and oxidized proteins indicates increased nitrative and oxidative stress in stria vascularis.*

Stria vascularis contains elevated levels of oxidized proteins

The presence of oxidized proteins was evaluated at P10 and P15 in the stria vascularis and the spiral ligament preparation of *Slc26a4⁻/⁻* and *Slc26a4⁺/⁻* mice (Fig. 3.3B). Detection of

oxidized proteins involved DNP-labeling of carbonyl groups in oxidized proteins by derivatization with DNPH. DNP-labeled proteins were detected by Western blot. No labeling was observed in the absence of derivatization. The levels of oxidized proteins were increased in stria vascularis but not in the spiral ligament preparation of $Slc26a4^{-/-}$ compared to $Slc26a4^{+/-}$ mice. The increased levels of oxidized proteins indicate that stria vascularis of $Slc26a4^{-/-}$ mice is under increased oxidative stress.

Antioxidant defenses are reduced in stria vascularis

Transcripts coding for superoxide dismutase (*Sod2*) and metallothionein (*Mt3*) were quantified in stria vascularis and in the spiral ligament preparation of $Slc26a4^{-/-}$ and $Slc26a4^{+/-}$ mice (Fig. 3.4). Expression of *Sod2* was reduced in stria vascularis of $Slc26a4^{-/-}$ mice at ages P10 and P30. Further, transcripts for *Mt3* were reduced in stria vascularis of $Slc26a4^{-/-}$ mice at P15. No changes in expression of *Sod2* and *Mt3* were found in spiral ligament. These observations suggest that defenses against free radical stress are weakened in stria vascularis of $Slc26a4^{-/-}$ mice before and after the onset of hearing.

Altered iron metabolism in stria vascularis is consistent with oxidative stress

Transcripts were quantified in stria vascularis and in the spiral ligament preparation of $Slc26a4^{+/-}$ and $Slc26a4^{-/-}$ mice (Fig. 3.5). Transcripts included the Fe uptake mechanism transferrin receptor (*Tfrc*), the Fe chelator transferrin (*Trf*), the Fe storage protein ferritin (*Ftl1*), and the expression regulator iron responsive protein (*Aco1*). Quantifications were performed before (P10) and after the onset of hearing (P15), after weaning (P30-P35) and in adulthood (P75). The numbers of transcripts coding for *Tfrc* were found to be reduced in $Slc26a4^{-/-}$ mice and this reduction was observed in stria vascularis at all ages including P10, and in the spiral ligament preparation at P75. The number of transcripts coding for *Trf* was elevated in $Slc26a4^{-/-}$ mice compared to $Slc26a4^{+/-}$ mice and this elevation was observed in stria vascularis from P35 onward but not in the spiral ligament preparation. Transcripts for *Ftl1* were found reduced in number and this reduction was seen in stria vascularis from P15 onward and in the spiral ligament preparation at P10 and at P75. In addition, transcripts for *Aco1* were present in stria vascularis and spiral ligament of $Slc26a4^{+/-}$ and $Slc26a4^{-/-}$ mice. No difference in the number of

transcripts was seen in stria vascularis of *Slc26a4*^{-/-} compared to *Slc26a4*^{+/-} mice, however, transcripts in the spiral ligament preparation were reduced at P15 and at P75.
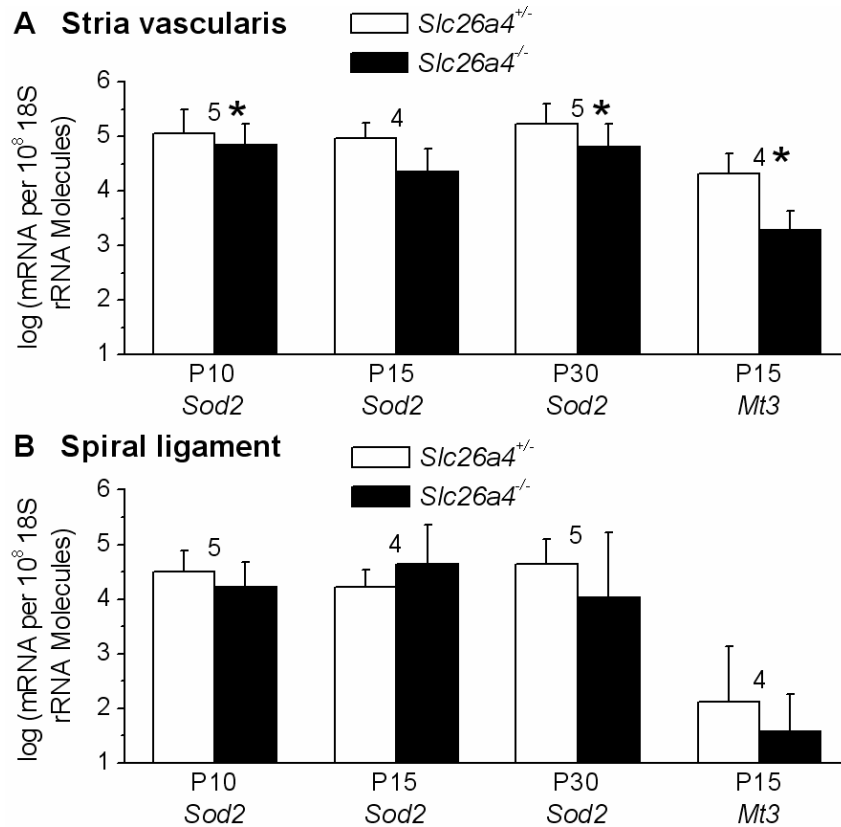
Figure 3.4: Quantification of transcripts coding for free radical defenses.
(A-B) Transcripts coding for superoxide dismutase (Sod2) and metallothionein (Mt3) were quantified relative to 18S in stria vascularis and in the preparation of spiral ligament from Slc26a4^{+/-} and Slc26a4^{-/-} mice at age P10, P15 and P30. Significant changes are marked (*) and numbers next to the data represent the number of animal pairs. Reductions in the number of transcripts, which indicates weakened defenses against free radical stress, were seen in stria vascularis but not in spiral ligament.

Protein expression of *Trf* and *Tfrc* was quantified at age P35 in stria vascularis and the spiral ligament preparation of *Slc26a4*^{+/-} and *Slc26a4*^{-/-} mice (Fig. 3.6). Protein expression of *Trf* was increased and protein expression of *Tfrc* was decreased in stria vascularis but not in the spiral ligament preparation of *Slc26a4*^{-/-} mice compared to *Slc26a4*^{+/-} mice. The increase in *Trf* expression is consistent with the increase in *Trf* transcripts (Fig. 3.5) and with *Aco1* mediated translational expression regulation via an elevated free Fe pool. The decrease in *Tfrc* expression is consistent with the observed decrease in transcripts and *Aco1* mediated transcriptional regulation via an elevated free Fe pool.
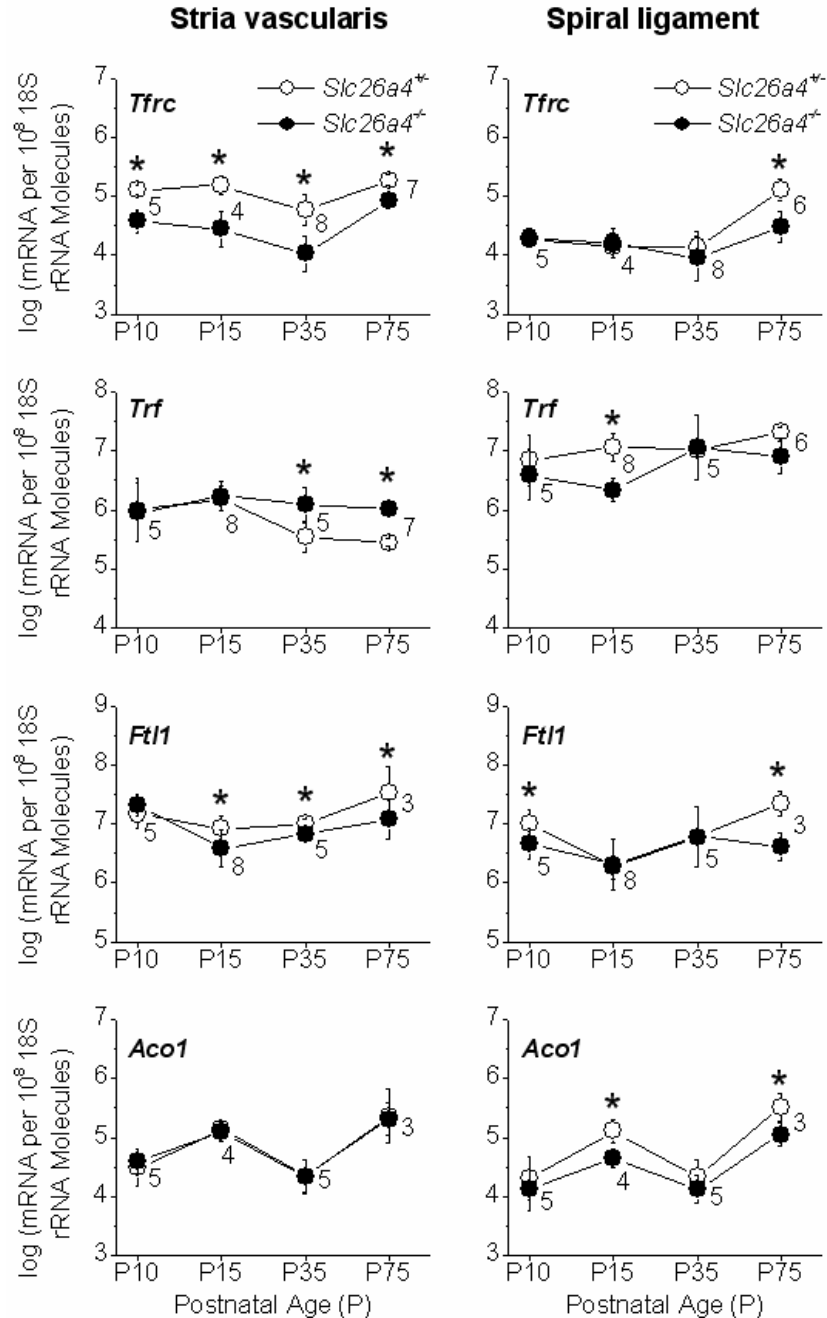
Figure 3.5: Quantification of transcripts coding for proteins involved in Fe metabolism.
Transcripts coding for transferrin receptor (Tfrc), transferrin (Trf), ferritin (Ftl1) and Fe responsive protein (Aco1) were quantified relative to 18S in stria vascularis (left-side graphs) and in the preparation of spiral ligament (right-side graphs) of Slc26a4$^{+/-}$ and Slc26a4$^{-/-}$ mice at different ages. Significant changes are marked (*) and numbers next to the data represent the number of animal pairs. The legend given pertains to all graphs. Reductions in Tfrc and Ftl1 transcripts were mainly seen in stria vascularis. The reduction in Tfrc transcripts is consistent with an elevated pool of free Fe and Aco1-regulated degradation of Tfrc mRNA and the reduction in Ftl1 transcripts is consistent with a reduced capacity to sequester Fe and Fe-mediated free radical stress.
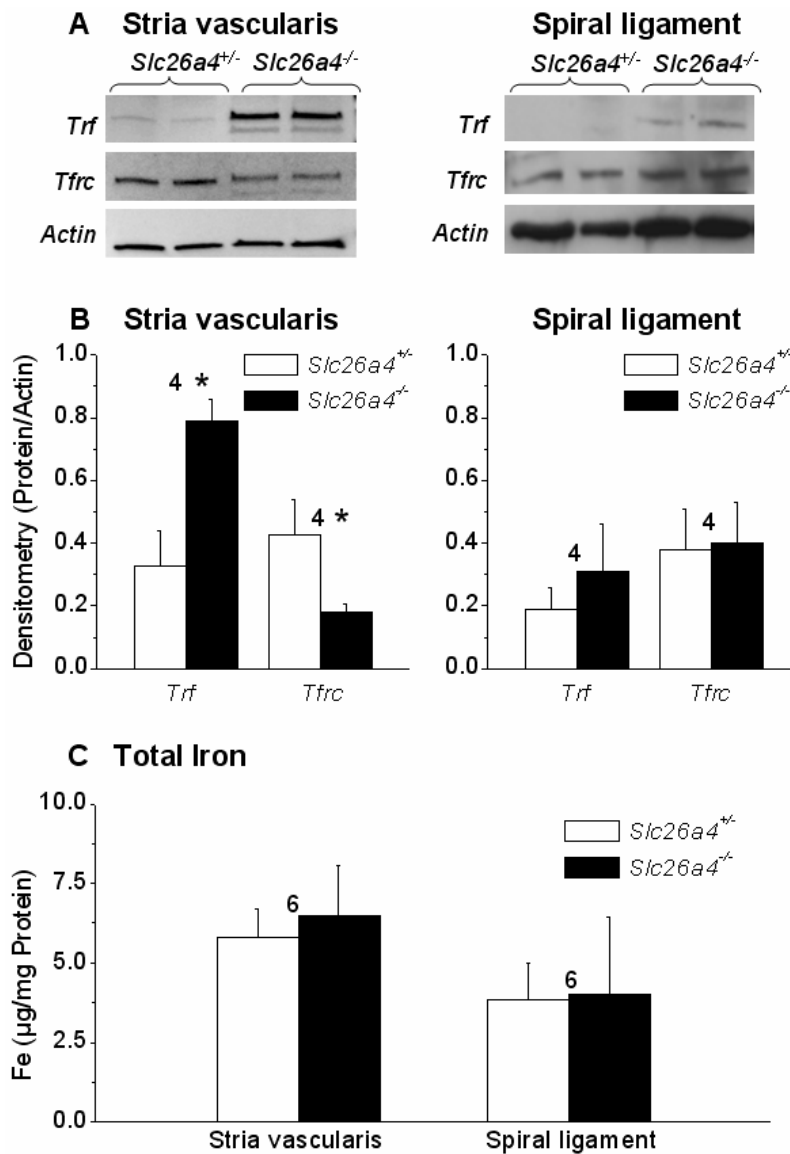
Figure 3.6: Quantification of proteins involved in Fe metabolism and total iron.
(A-B) Transferrin (Trf) and transferrin receptor (Tfrc) were quantified relative to actin *in stria vascularis and in the preparation of spiral ligament of Slc26a4$^{+/-}$ and Slc26a4$^{-/-}$ mice at age P35. Representative western blots and data summaries are shown. Significant changes are marked (*) and numbers next to the bars represent the number of blots. Changes in protein expression were seen in stria vascularis but not in the preparation of spiral ligament. (C) Tissue-Fe was quantified in stria vascularis and spiral ligament of Slc26a4$^{+/-}$ and Slc26a4$^{-/-}$ at age P10. No difference was found in tissue-Fe. The increase in Trf protein expression and the reduction in Tfrc protein expression is consistent with Fe-mediated free radical stress.*

Tissue-Fe was measured at age P10, before the onset of hearing, in stria vascularis and the spiral ligament preparation of *Slc26a4$^{+/-}$* and *Slc26a4$^{-/-}$* mice (Fig. 3.6). No difference in

Tissue-Fe was found in stria vascularis and spiral ligament of *Slc26a4$^{-/-}$* compared to *Slc26a4$^{+/-}$* mice.

The changes in the transcript and protein level expression of *Trf* and *Tfrc* indicate Fe-mediated oxidative stress in the stria vascularis of *Slc26a4$^{-/-}$* mice. The reduction in *Ftl1* transcripts is consistent with a reduced capacity to sequester Fe and weakened defenses against oxidative stress.

Western blot for Kcnj10 protein in stria vascularis

Before evaluating the effect of oxidative and nitrative stress on Kcnj10 protein expression, the specificity of Kcnj10 antibodies was evaluated. Western blots revealed a considerable interexperimental variability in the pattern of bands and smears detected by anti-Kcnj10 antibodies. Reprobing individual blots with two different anti-Kcnj10 antibodies, one of which was a monoclonal, revealed highly similar patterns of bands and smears (Fig. 3.7A vs. 3.7C and 3.7D vs. 3.7F). Differences in the pattern of bands and smears was a function of the protein extraction method. The interexperimental variability, however, was encountered with all methods of protein extraction (compare Fig. 3.7C and 3.7D). Immunoprecipitation with the mouse monoclonal and detection with the rabbit polyclonal antibody revealed monomers of Kcnj10 at ~40 kDa as well as higher molecular weight bands and smears (Fig. 3.7G). This observation confirmed that the mouse monoclonal and the rabbit polyclonal antibody recognized the same protein in samples from stria vascularis.

Further, incubating the primary antibody with a blocking peptide (KLEESLREQAEKEGSALSVR) resulted in the loss of all bands and smears (Fig. 3.7H and 3.7I). In this experiment, a single lane of a blot was probed for Kcnj10 protein using the rabbit polyclonal antibody, then stripped and cut into two pieces that were reprobed for Kcnj10 in the absence and presence of blocking peptide. The cut pieces were rejoined for detection. This experimental protocol was chosen to unambiguously demonstrate that the addition of blocking peptide is sufficient to prevent detection of Kcnj10. Taken together, these data verify that the rabbit polyclonal and the mouse monoclonal antibody detect Kcnj10 and that Kcnj10 in stria vascularis exists as monomers (~40 kDa), as well as in variable higher molecular weight

complexes. In subsequent experiments both smears and bands were regarded as Kcnj10 protein and quantification of expression was based on integrals of staining as shown in Fig. 3.2.

The variability in the pattern of Kcnj10 expression is likely due to the interaction with the dystrophin glycoprotein complex. This complex contains proteins that greatly vary in their mobility patterns due to variable glycosylations and stoichiometries. Kcnj10 protein has been shown to be associated with the dystrophin glycoprotein complex in brain and retina and with aquaporin 4 in retina (6; 7). Moreover, ubiquitination may contribute to the observed smears.

Progressive loss of Kcnj10 *expression in the stria vascularis of Slc26a4$^{-/-}$ mice*

Protein expression of Kcnj10 was quantified in stria vascularis before the onset of hearing (P10 and P11) and after the onset of hearing (P13 and P15) (Fig. 3.8). As expected stria vascularis of *Slc26a4$^{+/-}$* mice maintained and stria vascularis of *Slc26a4$^{-/-}$* mice progressively lost the expression of Kcnj10 protein. These results are consistent with previous studies showing loss of Kcnj10 protein expression at P15 by immunohistochemistry and the loss of endocochlear potential (44). The loss of Kcnj10 protein expression occurs at a time point when the stria vascularis of *Slc26a4$^{-/-}$* mice is under increased oxidative and nitrative stress. This finding suggests that increased oxidative and/or nitrative stress contributes to the loss of Kcnj10 protein expression in the stria vascularis of *Slc26a4$^{-/-}$* mice.

A: First Detection

Protein extraction: Urea | Triton | SDS

250 –
150 –
100 –
75 –
50 –
37 –

1⁰: anti-Kcnj10 mouse mAB
2⁰: anti-mouse-HRP

B: Stripped Blot

Protein extraction: Urea | Triton | SDS

1⁰: none
2⁰: anti-mouse-HRP

C: Second Detection

Protein extraction: Urea | Triton | SDS

250 –
150 –
100 –
75 –
50 –
37 –

1⁰: anti-Kcnj10 rabbit pAB
2⁰: anti-rabbit-HRP

D: First Detection

Protein extraction: Urea | Triton | SDS

250 –
150 –
100 –
75 –
50 –
37 –

1⁰: anti-Kcnj10 rabbit pAB
2⁰: anti-rabbit-HRP

E: Stripped Blot

Protein extraction: Urea | Triton | SDS

1⁰: none
2⁰: anti-rabbit-HRP

F: Second Detection

Protein extraction: Urea | Triton | SDS

250 –
150 –
100 –
75 –
50 –
37 –

1⁰: anti-Kcnj10 mouse mAB
2⁰: anti-mouse-HRP

G: Immunoprecipitation

Protein extraction: Triton | Triton

250 –
150 –
100 –
75 –
50 –
37 –

IP: anti-Kcnj10 mouse mAB
1⁰: anti-Kcnj10 rabbit pAB
2⁰: anti-rabbit-HRP

H: First Detection

Without peptide

250 –
150 –
100 –
75 –
50 –
37 –

1⁰: anti-Kcnj10 rabbit pAB
2⁰: anti-rabbit-HRP

I: Second Detection

With peptide | Without peptide

1⁰: anti-Kcnj10 rabbit pAB
2⁰: anti-rabbit-HRP

Figure 3.7: Western blot for Kcnj10 protein in stria vascularis.
(A-C) Protein was extracted from stria vascularis using three different methods and first probed for Kcnj10 *with a mouse monoclonal antibody. This blot was stripped and reprobed for* Kcnj10 *with a rabbit polyclonal antibody. Note that the pattern of staining varied with the method of*

75

extraction but not with the antibody used for probing (compare A and C). (D-F) Similar experiments were performed in reverse order. Protein was extracted from stria vascularis using three different methods and first probed for Kcnj10 *with a rabbit polyclonal antibody. The blot was then stripped and reprobed for* Kcnj10 *with a mouse monoclonal antibody. Note that considerable interexperimental variability in the pattern of bands and smears was encountered (compare C and D) but that the little variability was seen with the different antibodies (compare D and F). (G) Protein lysate from stria vascularis was immunoprecipitated with mouse monoclonal antibody for* Kcnj10 *and the resulting western blot was probed with a rabbit polyclonal antibody for* Kcnj10. *Note that a monomeric form of* Kcnj10 *(~40 kDa) and complexes that resulted in bands and smears of higher molecular weight were observed by immunoprecipitation as well as by western blotting of whole cell lysates (compare A and G). (H-I) A single lane containing stria vascularis protein was probed for* Kcnj10, *stripped, cut into two pieces (indicated by ✂) and probed again for* Kcnj10 *in the presence and absence of blocking peptide. These experiments confirmed that western blot for* Kcnj10 *in stria vascularis have both smears and bands.*
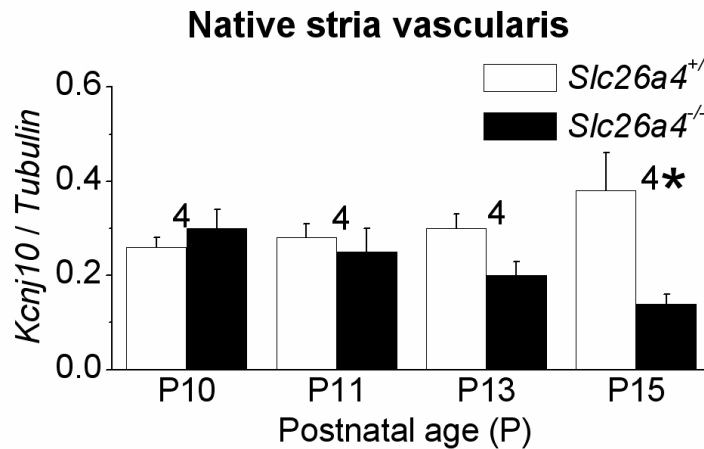
Figure 3.8: Quantification of Kcnj10 protein expression in native stria vascularis.

Levels of Kcnj10 *protein were quantified against* tubulin *at P10, P11, P13 and P15. Significant changes between corresponding time points are marked (*) and numbers next to the bars represent the number of experiments.* Kcnj10 *expression was progressively lost from the stria vascularis of Slc26a4$^{-/-}$ mice. The loss of* Kcnj10 *expression in native tissue that is under the influence of oxidative/nitrative stress supports a role for oxidative/nitrative stress mediated loss of* Kcnj10 *expression.*

Protocol development for organ culture of stria vascularis

A previous study has shown that stria vascularis in organ culture is poorly preserved and shows signs of degeneration in strial marginal and intermediate cells within 5 days (2). The degeneration of stria vascularis could be due to low apical concentration of K$^+$ in organ culture that would lead to elevated rates of K$^+$ secretion from strial marginal cells (43). Increased ion transport rates would increase ATP consumption, ATP production and thereby enhance

mitochondrial stress (25). Furosemide and furosemide analogs have been shown to reduce ATP consumption and inhibit K^+ secretion by strial marginal cells (23; 43). Reduced ATP consumption would reduce ATP production and thereby lower oxidative stress. Therefore furosemide supplementation might be useful in preserving the integrity of stria vascularis in organ culture. Stria vascularis was cultured in media with/without furosemide for 0, 1, 3 and 5 days and evaluated for viability by quantifying the levels of tubulin. In the absence of furosemide tubulin expression was gradually lost. In the presence of furosemide stria vascularis could be cultured for at least 5 days (Fig. 3.9). Therefore to evaluate the expression of Kcnj10 in organ culture, stria vascularis was cultured in media supplemented with furosemide.

A   Organ culture of stria vascularis
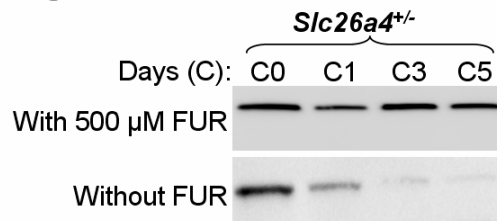
B   Organ culture of stria vascularis
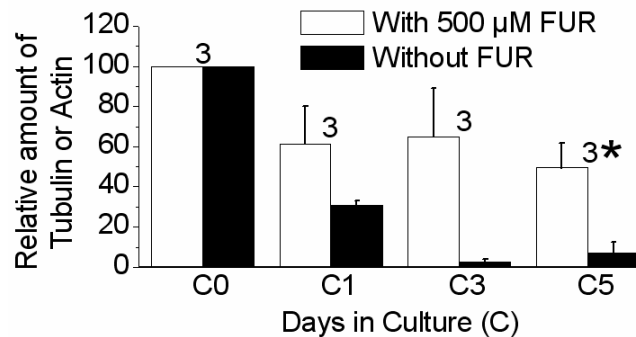
Figure 3.9: Quantification of tubulin or actin protein expression in organ culture of stria vascularis.
(A-B) Levels of tubulin or actin were quantified in P10 stria vascularis of Slc26a4$^{+/-}$ mice at 0, 1, 3 and 5 days in organ culture. Data are presented as percent of tubulin or actin protein at 0 day of culture, which corresponds to age P10. Significant changes between corresponding time points are marked (*) and numbers next to the bars represent the number of experiments. Tubulin or actin expression was gradually lost in organ culture of stria vascularis in the absence of furosemide (FUR). Stria vascularis can be cultured for at least 5 days when the media is supplemented with 500 μM furosemide (FUR).

Similar expression of Kcnj10 in organ culture of Slc26a4$^{-/-}$ and Slc26a4$^{+/-}$ mice

Stria vascularis from P10 *Slc26a4*$^{-/-}$ and *Slc26a4*$^{+/-}$ mice, were cultured. Protein expression of Kcnj10 was quantified in organ culture at 1, 3 and 5 days, corresponding to the time points of measurements in native tissue at P11, P13 and P15. Under conditions of equal oxidative stress in organ culture, stria vascularis of *Slc26a4*$^{-/-}$ mice was able to maintain Kcnj10 expression at a level similar to *Slc26a4*$^{+/-}$ mice (Fig. 3.10). These observations suggest that oxidative stress mediates the loss of Kcnj10 expression in the native tissue.
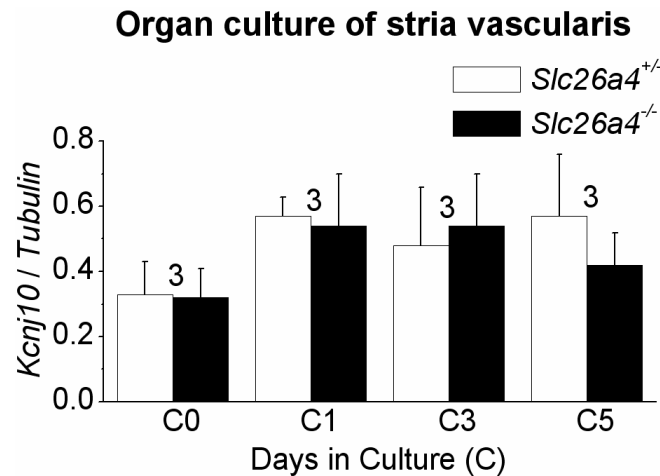
Figure 3.10: Quantification of Kcnj10 protein expression in organ culture of stria vascularis.
Levels of Kcnj10 *protein were quantified against* tubulin *in P10 stria vascularis of Slc26a4*$^{+/-}$ *and Slc26a4*$^{-/-}$ *mice at 0, 1, 3 and 5 days in organ culture. Significant changes between corresponding time points are marked (*) and numbers next to the bars represent the number of experiments. In contrast to native stria vascularis shown in Fig. 9,* Kcnj10 *expression level in organ culture (shown here) followed the same trend in Slc26a4*$^{+/-}$ *and Slc26a4*$^{-/-}$ *mice. Similar levels of* Kcnj10 *expression in stria vascularis of Slc26a4*$^{+/-}$ *and Slc26a4*$^{-/-}$ *mice under conditions of equal oxidative challenge in organ culture conditions supports oxidative stress mediated loss of* Kcnj10 *expression.*

Loss of Kcnj10 protein expression under oxidative and nitrative stress

The effect of oxidative and nitrative stress on protein expression of Kcnj10 was evaluated in an heterologous expression system (Fig. 3.11). Cells were transfected with a vector that contains *Kcnj10-GFP*-Export-sequence. This plasmid was used in our study because the localization of Kcnj10 to plasma membrane in native tissues is lost under cell culture. However, insertion of the ER export sequence for Kir2.1 into the C-terminal of Kcnj10 enables it to translocate to the plasma membrane (39). Cells were treated with 500 µM furosemide to replicate

the conditions present in organ culture. Oxidative stress was induced by incubation with 10 µM H_2O_2. Further, oxidative and nitrative stress was induced by incubation with 1mM SIN-1. SIN-1 releases equimolar amounts of $O_2^{\bullet-}$ and •NO that react to produce peroxynitrite (27). Kcnj10 expression was reduced in cells treated with SIN-1 but not in cells treated with H_2O_2. No significant change was found in the expression levels of tubulin suggesting that the observed differences in Kcnj10 expression are not due to cell death or degeneration. SIN-1 mediated loss of Kcnj10 suggests that free radical stress comprising of both oxygen and nitrogen radicals is capable of reducing Kcnj10 expression. It is conceivable that observed loss of Kcnj10 expression in stria vascularis of $Slc26a4^{-/-}$ mice is due to the combined effect of oxidative and nitrative stress.

Discussion

The most salient findings of the present study are that 1) Free radical stress is increased in stria vascularis of $Slc26a4^{-/-}$ mice as early as P10, which is before the onset of hearing; 2) Kcnj10 expression is lost progressively in the stria vascularis of $Slc26a4^{-/-}$ mice; 3) Under conditions of equal oxidative stress, stria vascularis of P10 $Slc26a4^{-/-}$ and $Slc26a4^{+/-}$ mice have a similar pattern of expression in organ culture; 4) Kcnj10 expression is reduced under free radical stress in cell culture. These results suggest that free radical stress is involved in the etiology of hearing loss in Pendred syndrome.

Free radical stress that exceeds the capacity of defense mechanisms has been implicated in inner ear pathogenesis including acoustic trauma and drug-induced ototoxicity (17; 33). Stria vascularis is prone to free radical stress due to its high metabolic activity and dense vascular system (25). Oxygen free radical $O_2^{\bullet-}$ is a product of energy metabolism in the mitochondria and the nitrogen free radical •NO is generated by nitric oxide synthase in the endothelial cells of stria vascularis. The reaction between $O_2^{\bullet-}$ and •NO produces peroxynitrite ($ONOO^-$). $ONOO^-$ decomposes to form the very aggressive nitrate radical ($\bullet NO_2$), that causes nitration of proteins. The formation of $\bullet NO_2$ from $ONOO^-$ is facilitated under acidic conditions or in the presence of CO_2 (5; 24). The sensitivity of Kcnj10 protein expression to free radical stress and the presence of oxidative and nitrative stress in stria vascularis suggest that free radical stress is responsible for the loss of Kcnj10 in Pendred syndrome.
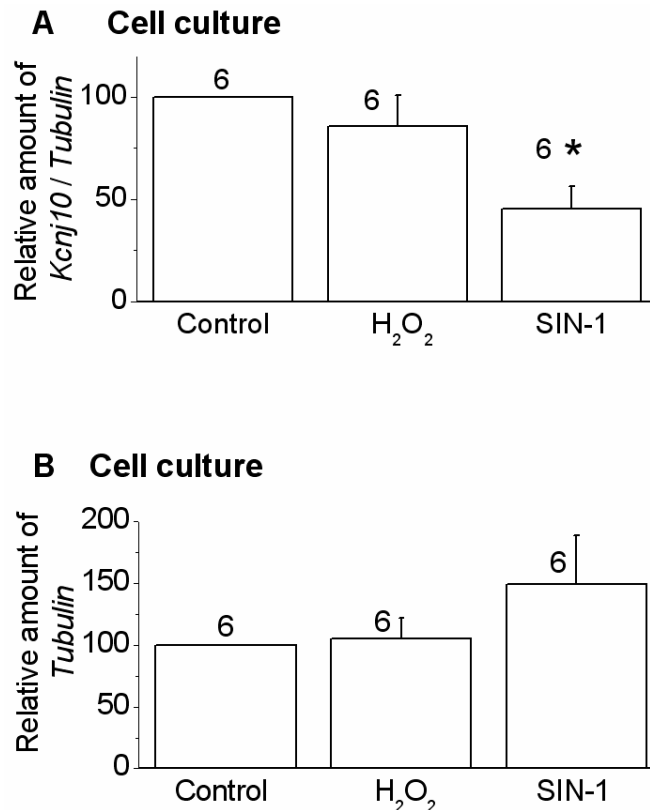
Figure 3.11: Quantification of Kcnj10 protein expression under free radical stress.
(A-B) Levels of Kcnj10 *protein were quantified against* tubulin *in cell culture under the influence of 10 μM H_2O_2 and 1 mM SIN-1. Data are presented as percent of* Kcnj10 *expression in control samples. Decrease in the expression of* Kcnj10 *protein was found in SIN-1 mediated oxidative and nitrative stress but not in H_2O_2 mediated oxidative stress. No significant change was found in the expression levels of* tubulin *between control and H_2O_2 or SIN-1 treatments. The loss of* Kcnj10 *expression under free radical stress provides with a mechanism for the observed loss of* Kcnj10 *in the stria vascularis of Slc26a4$^{-/-}$ mice.*

Reduction of Kcnj10 protein expression under free radical stress is a pathobiologic mechanism that is not limited to Pendred syndrome. Loss of Kcnj10 under free radical stress is also implicated in other disease models. Kcnj10 protein expression, unlike the expression of other K^+ channels, is reduced in the retina after ischemia-reperfusion injury, an insult that is associated with oxidative stress (19). Furthermore, mice expressing a mutant superoxide dismutase (SOD1-G93A) have increased oxidative stress and reduced expression of Kcnj10 protein in spinal cord tissues (1; 22).

The origin of increased free radical stress in stria vascularis may be related to the enlarged endolymphatic volume or the acidified endolymphatic pH of *Slc26a4$^{-/-}$* mice.

Enlargement of the cochlear and vestibular endolymphatic compartments develop in $Slc26a4^{-/-}$ mice prenatally after embryonic day 13 (E13), when the onset of pendrin expression fails to occur in $Slc26a4^{-/-}$ mice (12). Shortly after birth, the composition of endolymph changes from a Na^+ rich fluid to a K^+ rich fluid. The onset of K^+ secretion occurs at P3 (3; 45). K^+ is secreted by stria vascularis and the rate of K^+ secretion is controlled by the endolymphatic K^+ concentration (41; 43). Enlarged endolymphatic spaces with an inherently less favorable surface-to-volume ratio may require larger rates of K^+ secretion to offset leakage and maintain the normal high endolymphatic K^+ concentration found in $Slc26a4^{-/-}$ mice (42). Higher rates of K^+ secretion can be associated with higher rates of oxidative stress since metabolism and ATP production in stria vascularis are tightly linked to the rate of ion transport (23; 25). It is conceivable that the onset of oxidative stress in stria vascularis coincides with the onset of K^+ secretion at P3, which is prior to the onset of Kcnj10 expression and rise of endocochlear potential at P8 and the onset of hearing at P12 (3; 18; 35; 44).

Acidification of endolymph was observed in $Slc26a4^{-/-}$ mice at P10 and older ages (28; 44). Acidification could contribute to free radical stress in stria vascularis if the lowered pH of endolymph would decrease the cytosolic pH of the adjacent stria marginal cells that are the most likely source of $O_2^{\bullet-}$. The cytosolic pH could induce oxidative stress by enhancing the stability of $^{\bullet}OH^-$ and by promoting the formation of the aggressive $^{\bullet}OH^-$, $\bullet NO_2$ from $O_2^{\bullet-}$ and $\bullet NO$ (5; 10).

In conclusion, the data demonstrate that loss of pendrin leads to free radical stress in stria vascularis and that free radical stress is sufficient to cause the loss Kcnj10 expression. The loss of Kcnj10 expression in stria vascularis leads to the loss of the endocochlear potential and the failure to develop hearing in the mouse model of Pendred syndrome.

Acknowledgments

Grants

References

1. **Andrus PK, Fleck TJ, Gurney ME and Hall ED**. Protein oxidative damage in a transgenic mouse model of familial amyotrophic lateral sclerosis. *J Neurochem* 71: 2041-2048, 1998.

2. **Anniko M**. The post-natal mammalian labyrinthine secretory epithelium *in vitro*. *Acta Otolaryngol* 90: 237-243, 1980.

3. **Anniko M and Nordemar H**. Embryogenesis of the inner ear. IV. Post-natal maturation of the secretory epithelia of the inner ear in correlation with the elemental composition in the endolymphatic space. *Arch Otorhinolaryngol* 229: 281-288, 1980.

4. **Balagopalakrishna C, Paka L, Pillarisetti S and Goldberg IJ**. Lipolysis-induced iron release from diferric transferrin: Possible role of lipoprotein lipase in LDL oxidation. *J Lipid Res* 40: 1347-1356, 1999.

5. **Beckman JS, Beckman TW, Chen J, Marshall PA and Freeman BA**. Apparent hydroxyl radical production by peroxynitrite: implications for endothelial injury from nitric oxide and superoxide. *Proc Natl Acad Sci U S A* 87: 1620-1624, 1990.

6. **Connors NC, Adams ME, Froehner SC and Kofuji P**. The potassium channel Kir4.1 associates with the dystrophin-glycoprotein complex via alpha-syntrophin in glia. *J Biol Chem* 279: 28387-28392, 2004.

7. **Connors NC and Kofuji P**. Potassium channel Kir4.1 macromolecular complex in retinal glial cells. *Glia* 53: 124-131, 2006.

8. **Cox LA and Adrian GS**. Posttranscriptional regulation of chimeric human transferrin genes by iron. *Biochemistry* 32: 4738-4745, 1993.

9. **Cremers CW, Admiraal RJ, Huygen PL, Bolder C, Everett LA, Joosten FB, Green ED, van Camp G and Otten BJ**. Progressive hearing loss, hypoplasia of the cochlea and widened vestibular aqueducts are very common features in Pendred's syndrome. *Int J Pediatr Otorhinolaryngol* 45: 113-123, 1998.

10. **Crow JP, Spruell C, Chen J, Gunn C, Ischiropoulos H, Tsai M, Smith CD, Radi R, Koppenol WH and Beckman JS**. On the pH-dependent yield of hydroxyl radical products from peroxynitrite. *Free Radic Biol Med* 16: 331-338, 1994.

11. **Eisenstein RS**. Iron regulatory proteins and the molecular control of mammalian iron metabolism. *Annu Rev Nutr* 20: 627-662, 2000.

12. **Everett LA, Belyantseva IA, Noben-Trauth K, Cantos R, Chen A, Thakkar SI, Hoogstraten-Miller SL, Kachar B, Wu DK and Green ED**. Targeted disruption of mouse *Pds* provides insight about the inner-ear defects encountered in Pendred syndrome. *Hum Mol Genet* 10: 153-161, 2001.

13. **Everett LA, Glaser B, Beck JC, Idol JR, Buchs A, Heyman M, Adawi F, Hazani E, Nassir E, Baxevanis AD, Sheffield VC and Green ED**. Pendred syndrome is caused by mutations in a putative sulphate transporter gene (*PDS*). *Nat Genet* 17: 411-422, 1997.

14. **Everett LA, Morsli H, Wu DK and Green ED**. Expression pattern of the mouse ortholog of the Pendred's syndrome gene (*Pds*) suggests a key role for pendrin in the inner ear. *Proc Natl Acad Sci U S A* 96: 9727-9732, 1999.

15. **Fish WW**. Rapid colorimetric micromethod for the quantitation of complexed iron in biological samples. *Methods Enzymol* 158: 357-364, 1988.

16. **Fraser GR**. Association of congenital deafness with goitre (pendred's syndrome) a study of 207 families. *Ann Hum Genet* 28: 201-249, 1965.

17. **Henderson D, Bielefeld EC, Harris KC and Hu BH**. The role of oxidative stress in noise-induced hearing loss. *Ear Hear* 27: 1-19, 2006.

18. **Hibino H, Higashi-Shingai K, Fujita A, Iwai K, Ishii M and Kurachi Y**. Expression of an inwardly rectifying K^+ channel, Kir5.1, in specific types of fibrocytes in the cochlear lateral wall suggests its functional importance in the establishment of endocochlear potential. *Eur J Neurosci* 19: 76-84, 2004.

19. **Iandiev I, Tenckhoff S, Pannicke T, Biedermann B, Hollborn M, Wiedemann P, Reichenbach A and Bringmann A**. Differential regulation of Kir4.1 and Kir2.1 expression in the ischemic rat retina. *Neurosci Lett* 396: 97-101, 2006.

20. **Jabba SV, Oelke A, Singh R, Maganti RJ, Fleming S, Wall SM, Everett LA, Green ED and Wangemann P**. Macrophage invasion contributes to degeneration of stria vascularis in Pendred syndrome mouse model. *BMC Med* 4: 37, 2006.

21. **Johnsen T, Larsen C, Friis J and Hougaard-Jensen F**. Pendred's syndrome. Acoustic, vestibular and radiological findings in 17 unrelated patients. *J Laryngol Otol* 101: 1187-1192, 1987.

22. **Kaiser M, Maletzki I, Hulsmann S, Holtmann B, Schulz-Schaeffer W, Kirchhoff F, Bahr M and Neusch C**. Progressive loss of a glial potassium channel (KCNJ10) in the spinal cord of the SOD1 (G93A) transgenic mouse model of amyotrophic lateral sclerosis. *J Neurochem* 99: 900-912, 2006.

23. **Kusakari J, Ise I, Comegys TH, Thalmann I and Thalmann R**. Effect of ethacrynic acid, furosemide, and ouabain upon the endolymphatic potential and upon high energy phosphates of the stria vascularis. *Laryngoscope* 88: 12-37, 1978.

24. **Lymar SV, Jiang Q and Hurst JK**. Mechanism of carbon dioxide-catalyzed oxidation of tyrosine by peroxynitrite. *Biochemistry* 35: 7855-7861, 1996.

25. **Marcus DC, Thalmann R and Marcus NY**. Respiratory rate and ATP content of stria vascularis of guinea pig in vitro. *Laryngoscope* 88: 1825-1835, 1978.

26. **Marcus DC, Wu T, Wangemann P and Kofuji P**. *KCNJ10* (*Kir4.1*) potassium channel knockout abolishes endocochlear potential. *Am J Physiol Cell Physiol* 282: C403-C407, 2002.

27. **Muijsers RB, van Den WE, Folkerts G, Beukelman CJ, Koster AS, Postma DS and Nijkamp FP**. Apocynin inhibits peroxynitrite formation by murine macrophages. *Br J Pharmacol* 130: 932-936, 2000.

28. **Nakaya K, Harbidge DG, Wangemann P, Schultz BD, Green ED, Wall SM and Marcus DC**. Lack of pendrin HCO_3^- transport elevates vestibular endolymphatic $[Ca^{2+}]$ by inhibition of acid-sensitive TRPV5 and TRPV6 channels. *Am J Physiol Renal Physiol* 292: F1314-F1321, 2007.

29. **Pendred V.** Deaf-mutism and goitre. *Lancet* 11: 532, 1896.

30. **Radi R**. Nitric oxide, oxidants, and protein tyrosine nitration. *Proc Natl Acad Sci U S A* 101: 4003-4008, 2004.

31. **Ramakers C, Ruijter JM, Deprez RH and Moorman AF**. Assumption-free analysis of quantitative real-time polymerase chain reaction (PCR) data. *Neurosci Lett* 339: 62-66, 2003.

32. **Reardon W, Coffey R, Phelps PD, Luxon LM, Stephens D, Kendall-Taylor P, Britton KE, Grossman A and Trembath R**. Pendred syndrome--100 years of underascertainment? *QJM* 90: 443-447, 1997.

33. **Rybak LP and Whitworth CA**. Ototoxicity: therapeutic opportunities. *Drug Discov Today* 10: 1313-1321, 2005.

34. **Sabolic I**. Common mechanisms in nephropathy induced by toxic metals. *Nephron Physiol* 104: 107-114, 2006.

35. **Sadanaga M and Morimitsu T**. Development of endocochlear potential and its negative component in mouse cochlea. *Hear Res* 89: 155-161, 1995.

36. **Sargent PJ, Farnaud S and Evans RW**. Structure/function overview of proteins involved in iron storage and transport. *Curr Med Chem* 12: 2683-2693, 2005.

37. **Scott DA, Wang R, Kreman TM, Sheffield VC and Karniski LP**. The Pendred syndrome gene encodes a chloride-iodide transport protein. *Nat Genet* 21: 440-443, 1999.

38. **Stadtman ER**. Metal ion-catalyzed oxidation of proteins: biochemical mechanism and biological consequences. *Free Radic Biol Med* 9: 315-325, 1990.

39. **Stockklausner C, Ludwig J, Ruppersberg JP and Klocker** N. A sequence motif responsible for ER export and surface expression of Kir2.0 inward rectifier K^+ channels. *FEBS Lett* 493: 129-133, 2001.

40. **Vesela A and Wilhelm J**. The role of carbon dioxide in free radical reactions of the organism. *Physiol Res* 51: 335-339, 2002.

41. **Wangemann P**. Supporting sensory transduction: cochlear fluid homeostasis and the endocochlear potential. *J Physiol* 576: 11-21, 2006.

42. **Wangemann P, Itza EM, Albrecht B, Wu T, Jabba SV, Maganti RJ, Lee JH, Everett LA, Wall SM, Royaux IE, Green ED and Marcus DC**. Loss of KCNJ10 protein expression abolishes endocochlear potential and causes deafness in Pendred syndrome mouse model. *BMC Med* 2: 30, 2004.

43. **Wangemann P, Liu J and Marcus DC**. Ion transport mechanisms responsible for K^+ secretion and the transepithelial voltage across marginal cells of stria vascularis in vitro. *Hear Res* 84: 19-29, 1995.

44. **Wangemann P, Nakaya K, Wu T, Maganti RJ, Itza EM, Sanneman JD, Harbidge DG, Billings S and Marcus DC**. Loss of cochlear HCO_3^- secretion causes deafness via endolymphatic acidification and inhibition of Ca^{2+} reabsorption in a Pendred syndrome mouse model. . *Am J Physiol Renal Physiol* 292: F1345-F1353, 2007.

45. **Yamasaki M, Komune S, Shimozono M, Matsuda K and Haruta A**. Development of monovalent ions in the endolymph in mouse cochlea. *ORL J Otorhinolaryngol Relat Spec* 62: 241-246, 2000.

46. **You HJ, Oh DH, Choi CY, Lee DG, Hahm KS, Moon AR and Jeong HG**. Protective effect of metallothionein-III on DNA damage in response to reactive oxygen species. *Biochim Biophys Acta* 1573: 33-38, 2002.

CHAPTER 4 - The *Slc26a4*^{-/-} mice has no apparent thyroid dysfunction

These data will be submitted as part of an article to a peer reviewed journal.

Ruchira Singh, Christa Linsenmeyer, Kazuhiro Nakaya, Peying Fong, Daniel Marcus, and Philine Wangemann

Loss of pendrin in the mouse acidifies luminal pH of thyroid follicles but does not alter thyroxine production.

Abstract

Pendred syndrome is caused by mutations in the anion exchanger pendrin (*SLC26A4*) and is characterized by deafness, post-pubertal goiter and iodide organification defects. Studies were performed on thyroids from *Slc26a4$^{+/-}$* and *Slc26a4$^{-/-}$* mice at various ages: postnatal days 10 (P10), P15 (corresponding to the time point of maximal thyroid gland activity), P30 (post-weaning) and P80 (young adults). Global gene expression levels in the thyroid were evaluated by gene arrays performed at P15. Thyroxine (T4) levels in the serum were quantified by immunoassay. Gene expression was quantified by qRT-PCR. Western blotting was used to evaluate the expression of two proteins involved in thyroid hormone synthesis, Tpo and Duox1, as well as the chloride channel, ClC-5, oxidized proteins, eNOS and proteins involved in iron metabolism. Nitrated and oxidized proteins were quantified by ELISA. Total iron was measured by ferrozine spectrophotometry. *Slc26a4* mRNA expression was modest in the thyroid of *Slc26a4$^{+/-}$* mice at all ages. Decreased levels of nitrated proteins were observed in the thyroid of *Slc26a4$^{-/-}$* mice at P35. Between the *Slc26a4$^{+/-}$* and *Slc26a4$^{-/-}$* mice: a) no differences in the serum T4 levels were observed, b) no differences in the expression of Tpo and Duox1 were observed and c) no differences in the levels of oxidized proteins were observed. The absence of elevated levels of oxidized proteins suggests that increased oxidative stress is not present in the thyroid of *Slc26a4$^{-/-}$* mice. The low expression of *Slc26a4* in mouse thyroid and the normal thyroid gland function in the Pendred syndrome mouse model suggests a distinction between the roles of pendrin in murine and human thyroids.

Introduction

Pendred syndrome is an inherited autosomal recessive condition that primarily affects the thyroid and the inner ear. It is characterized by a positive perchlorate discharge test, goiter, and prelingual sensorineural deafness (6; 15; 19). Pendred syndrome is caused by loss-of-function mutations in the gene *SLC26A4*, which encodes pendrin. Pendrin is primarily expressed in the inner ear, the thyroid and the kidney (10; 24; 29). In the thyroid, pendrin localizes to the apical membrane of thyrocytes and mediates iodide transport (9; 24; 32). Pendrin has been hypothesized to play a role in iodide organification by transporting iodide to the follicular lumen

(4). Therefore, lack of pendrin function has been suggested to limit the iodination of thyroglobulin, thereby affecting the synthesis of thyroid hormone (9; 15; 26).

Clinical studies suggest a role for pendrin in thyroid hormone metabolism. Patients with non-functional pendrin can present with goiter, which can be either hypothyroid or euthyroid. Moreover, mutations in *Slc26a4* have been found in congenital hypothyroidism (2). Decreased expression of proteins that are involved in thyroid iodide metabolism, including pendrin, has been shown in thyroid cancer in humans (7; 27; 31). Thyroid carcinomas have also been reported in patients with Pendred syndrome (1; 3; 18).

In the mouse, the thyroid gland activity peaks around postnatal day 15 (P15) (5). However, a study that investigated the thyroid histology and serum T3, T4 and TSH levels in adult mice identified no differences between *Slc26a4$^{+/+}$* and *Slc26a4$^{-/-}$* mice (8). Because the previous study was carried out on adult mice, we were prompted to re-evaluate the thyroid pathology in thyroid of *Slc26a4$^{-/-}$* mice in a developmental study (9; 25). Thus, the first aim of the present study was to determine the time course of *Slc26a4* expression in the mouse thyroid and to evaluate the effect of absence of pendrin on the expression of genes/proteins involved in the synthesis of thyroid hormone and on serum T4 levels.

Pendrin-mediated iodide/Cl$^-$ exchange in the apical membrane of the thyrocyte requires the presence of Cl$^-$ in the follicular lumen. It has been suggested that the Cl$^-$ channel, ClC-5, may assist in Cl$^-$ cycling by transporting Cl$^-$ into the follicular lumen. If Cl$^-$ transport by ClC-5 and iodide transport by pendrin are a coupled mechanism, it is conceivable that lack of pendrin will have an effect on the expression of ClC-5. In one study, *Clcn5$^{-/-}$* (*Clcn5* encodes ClC-5*)* mice have been shown to develop euthyroid goiter that correlates with delayed iodide organification and reduced pendrin expression (30). The second aim of this study was to determine whether absence of pendrin affects ClC-5 protein expression in the mouse model of Pendred syndrome.

The third aim of this study was to address whether free radical stress and iron metabolism are altered in the thyroid of *Slc26a4$^{-/-}$* mice. Absence of pendrin is associated with increased free radical stress and altered iron metabolism in the stria vascularis of *Slc26a4$^{-/-}$* mice(28), raising the possibility that it also may lead to increased oxidative stress in the thyroid gland. This is

particularly feasible, given that hydrogen peroxide (H_2O_2), a well known oxidant, is involved in the process of thyroid hormone synthesis (16; 21). Indeed, cumulative oxidative stress in the thyroid could underly the goiter formation and thyroid carcinomas observed in human patients with Pendred syndrome (1; 14; 22).

Methods

Animal use

The *Slc26a4*^{-/-} and *Slc26a4*^{+/-} mice used in the experiments were raised in a colony at Kansas State University, established with breeders kindly provided by Dr. Susan Wall (Emory University, Atlanta, GA). Deeply anesthetized mice (tribromoethanol, 560 mg/kg, i.p.) were sacrificed either by decapitation or by transcardial perfusion with Cl^{-}-free solution (150 mM Na-gluconate, 4 mM Ca^{2+}-gluconate, 5 mM glucose 1.6 mM K_2HPO_4, 1 mM $MgSO_4$, 0.4 mM KH_2PO_4, pH 7.4) and dissection was carried out in the same solution at -10 °C. All procedures performed on animals were approved by the Institutional Animal Care and Use Committee of Kansas State University.

Gene array

Total RNA was isolated from the thyroid of three P15 *Slc26a4*^{-/-} and *Slc26a4*^{+/-} mice (RNeasy micro, Qiagen, Valencia, CA, USA) and stored at -80 °C until further processing. RNA was processed at the Gene Expression Facility at Kansas State University. A total of six arrays were run from sex-matched littermates. Three chips, each, hybridized with cDNA from thyroids of *Slc26a4*^{+/-} and *Slc26a4*^{-/-} mice, were compared. RNA was amplified to produce cDNA, which was fragmented, biotinylated and hybridized to high-density oligonucleotide gene chips (Ovation™ RNA Amplification System V2, Cat # 3100-12, NuGen, San Carlos, CA and FL-Ovation™ cDNA Biotin Module V2, Cat # 4200-12, NuGen; mouse 430 2.0 gene chip, Cat # 900496, Affymetrix, Santa Clara, CA, USA). Gene array data were analyzed using commercial software (GCOS, Affymetrix) and with custom-written macros (Excel, Microsoft, Redmond, WA, USA), as described previously (13). Present/absent calls were used to determine the expression, and averaged signal intensities (average of data obtained from three chips) were used to determine changes in expression levels. 'Intensity' for gene array data from *Slc26a4*^{+/-} and for

Slc26a4^{-/-} samples represents averages of data from one or more probes. For example, the gene *Tg* is represented on the chip by two probes. Present calls (P) were summarized for all three chips. For example, 6/6 indicates that this gene was called present by all 6 probes ($2 \times 3 = 6$); 4/6 indicates that the gene is represented by 2 probes on the 3 chips ($2 \times 3 = 6$) and that the gene was called present by 4 of the 6 probes. Ratios of intensity values (*Slc26a4*^{-/-} to *Slc26a4*^{+/-}) were calculated for each probe and averaged.

Quantitative RT-PCR

Total RNA was isolated from the thyroid (RNeasy micro, Qiagen) and kidney (RNeasy mini, Qiagen) of sex-matched *Slc26a4*^{+/-} and *Slc26a4*^{-/-} littermates and stored at -80 °C until further processing. Real time RT-PCR in the presence of SYBR green (Molecular Probes, Eugene, OR) was carried out in 96-well plates (QuantiTect SYBR Green RT-PCR Kit Cat# 204243, Qiagen, Valencia, CA; iCycler, BioRad, Hercules,CA) using gene specific primers (Table. 4.1).

Table 4.1: Gene specific primers

Gene	Primers	Product size
18S	gag gtt cga aga cga tca ga (sense) gtt ctt agt tgg tgg agc ga (antisense)	316 bp
Slc26a4	tcg gaa cat caa gac aca tc (*sense*) acc tca cta tga atc caa tct g (*antisense*)	252 bp
Ferritin heavy chain (*Fth*)	ttt gag cct gag ccc ttt (sense) tca aag aga tat tct gcc atg c (antisense)	706 bp
Actb	gga cct gac aga cta cct c (*sense*) tcg ttg cca ata gtg atg ac (*antisense*)	210 bp

The RT-PCR plate was set up by programming an automatic pipetting station (Biomek NX[P], Beckman Coulter, Fullerton, CA). RT-PCR was performed as described previously (28). Single product amplification was verified by gel electrophoresis and the identity of the product was confirmed by sequencing. The number of template molecules (T) was calculated according to the following formula: T = 10^ log (number of molecules at C_t) / (PCR efficiency^C_t), where C_t represents the cycle at which the fluorescence of the product molecules reached a set threshold. Samples that failed to reach the set threshold within the 40 cycles of PCR were assigned a default C_t value of 40. The number of molecules at C_t was calibrated by amplifying known numbers of 18S rRNA molecules. The content of 18S in total RNA was estimated under

the assumption that total RNA consists of 90% 18S and 28S rRNA. PCR efficiency was obtained from the slope of the log-linear phase of the growth curve (20).

Serum T4 measurements

Blood samples were collected by cardiac puncture, transferred into microcentrifuge tubes and allowed to clot for 30 min at room temperature. The clotted samples were centrifuged at 1500 rpm for 10 min at room temperature. The serum was collected and centrifuged again at 1500 rpm for 10 min at room temperature. The collected supernatant was stored at -20 °C until further processing. The total serum T4 was measured by a chemiluminescent enzyme immunoassay (Immulite[®] total T4, Siemens Healthcare Diagnostics, Deerfield, IL) according to the manufacturer's instructions.

Isolation of protein

Freshly dissected thyroids were transferred into microcentrifuge tubes and excess Cl⁻-free solution was removed. Freshly dissected spleens were flash-frozen in liquid nitrogen, then pulverized. Proteins from both tissues were extracted by adding 30 µl of Tris-Triton buffer (50 mM Tris, 150 mM NaCl, 1% Triton-X) and bath sonicated for 30 min at 0 °C (Fisher Scientific, Pittsburgh, PA). The samples were centrifuged at 14,000 rpm for 10 min at 4 °C. The supernatant fractions were collected and either used immediately or stored at -80 °C.

Quantification of nitrated proteins

The level of nitrotyrosine in isolated proteins was quantitated by two different immunoabsorbent assays (Cat # HK501, Cell sciences, Canton, MA; Cat #17-376, Millipore, Billerica, MA) according to the manufacturers' instructions. (The total protein content of the sample was measured (NanoOrange protein quantitation kit, Cat # N666, Invitrogen, Carlsbad, CA). Differences in the amount of nitrotyrosine were evaluated by comparison of nitrated protein content to the total protein content.

Quantification of oxidized proteins

Two different techniques were used to quantitate the oxidized proteins in tissue samples. *Oxyblots:* Carbonyl groups of oxidized proteins were derivatized with dinitrophenylhydrazine (Oxyblot Kit, Cat # S7150, Millipore,) to form denitrophenylhydrazone (DNP). DNP-labeled proteins were separated by SDS gel electrophoresis (5 µl/lane) and detected in western blots. Procedures were carried out according to the manufacturer's recommendations. Differences in the presence of oxidized proteins were evaluated by comparison to the expression of actin or GAPDH. *ELISA:* Protein was isolated and the level of oxidized proteins was quantified by an immunoabsorbent assay (Cat # STA-310, Cell Biolabs, San Diego, CA;) according to manufacturer's recommendation.

Quantitative western blotting

An equal volume of Laemmli buffer containing 5% β-mercaptoethanol was added to the protein samples. Protein samples were either incubated at 75 °C for 10 min or at 37 °C for 1 hour. Protein samples (15 µl) were separated by SDS-PAGE (4-15% Tris-SDS Polyacrylamide Precast Gels, Cat # 161-1104, BioRad Laboratories, Hercules, CA). After separation, proteins were transferred to PVDF membranes (0.2 µm pore size, Cat # 162-0174, BioRad), blocked with 5% dry milk in TBS-Tween (137 mM NaCl, 20 mM Tris-Cl, 0.1% Tween-20, pH 7.6) and probed with primary antibodies (rabbit anti-ClC-5, 1:1000, a gift from Professor Thomas Jentsch, FMP/ Max-Delbrück-Centrum für Molekulare Medizin, Berlin, Germany; goat anti-Tpo, 1:200, Cat # sc-48951, Santa Cruz Biotechnology, Santa Cruz, CA; goat anti-Duox1, 1:200, Cat # sc-49939, Santa Cruz Biotechnology; rabbit anti-Trf, 1:750, Cat #A76, Biomeda, Foster City, CA; mouse anti-Tfrc 1:2,000, Cat #13-6800, Zymed, San Francisco, CA; rabbit anti-eNOS, 1:500, Cat # 610296, BD Biosciences, San Jose, CA; rabbit anti-actin, 1:1000, Cat # A2066, Sigma, St. Louis, MO; mouse anti-GAPDH, 1:300, Cat # MAB374, Chemicon International, Billerica, MA; rabbit anti-tubulin, 1:500, Cat # ab6046, Abcam Inc., Cambridge, MA). Membranes were washed 4x for 15 min each in TBS-Tween and incubated with the appropriate HRP-conjugated secondary antibodies (anti-rabbit, 1:5,000, Cat # 1858415; anti-mouse, 1:5,000, Cat # 1858416, Pierce, Rockford, IL; anti-rabbit, 1:5,000, Cat # anti-goat, 1:5,000, Cat # sc-2033, Santa Cruz Biotechnology). After washing 4x for 15 min each in TBS-Tween, HRP was

detected by chemiluminescence (SuperSignal West Femto Maximum Sensitivity Substrate, Cat # 34095, Pierce, Rockford, IL) using a camera-based imaging workstation (4000MM, Kodak). Membranes were stripped and reprobed with an antibody to a reference protein. Differences in protein expression were evaluated by comparison to the expression of actin, GAPDH or tubulin.

Quantification of total tissue Fe content

A ferrozine-based assay was modified and used for total iron measurement in the tissue (11). *Iron measurement in thyroid:* Each freshly dissected thyroid was transferred into a microcentrifuge tube and excess Cl⁻-free solution was removed. Guanidine hydrochloride (2 µl) was added to the tissue and mixed by a pulse spin. After incubation for 45 min at 60°C, 2 µl of FAT solution (0.5 M ferrozine, 0.5 M ascorbic acid and 1 M Tris-Cl, pH 7) was added. After mixing by pulse-spinning, the tissue was incubated for 45 min at 60°C. Absorbance at 562 nm of the supernatant was measured (ND1000, Nanodrop Technologies) and standards containing $FeCl_2$ were processed in parallel. Measurements of the total iron (Tissue-Fe) are reported per mg of wet tissue weight. *Iron measurement on spleen:* Freshly dissected spleens were flash-frozen in liquid nitrogen, then pulverized. Guanidine hydrochloride (100 µl) was added to the tissue and mixed by a pulse spin. After incubation for 45 min at 60°C, 100 µl of FAT solution was added. Mixing was facilitated by a pulse spin and the tissue was incubated for 10 min at room temperature. Absorbance at 562 nm was measured in the supernatant of the 200 µl sample (ND1000, Nanodrop Technologies) and standards containing $FeCl_2$ were processed in parallel. Measurements of the Tissue-Fe are reported per mg of wet tissue weight.

Statistical analysis

Data for the quality metrics on the gene array experiment are expressed as mean ± S.D. For all other experiments, data are reported as mean ± sem. Data throughout the manuscript were compared by unpaired t-test. Significance was assumed at $P < 0.05$.

Results

Slc26a4 transcript expression does not correlate with the thyroid gland activity

To determine whether pendrin expression correlates with the thyroid gland activity, the mRNA expression of *Slc26a4* in the mouse thyroid was evaluated at various ages (Fig. 4.1). RNA was isolated from two pendrin-expressing tissues, thyroid and kidney, of *Slc26a4*^{+/−} mice at the following ages: P10, P15, post-weaning mice (P30) and young adults (P80), and quantitative RT-PCR was performed. As a quality control to ensure that the RT-PCR reaction worked and that sufficient level of RNA was present, transcript levels coding for ferritin heavy chain (*Fth*) and *ActB* were evaluated in parallel with *Slc26a4* from the RNA samples. In comparison to the kidney where *Slc26a4* was highly expressed at all ages, *Slc26a4* expression in the thyroid of *Slc26a4*^{+/−} mice was modest. No age dependence was observed in the expression pattern of *Slc26a4* in either the thyroid or the kidney. Moreover, in a few experiments, *Slc26a4* expression was below the level of detection in the thyroid samples since the fluorescence failed to reach the set threshold. Consistent with these results, *Slc26a4* was called absent in the gene arrays performed on the thyroid of Slc26a4^{+/-} mice. The relatively low and constant expression of *Slc26a4* at all ages in the mouse thyroid indicates that *Slc26a4* expression does not increase during the peak of thyroid gland activity at P15 in the mouse.
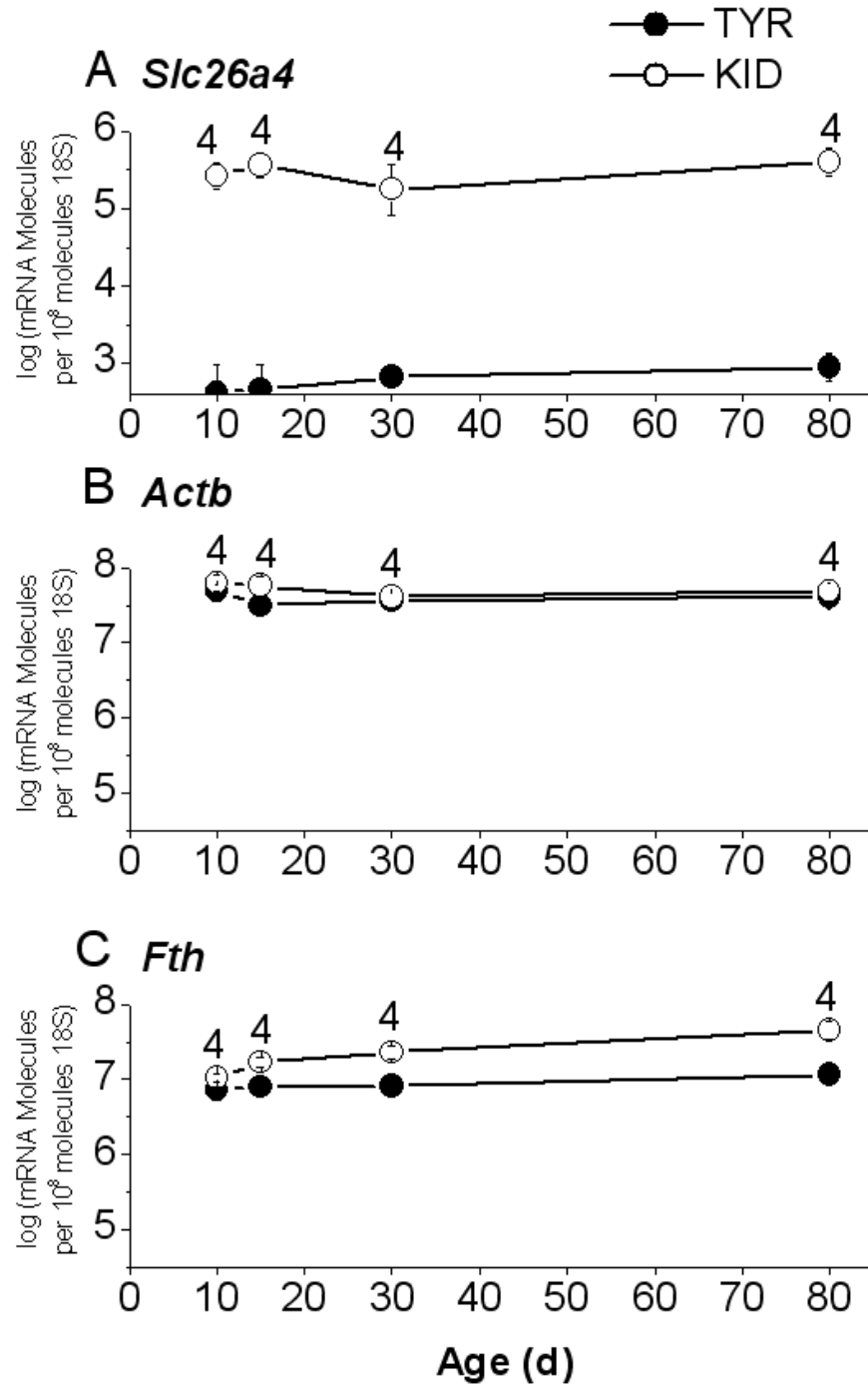
Figure 4.1: *Slc26a4* mRNA expression in the thyroid is constant over various ages
*Transcripts coding for **A)** Slc26a4, **B)** Actb and **C)** ferritin heavy chain (Fth) were quantified relative to 18S RNA isolated from thyroid (TYR) and kidney (KID) from Slc26a4$^{+/-}$ mice at P10, P15, P30 and P80 (n=4). Slc26a4 was highly expressed in the kidney and modestly expressed in the thyroid at all ages. Fth and Actb were highly expressed in the thyroid and kidney of Slc26a4$^{+/-}$ mice at all ages.*

Lack of pendrin does not affect the expression of genes involved in thyroid hormone synthesis

Gene array data from P15 *Slc26a4$^{+/-}$* and *Slc26a4$^{-/-}$* mice were analyzed to evaluate the expression of genes involved in thyroid hormone synthesis (Table 4.2). Gene array data analysis revealed no differences in the expression of *Tg, Tpo, Duox2, Dio1* and *Dio2* between the *Slc26a4$^{+/-}$* and *Slc26a4$^{-/-}$* mice.

Table 4.2: Genes involved in thyroid hormone synthesis

#	Gene	Description	*Slc26a4$^{+/-}$* Intensity	P	*Slc26a4$^{-/-}$* Intensity	P	Fold	Significance
1	*Tg*	Thyroglobulin	6,619	6/6	6,507	6/6	1.25	n.s
2	*Tpo*	Thyroid peroxidase	2,737	3/3	2,967	3/3	1.08	n.s
3	*Duox2*	Dual oxidase 2	43	2/3	34	2/3	1.28	n.s
4	*Dio1*	Deiodinase 1	4,028	3/3	3,830	3/3	1.05	n.s
5	*Dio2*	Deiodinase 2	735	9/9	1114	9/9	1.56	n.s
6	*Slc26a4*	Pendrin	7	0/3	8	0/3	-	-
7	*NIS*	Sodium iodide symporter	1,157	6/6	935	6/6	1.12	n.s

For parameters 'P', and 'Fold' see section: Methods.Genearray. Fold differences are given when a gene was called Present (P) in Slc26a4$^{+/-}$ and Slc26a4$^{-/-}$ samples in at least half of the available probes.

Western blots were performed to evaluate the protein levels of Tpo and Duox1 in the *Slc26a4*^{+/–} and *Slc26a4*^{–/–} mice at various ages (Fig. 4.2). Although densitometry was not performed, visual inspection did not reveal obvious differences in the protein expression of Tpo and Duox1 between *Slc26a4*^{+/–} and *Slc26a4*^{–/–} mice. These observations suggest that the absence or presence of pendrin does not affect the expression of genes/ proteins that are involved in the synthesis of thyroid hormone.
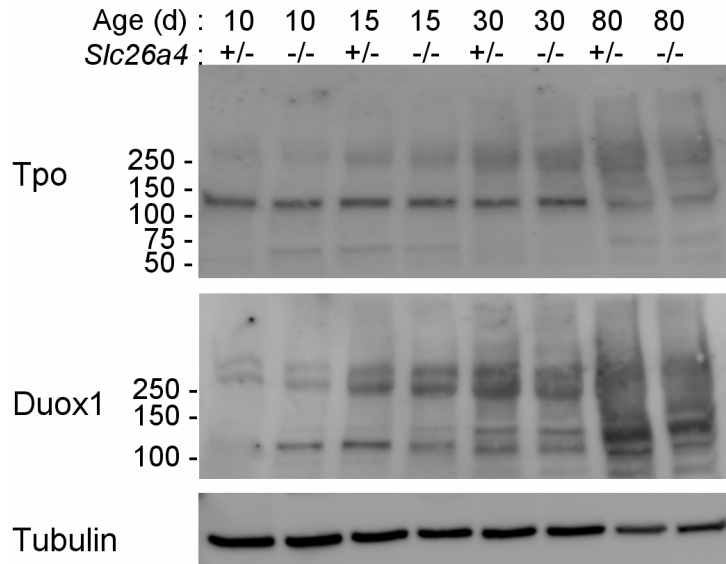

Figure 4.2: No visible difference between the protein expression of Tpo and Duox1 in the thyroid of *Slc26a4*^{+/-} and *Slc26a4*^{-/-} mice.
*Representative western blots for Thyroid peroxidase (*Tpo*), dual oxidase 2 (*Duox1*) and tubulin in thyroid of Slc26a4*^{+/-} *and Slc26a4*^{-/-} *mice at P10, P15, P30 and P80 (n=3). Consistent with the gene expression data, no differences in the protein expression of* Tpo *and* Duox1 *were detected in the thyroid of Slc26a4*^{-/-} *mice as compared to Slc26a4*^{+/-} *mice. Data were collected by Christa Linsenmeyer and Ruchira Singh*

Lack of pendrin does not affect serum T4 levels

Fig. 4.3 shows a time course of serum T4 level as measured by immunoassay of the serum samples from *Slc26a4*$^{+/-}$ and *Slc26a4*$^{-/-}$ mice. No differences in the T4 levels in the serum of *Slc26a4*$^{+/-}$ and *Slc26a4*$^{-/-}$ mice were observed at any time point included in this study. These data are consistent with results from previous studies suggesting the lack of overt hypothyroidism in *Slc26a4*$^{-/-}$ mice (8).
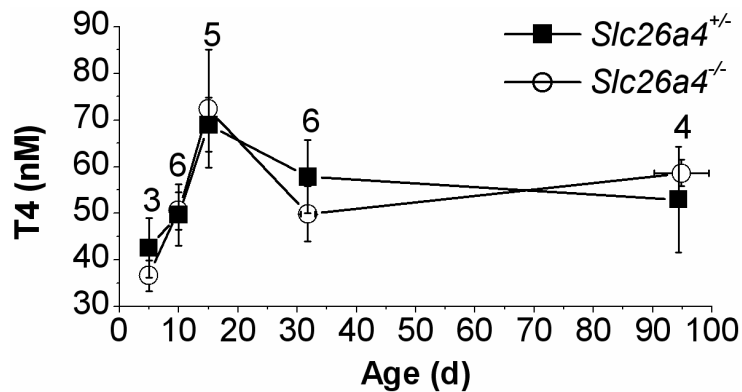

Figure 4.3: No difference in serum T4 levels is observed between *Slc26a4*$^{+/-}$ and *Slc26a4*$^{-/-}$ mice.

Measurement of serum T4 levels in Slc26a4$^{+/-}$ and Slc26a4$^{-/-}$ mice at ages P5, P10 P15, P30 and ~ P90. Numbers next to the bars represent the number of observations. No differences in the T4 levels in the serum of Slc26a4$^{+/-}$ and Slc26a4$^{-/-}$ mice were found at any age, indicating that Slc26a4$^{-/-}$ mice do not develop systemic hypothyroidism. Data were collected by Christa Linsenmeyer.

Lack of pendrin does not affect ClC-5 protein expression in the thyroid

Clcn5^{-/-} mice show selective loss of pendrin expression in the thyroid (30). This finding led us to investigate whether the knockout of pendrin affects ClC-5 protein expression. The expression of ClC-5 was compared between the *Slc26a4^{+/-}* and *Slc26a4^{-/-}* mice using western blots (Fig. 4.4). No difference in the expression of ClC-5 in the thyroids from *Slc26a4^{+/-}* and *Slc26a4^{-/-}* mice was found at any time point included in this study. This finding suggests that lack of pendrin does not affect the expression of ClC-5 in the thyroid.
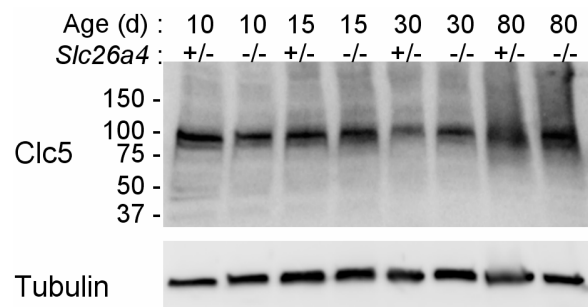

Figure 4.4: No visible difference is observed in the ClC-5 protein expression level in the thyroid of *Slc26a4^{+/-}* and *Slc26a4^{-/-}* mice.
Representative western blots for ClC-5 protein and tubulin *in thyroid of Slc26a4^{+/-} and Slc26a4^{-/-} mice at P10, P15, P30 and P80 (n=3). Based on visual inspection, no difference in thyroid ClC-5 protein expression was seen at any age in Slc26a4^{-/-} mice as compared to Slc26a4^{+/-} mice. Data were collected by Dr. Peying Fong, Christa Linsenmeyer and Ruchira Singh.*

Lack of pendrin leads to reduced nitrative stress in the thyroid

The finding that free radical stress is increased in the stria vascularis of *Slc26a4^{-/-}* mice led us to investigate oxidative and nitrative stress in other tissues (28). Oxidative stress was evaluated in: a) a pendrin-expressing tissue, thyroid, and b) a non-pendrin-expressing tissue, spleen. Oxidized proteins, using DNP-labeling of carbonyl groups by derivatization with DNPH, were detected by: a) western blot at P35 (Fig. 4.5A, 4.5B) and b) ELISA at P15 (Fig. 4.5C). Note that no labeling was observed in the absence of derivatization in western blot (Fig. 4.5A). No difference in the levels of oxidized proteins was found between the thyroids of *Slc26a4^{+/-}* and *Slc26a4^{-/-}* mice. It is important to note that two different techniques were used to quantitate oxidized proteins at P15 and P35. Although data from two different techniques cannot be compared, both data sets are presented. (The reason for using two different techniques at P15 and

P35 is due to the use of P35 mice for our initial experiments. In later experiments we decided to focus on P15, an age that corresponds to the maximal activity of thyroid gland.)
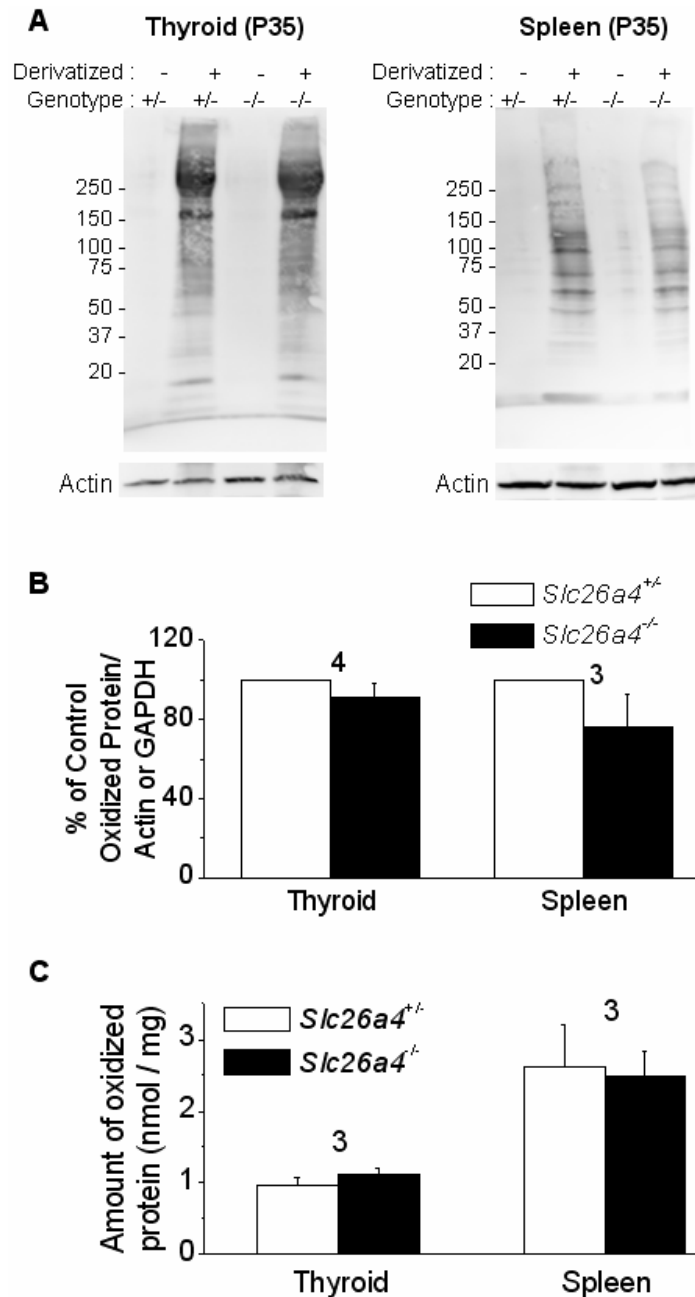

Figure 4.5 The levels of oxidized proteins were not different in the thyroid of *Slc26a4*^{+/-} and *Slc26a4*^{-/-} mice.
(A-B) Oxidized proteins were quantified against actin *or* GAPDH *in thyroid and spleen from Slc26a4*^{+/-} *and Slc26a4*^{-/-} *mice at P35. Representative western blots and data summaries are shown. (C) Relative amount of oxidized protein was determined by ELISA in thyroids from Slc26a4*^{+/-} *and Slc26a4*^{-/-} *mice at P15. No difference in the levels of oxidized proteins was found between thyroid or spleen of Slc26a4*^{+/-} *and Slc26a4*^{-/-} *mice.*

The protein expression of eNOS was evaluated by western blots in a developmental study (Fig. 4.6A, 4.6B). The amount of nitrated proteins in relationship to the total protein was quantified at P15 and P35 in the thyroid of *Slc26a4*$^{-/-}$ and *Slc26a4*$^{+/-}$ mice (Fig. 4.6C). No difference in the levels of eNOS was found between the thyroid of *Slc26a4*$^{-/-}$ and *Slc26a4*$^{+/-}$ mice. Although *Slc26a4*$^{+/-}$ and *Slc26a4*$^{-/-}$ mice show similar levels of nitration at P15, nitration is reduced at P35 in *Slc26a4*$^{-/-}$ mice, suggesting that thyroid of *Slc26a4*$^{-/-}$ mice experience reduced nitrative stress. It is conceivable that reduction of nitrative stress occurs between P15 and P35.
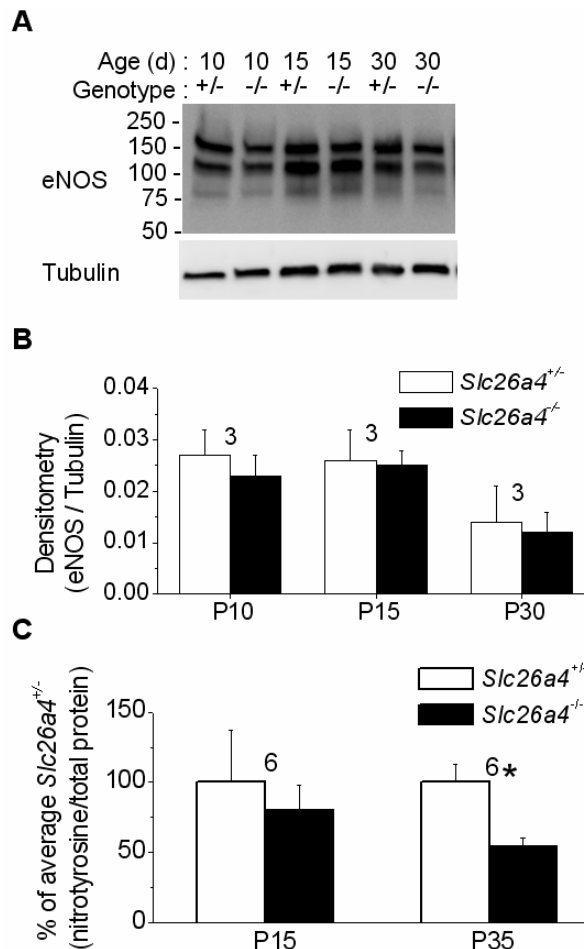

Figure 4.6: The amounts of nitrated proteins in the thyroid of *Slc26a4*$^{-/-}$ mice were decreased in comparison to the thyroid of *Slc26a4*$^{+/-}$ mice.
(A-B) Protein expression of eNOS *was quantified relative to* tubulin *in thyroid of Slc26a4*$^{+/-}$ *and Slc26a4*$^{-/-}$ *mice at P10, P15 and P30. Representative western blots and data summaries are shown. No difference in* eNOS *expression was found between Slc26a4*$^{+/-}$ *and Slc26a4*$^{-/-}$ *mice at any age. (C) The level of nitrotyrosine by ELISA was quantified against total protein in thyroids from Slc26a4*$^{+/-}$ *and Slc26a4*$^{-/-}$ *mice at P15 and P35. Significant changes are marked (*) and numbers next to the bars represent the number of observations. Reduced levels of nitrated protein were seen at P35 in the thyroid of Slc26a4*$^{-/-}$ *mice.*

*Lack of pendrin does not affect the expression of **Trf** and **Tfrc** in thyroid and spleen.*

The observation that the expression of genes involved in iron metabolism is altered in the stria vascularis of $Slc26a4^{-/-}$ mice led us to investigate the expression of Trf and Tfrc, two proteins involved in iron metabolism, in a pendrin-expressing tissue, thyroid, and in a non-pendrin expressing tissue, spleen (28). Protein levels of Trf and Tfrc were quantified in the thyroid and spleen of $Slc26a4^{+/-}$ and $Slc26a4^{-/-}$ mice at P35 (Fig. 4.7A). Further, the tissue iron levels (Tissue-Fe) were measured at P15 corresponding to the time point of maximal activity of thyroid gland (Fig. 4.7B). No differences in protein expression of Trf and Tfrc were found in the thyroids and spleens of $Slc26a4^{+/-}$ and $Slc26a4^{-/-}$ mice at P35. No differences in tissue-Fe were found in the thyroids and spleens of $Slc26a4^{-/-}$ compared to $Slc26a4^{+/-}$ mice at P15.
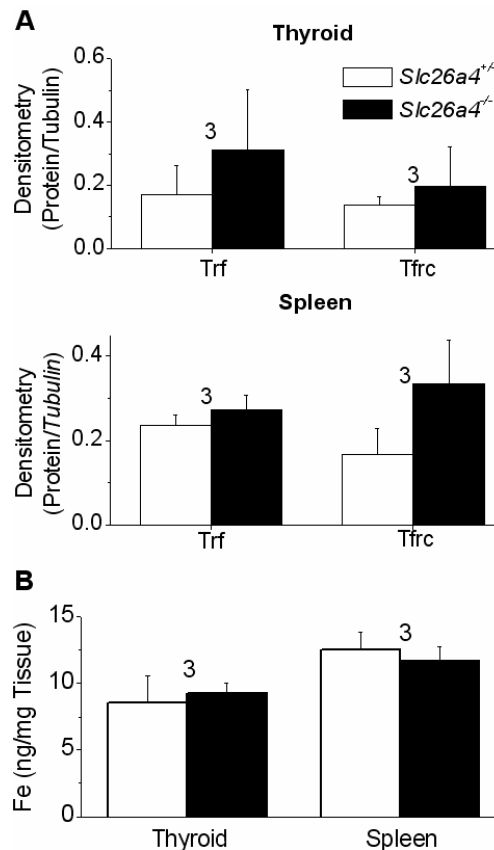

Figure 4.7: Tissue iron levels and protein expression of Trf, Tfrc was unchanged in the thyroid and spleen of $Slc26a4^{+/-}$ and $Slc26a4^{-/-}$ mice.
(A) Transferrin (Trf) and transferrin receptor (Tfrc) were quantified relative to tubulin in thyroid and spleen of Slc26a4$^{+/-}$ and Slc26a4$^{-/-}$ mice at age P35. (B) Tissue-iron was quantified in thyroid and spleen of Slc26a4$^{+/-}$ and Slc26a4$^{-/-}$ at age P15. Numbers next to the bars represent the number of observations. No difference was found in tissue-Fe or the levels of Trf and Tfrc between thyroid or spleen of Slc26a4$^{+/-}$ and Slc26a4$^{-/-}$ mice.

Discussion

The most salient finding of the present study is that no difference between the thyroid gland function was observed between littermates of $Slc26a4^{+/-}$ and $Slc26a4^{-/-}$ mice. The inference that $Slc26a4$ expression is not essential for thyroid gland function is derived from the following observations: 1) $Slc26a4$ mRNA expression is very low in the mouse thyroid and its levels do not increase at the time point corresponding to maximal thyroid gland activity, 2) no observable effect of lack of pendrin is seen on the expression of genes involved in thyroid hormone synthesis and 3) serum T4 levels are unaffected in $Slc26a4^{-/-}$ mice.

It is conceivable that the variability in thyroid phenotype between human patients and $Slc26a4^{-/-}$ mice is due to differences in $Slc26a4$ expression between humans and rodents. $Slc26a4$ transcript is highly expressed in the human thyroid at levels much higher than in the kidney (9). In contrast, our results show very little $Slc26a4$ mRNA expression in the mouse thyroid at all time points, including those of maximal gland activity. Consistent with our finding, another group has reported that $Slc26a4$ mRNA expression in thyroids from adult mice is only 2% of the kidney expression (30).

Pendrin in the thyroid has been implicated in iodide transport across the apical membrane of the thyrocytes (24; 32). Iodide organification defects are seen in human Pendred syndrome patients, and reduced expression of pendrin has been implicated as the cause of euthyroid goiter due to delayed iodide organification in $Clcn5^{-/-}$ mice (30). However, our current observations suggest that pendrin is not necessary for thyroid gland function, at least not in the 129Sv/Ev strain of mice. Two possible reasons for the presence of euthyroid goiter in $Clcn5^{-/-}$ mice could be that 1) although a lack of ClC-5 is associated with reduced pendrin expression, the euthyroid goiter observed in $Clcn5^{-/-}$ mice is caused by a different mechanism and 2) the two mouse strains, 129Sv/Ev and C57BL/6J, respond differently to absence of pendrin in the thyroid gland. Pendrin has not been shown to transport iodide *in vivo,* which could imply that 1) the apical iodide transporter in the thyroid remains to be identified, 2) the apical iodide transporter differs between human (pendrin) and mouse thyroid (unidentified) or 3) an unidentified iodide transporter compensates for the absence of pendrin in the mouse thyroid.

The absence of *Slc26a4* leads to increased free radical stress in the stria vascularis of *Slc26a*$^{-/-}$ mice (28). The absence of increased levels of free radical stress markers in the thyroid of *Slc26a4*$^{-/-}$ mice suggests that complete absence of *Slc26a4* in itself may not be sufficient to cause free radical stress. Alternatively, it is possible that increased free radical stress is present in the thyroid but is restricted to a few cells and hence was not detected in analysis of whole tissue lysate.

One of the consistent features of Pendred syndrome in human patients is deafness (12). Hypothyroidism at birth is known to lead to deafness. Since most Pendred syndrome patients are deaf at birth and mutations in *Slc26a4* are found in congenital hypothyroidism, it difficult to completely rule out systemic hypothyroidism as the cause of deafness in Pendred syndrome (2). Our present finding that the overt hypothyroidism is not present in *Slc26a4*$^{-/-}$ mice together with the fact that deafness is a consistent feature of Pendred syndrome mouse model establishes that absence of *Slc26a4* in the cochlea is sufficient to affect hearing. However, it is still possible that lack of *Slc26a4* leads to conditions of local hypothyroidism in the cochlea that could contribute to deafness in Pendred syndrome. Tissue-specific hypothyroidism limited to the cochlea has been demonstrated as the cause of deafness in *Dio2*$^{-/-}$ mice (17).

The normal function of the thyroid gland in the Pendred syndrome mouse model and the difference in *Slc26a4* expression between mouse and human thyroid suggest that pendrin has a different functional role in mouse and human thyroids.

Acknowlegements

References

1. **Abs R, Verhelst J, Schoofs E and De Somer E**. Hyperfunctioning metastatic follicular thyroid carcinoma in Pendred's syndrome. *Cancer* 67: 2191-2193, 1991.

2. **Banghova K, Taji EA, Cinek O, Novotna D, Pourova R, Zapletalova J, Hnikova O and Lebl J**. Pendred syndrome among patients with congenital hypothyroidism detected by neonatalscreening: identification of two novel *PDS/SLC26A4* mutations. *Eur J Pediatr* 2007.

3. **Bashir EA, Ahmed S, Murtaza B, Abbasi MH, Shah SS, Tamimy MS and Awan AS**. Follicular carcinoma thyroid in Pendred syndrome. *J Coll Physicians Surg Pak* 14: 679-680, 2004.

4. **Bidart JM, Mian C, Lazar V, Russo D, Filetti S, Caillou B and Schlumberger M**. Expression of pendrin and the Pendred syndrome (*PDS*) gene in human thyroid tissues. *J Clin Endocrinol Metab* 85: 2028-2033, 2000.

5. **Campos-Barros A, Amma LL, Faris JS, Shailam R, Kelley MW and Forrest D**. Type 2 iodothyronine deiodinase expression in the cochlea before the onset of hearing. *Proc Natl Acad Sci U S A* 97: 1287-1292, 2000.

6. **Cremers CW, Admiraal RJ, Huygen PL, Bolder C, Everett LA, Joosten FB, Green ED, van Camp G and Otten BJ**. Progressive hearing loss, hypoplasia of the cochlea and widened vestibular aqueducts are very common features in Pendred's syndrome. *Int J Pediatr Otorhinolaryngol* 45: 113-123, 1998.

7. **Elisei R, Pinchera A, Romei C, Gryczynska M, Pohl V, Maenhaut C, Fugazzola L and Pacini F**. Expression of thyrotropin receptor (TSH-R), thyroglobulin, thyroperoxidase, and calcitonin messenger ribonucleic acids in thyroid carcinomas: evidence of TSH-R gene transcript in medullary histotype. *J Clin Endocrinol Metab* 78: 867-871, 1994.

8. **Everett LA, Belyantseva IA, Noben-Trauth K, Cantos R, Chen A, Thakkar SI, Hoogstraten-Miller SL, Kachar B, Wu DK and Green ED**. Targeted disruption of mouse *Pds* provides insight about the inner-ear defects encountered in Pendred syndrome. *Hum Mol Genet* 10: 153-161, 2001.

9. **Everett LA, Glaser B, Beck JC, Idol JR, Buchs A, Heyman M, Adawi F, Hazani E, Nassir E, Baxevanis AD, Sheffield VC and Green ED**. Pendred syndrome is caused by mutations in a putative sulphate transporter gene (*PDS*). *Nat Genet* 17: 411-422, 1997.

10. **Everett LA, Morsli H, Wu DK and Green ED**. Expression pattern of the mouse ortholog of the Pendred's syndrome gene (*Pds*) suggests a key role for pendrin in the inner ear. *Proc Natl Acad Sci U S A* 96: 9727-9732, 1999.

11. **Fish WW**. Rapid colorimetric micromethod for the quantitation of complexed iron in biological samples. *Methods Enzymol* 158: 357-364, 1988.

12. **Fraser GR**. Association of congenital deafness with goitre (Pendred's syndrome) a study of 207 families. *Ann Hum Genet* 28: 201-249, 1965.

13. **Jabba SV, Oelke A, Singh R, Maganti RJ, Fleming S, Wall SM, Everett LA, Green ED and Wangemann P**. Macrophage invasion contributes to degeneration of stria vascularis in Pendred syndrome mouse model. *BMC Med* 4: 37, 2006.

14. **Karbownik M and Lewinski A**. The role of oxidative stress in physiological and pathological processes in the thyroid gland; possible involvement in pineal-thyroid interactions. *Neuro Endocrinol Lett* 24: 293-303, 2003.

15. **Morgans ME and Trotter WR**. Association of congenital deafness with goitre; the nature of the thyroid defect. *Lancet* 1: 607-609, 1958.

16. **Nakamura M and Ohtaki S**. [Molecular mechanism of thyroid hormone synthesis]. *Nippon Rinsho* 52: 857-863, 1994.

17. **Ng L, Goodyear RJ, Woods CA, Schneider MJ, Diamond E, Richardson GP, Kelley MW, Germain DL, Galton VA and Forrest D**. Hearing loss and retarded cochlear development in mice lacking type 2 iodothyronine deiodinase. *Proc Natl Acad Sci U S A* 101: 3474-3479, 2004.

18. **Ozluk A, Yildirim E, Oral S, Celen O and Berberoglu U**. Carcinomas of the thyroid and breast associated with Pendred's syndrome: report of a case. *Surg Today* 28: 673-674, 1998.

19. **Pendred V.** Deaf-mutism and goitre. *Lancet* 11: 532, 1896.

20. **Ramakers C, Ruijter JM, Deprez RH and Moorman AF**. Assumption-free analysis of quantitative real-time polymerase chain reaction (PCR) data. *Neurosci Lett* 339: 62-66, 2003.

21. **Ramasarma T**. H2O2 has a role in cellular regulation. *Indian J Biochem Biophys* 27: 269-274, 1990.

22. **Reardon W, Coffey R, Phelps PD, Luxon LM, Stephens D, Kendall-Taylor P, Britton KE, Grossman A and Trembath R**. Pendred syndrome--100 years of underascertainment? *QJM* 90: 443-447, 1997.

23. **Reardon W and Trembath RC**. Pendred syndrome. *J Med Genet* 33: 1037-1040, 1996.

24. **Royaux IE, Suzuki K, Mori A, Katoh R, Everett LA, Kohn LD and Green ED**. Pendrin, the protein encoded by the Pendred syndrome gene (*PDS*), is an apical porter of iodide in the thyroid and is regulated by thyroglobulin in FRTL-5 cells. *Endocrinology* 141: 839-845, 2000.

25. **Royaux IE, Wall SM, Karniski LP, Everett LA, Suzuki K, Knepper MA and Green ED**. Pendrin, encoded by the Pendred syndrome gene, resides in the apical region of renal intercalated cells and mediates bicarbonate secretion. *Proc Natl Acad Sci U S A* 98: 4221-4226, 2001.

26. **Sheffield VC, Kraiem Z, Beck JC, Nishimura D, Stone EM, Salameh M, Sadeh O and Glaser B**. Pendred syndrome maps to chromosome 7q21-34 and is caused by an intrinsic defect in thyroid iodine organification. *Nat Genet* 12: 424-426, 1996.

27. **Sheils OM and Sweeney EC**. TSH receptor status of thyroid neoplasms--TaqMan RT-PCR analysis of archival material. *J Pathol* 188: 87-92, 1999.

28. **Singh R and Wangemann P**. Free radical stress mediated loss of Kcnj10 protein expression in stria vascularis contributes to deafness in Pendred syndrome mouse model. *Am J Physiol Renal Physiol* 2007.

29. **Soleimani M, Greeley T, Petrovic S, Wang Z, Amlal H, Kopp P and Burnham CE**. Pendrin: an apical Cl^-/OH^-. *Am J Physiol Renal Physiol* 280: F356-F364, 2001.

30. **van den Hove MF, Croizet-Berger K, Jouret F, Guggino SE, Guggino WB, Devuyst O and Courtoy PJ**. The loss of the chloride channel, ClC-5, delays apical iodide efflux and induces a euthyroid goiter in the mouse thyroid gland. *Endocrinology* 147: 1287-1296, 2006.

31. **Xing M, Tokumaru Y, Wu G, Westra WB, Ladenson PW and Sidransky D**. Hypermethylation of the Pendred syndrome gene *SLC26A4* is an early event in thyroid tumorigenesis. *Cancer Res* 63: 2312-2315, 2003.

32. **Yoshida A, Taniguchi S, Hisatome I, Royaux IE, Green ED, Kohn LD and Suzuki K**. Pendrin is an iodide-specific apical porter responsible for iodide efflux from thyroid cells. *J Clin Endocrinol Metab* 87: 3356-3361, 2002.

The American Physiological Society
9650 Rockville Pike, Bethesda, MD 20814-3991, USA
Phone: (301) 634-7070
Fax: (301) 634-7243

December 19, 2007

Ms. Ruchira Singh
Department of Anatomy and Physiology
Kansas State University
Room 204 Coles Hall
1600 Dension Avenue
Manhattan, Kansas-66502

Dear Ms. Singh:

The American Physiological Society grants you permission to use the following two articles for your doctoral dissertation:

1..Ruchira Singh, Rajanikanth J. Maganti, Sairam V. Jabba, Martin Wang, Glenn Deng, Joe Don Heath, Nurith Kurn, and Philine Wangemann
> **Microarray-based comparison of three amplification methods for nanogram amounts of total RNA**
> *Am J Physiol Cell Physiol* 288: C1179-C1189, 2005.

2. Ruchira Singh and Philine Wangemann
> **Free radical stress mediated loss of *Kcnj10* protein expression in stria vascularis contributes to deafness in Pendred syndrome mouse model.**
> *Am J Physiol Renal Physiol* (October 24, 2007). doi:10.1152/ajprenal.00433.2007

ProQuest/UMI may provide single copies of the thesis on demand.

The American Physiological Society publication must be credited as the source with the words "used with permission" added.

Sincerely,

Ms. Margaret Reich
Director of Publications
The American Physiological Society
MR/pr